TRENDS OF STRUCTURES IN THE SOKOTO BASIN OF NORTH-WESTERN NIGERIA FROM THE INTERPRETATION OF AEROMAGNETIC ANOMALIES.

BY
ROGER KENYUY ISHAKU

B.Sc. (Hons) PHYSICS, ABU. A thesis submitted to the

Hello University, Zaria in partial fulfilment of the requirements for the award of the Degree of Master of Science in Applied Geophysics.

Department of Physics
Faculty of Science
Ahmadu Bello University
Zaria, Nigeria

March, 2000

DECLARATION

I hereby declare that:

(1) the report presented in this thesis is the result of original research of the author;

(2) this thesis has not been submitted to any other institution, organization or body for any award other than Ahmadu Bello University; and

(3) all inclusions from the works of others have been duely acknowledged.

Date: 18-05-2000

ROGER KENYUY ISHAKU

CERTIFICATION

This thesis entitled "TRENDS OF STRUCTURES IN THE SOKOTO BASIN OF NORTH-WESTERN NIGERIA FROM THE INTERPRETATION OF AEROMAGNETIC ANOMALIES" by Roger Kenyuy Ishaku meets the regulations governing the award of the degree of Master of Science of Ahmadu Bello University, and is approved for its contribution to knowledge and literary presentation.

Dr. M.N. Umego
Chairperson, Supervisory Committee — Date: 18-05-2000

Professor S.B. Ojo
Member, Supervisory Committee — Date: 19/12/00

Professor I.B. Osazuwa
Head of Department — Date: 30-5-2000

Professor S.B. Ojo
Dean, Postgraduate School — Date: 26/03/01

DEDICATION

To Sister Barbara Knudsen, Wysenyuy and Alice:

" Hallelujah! Hallelujah! Come and see what God has done "

ACKNOWLEDGEMENTS

I am greatly indebted to my supervisor Dr. M.N. Umego, M.Sc Applied Geophysics Coordinator for providing me with digital aeromagnetic data for the entire study area, his encouragement in diverse forms, his invaluable guidance, keen interest and advice which he readily gave at all times during my project work and the writing of this report. I acknowledge with thanks the sustained interest of my co-supervisor Professor S.B. Ojo Dean of the Postgraduate School for his useful suggestions after reading the draft. I am particularly grateful that in spite of his tight duty demands, he sacrificed some of his time to proof-read the original draft.

I am very grateful to Dr. R. Kangkolo for his provision of the computer programs used for this project and his keen guidance. I sincerely express my gratitude to the Head of Department Professor I. B. Osazuwa for his assistance in the use of the computers which were completely at my disposal during the course of this programme. I am greatly indebted to Professor C.O. Ajayi for his sustained interest in my work and hospitality to me as a foreign student during my long study years.

Many people have helped in numerous ways during the development of this work. I would like to acknowledge such assistance and participation from Dr. P.O. Sule, Professor N. Hariharan, Engr. A.C. Bamgbelu and Mr. K. Lawal and also to the entire staff of the Physics Department. Special thanks

are due to my course mates, namely, Augustine, Fidelis, Gabriel and Moshood for their timely co-operation throughout the study years.

Finally, I wish to thank my family and numerous friends at home who in their own ways helped me during the period of study, when my activities appeared to be far removed from the traditional duties of a senior member of the family. Special recognition is due to my brother Mr. J. Wysenyuy for solely financing this programme in spite of his obvious financial limitations and commitments to the entire family. My ultimate gratitude is to the Almighty Father for making my dreams materialise and for whatever I am and will ever be.

KASHIM IBRAHIM LIBRARY

ABSTRACT

The total magnetic field data for the Sokoto Basin was obtained from aeromagnetic maps each of size 55 km x 55 km within the Basin. A qualitative study of the structural trends in the total field map reveals an alignment of anomalous zones in approximately linear patterns oriented in the N-S, NNE-SSW and NW-SE directions. The residual field map and the regional field were obtained by the method of polynomial fitting using the least square technique. The residual anomalies in the study area change little from the anomalies of the observed total field.

The residual field was further analyzed by computing the zero contours of the second vertical derivative. These zero contours delineate the magnetic boundaries in the subsurface structures. The elongation of these contours are mostly in the NE-SW and E-W directions, though broken off at shorter distances in some sections.

The method of crosscorrelatidn was used to determine the structural trends and alignments for the twenty maps covering the area of study. The main trends for most of the maps are in the ENE-WSW and E-W directions with a moderately high degree of correlation over data values in the northern section of the area as opposed to the southwestern section where a low degree of correlation is common.

Spectral analysis of the residual magnetic field over forty eight overlapping blocks of size 55 km x 55 km was carried out. Two prominent magnetic layers were detected. The results reveal that the depths to the first layer vary from 0.9 km to 2.2 km with an average depth of 1.4 km. The second layer depths vary from 2.2 km to 6.9 km with an average depth of 4.3 km. The third layer magnetic sources are not uniformly distributed. The first magnetic layer is attributed to magnetic rocks intruded on the basement surface. The second magnetic sources are considered to arise from magnetic rocks within the basement which could include fractures and faults. The depths to the basement map show that the magnetic basement beneath the sediments in the basin is generally shallow with the highest depth of 2.2 km recorded in the northwest corner of the study area. There are a series of ridges and troughs on the basement surface suggesting that the subsurface rocks must have undergone gentle folding.

All the analyses carried out in the study confirm the fact that major structures are oriented in the NE-SW directions. However minor features could be trending in different directions as indicated in a few sections in the crosscorrelat.ion analyses.

TABLE OF CONTENTS

CHAPTER		PAGE
	Title page	i
	Declaration	ii
	Certification	iii
	Dedication	iv
	Acknowledgements	v
	Abstract	vii
	Table of content	ix
	List of tables	xii
	List of figures	xiii
	List of appendices	xiv
	Abbreviations and symbols	xv
1.	INTRODUCTION	
1.1	General Introduction	1
1.2	The magnetic method	2
1.3	The earth's magnetic field	4
1.4	Crosscorrelation function	6
1.5	Spectral analysis	6
1.6	Location of the area	7
1.7	Previous geophysical studies in the study area	8
1.8	Scope and objectives of the study	12
2	DETAILED GEOLOGY OF THE AREA	
2.1	Introduction	14
2.2	The basement complex	17

2.3	Pre-maastrichtian deposit	20
2.3.1	The basal conglomerates	21
2.3.2	Lateritic ironstones	22
2.4	Ma-maastrichtian deposits	22
2.5	Paleocene deposits	24
2.6	Faults and folds	26
2.7	Economic geology	26
3	DATA SOURCE OF PREPARATION	
3.1	Introduction	29
3.2	Regional-residual separation	29
3.2.1	Polynomial fitting method	30
3.3	Second vertical derivative	31
3.3.1	Basic mathematical theory of the second vertical derivative	33
4	THEORETICAL BACKGROUND OF QUANTITATIVE TECHNIQUES USED	
4.1	Introduction	35
4.2	Crosscorrelation function technique	35
4.3	Spectral analysis of aeromagnetic field	
4.3.1	Introduction	40
4.3.2	Fast Fourier analysis of two dimensional aeromagnetic data	40
4.3.3	Data treatment	42
4.3.4	An improved estimation of the source depth from magnetic spectra	46
5	Results and Interpretation	
5.1	Introduction	51
5.2	Qualitative Interpretation	52

5.2.1	Total field magnetic map	52
5.2.2	Anomaly alignments	54
5.3	The residual magnetic map and surface geology	55
5.4	Application and results of the second vertical derivative	59
5.5	Quantitative Interpretation	
5.5.1	Application of crosscorrelation	61
5.5.2	Results of crosscorrelation	61
5.6	Application of power spectral analysis	68
5.6.1	Results of power spectral analysis	69
5.6.2	Discussion of the depth to magnetic basement map	74
6	GENERAL DISCUSSIONS AND CONCLUSIONS	
6.1	Improved method of depth estimation	79
6.2	Summary of the results	80
6.3	Deduction	81
6.4	Limitations and assumptions	87
6.5	Conclusions	89
6.6	Recommendations	89
	References	91
	Appendices	96

LIST OF TABLES

TABLE	TITLE	PAGE
2.1	Geological sequence in the Sokoto Basin	19
5.1	Direction of the main trend and the correlation coefficient for each section	65
5.2	Latitude and longitude extension for each section	66
5.3	Locations and identification numbers for the blocks with their respective depths	72

LIST OF FIGURES

FIGURE	TITLE	PAGE
2.1	Structural map of the Iullemeden Basin	15
2.2	Simplified geological map of Nigeria showing the boundary of the study area	16
2.3	Geological map of Sokoto Basin	18
4.1(a)	Conventions for choosing $X_{j,k}$ from $Y_{j,k}$	38
4.1(b)	Schematic diagram from the sample sets $X_{j,k}$ and $Y_{j,k}$ used for the crosscorrelation technique	38
4.2(a)	Rectangular data window and the corresponding spectral window	45
4.2(b)	A cosine-bell data window and the corresponding spectral window	45
5.1	Total field magnetic map for the entire basin	53
5.2	Regional field for the entire basin	56
5.3	Residual field for the entire basin	58
5.4	Zero contours of the second vertical derivative	60
5.6	Cross coefficient maps for sections M009 and M010	62
5.7	Cross coefficient maps for sections M116 and M117	64
5.8	Sheet layout of the Sokoto Basin showing the direction of th main trend for each section	65
5.9	Power spectral analysis for blocks 5 and 6	70
5.10	Power spectral analysis for blocks 11 and 12	71
5.11	Generalised depth to the magnetic basement map	74
5.12	Depth to the second layer map	76

LIST OF APPENDICES

Appendix		Page
1	Fundamentals of spectral analysis	96
2	Crosscorrelation coefficient maps	100
3	Power spectrum analysis	109

LIST OF ABBREVIATIONS AND SYMBOLS

ABBREVIATION/SYMBOLS	DESCRIPTION
GSN	Geological Survey of Nigeria
JICA	Japanese International Cooperation Agency.
USAID	United States Agency for International Development.
LANDSAT	Land Resources Technology Satellite
°C	Degree Celsius
nT	nanotesla
m	metre
Km	Kilometre
N	north
E	east
W	west
S	south
Rep.	Republic

CHAPTER ONE

INTRODUCTION

1.1 General Introduction

Geophysical methods of exploration have played an increasingly important role in the economy of the world today. This is mainly as a result of the radical technical improvements in instrumentation, field methods, and modern interpretation techniques resulting from the emergence of large digital computers and their applications. The use of geophysics for geologic mapping has already been adopted by various international, national, and state organizations. Nigeria is no exception to this unavoidable wind of change. The Geological Survey of Nigeria (GSN) has responsibility for airborne magnetic surveying of the country and the publication of the airborne geophysical map series. The entire Nigeria's land mass has been effectively covered by airborne magnetic surveys carried out in the early and mid 1970s. Geophysical surveys of this type are often extended to provide geologic information which will perhaps stimulate and materially assist in a mineral exploration program.

It is certain that the future of applied geophysics in particular and the earth sciences in general appears enviably bright. Regardless of the synthetic and substitute materials, man's insatiable demand for basic resources will surely continue to expand, and will accelerate as the populous underdeveloped nations begin to emerge. However, geophysical prospecting does not constitute a panacea with regard to our

economic problems as it has its limitations and seldom gives a unique indication in the effort to discover concealed or obscured deposits of economic material.

1.2 The Magnetic Method

The magnetic method of applied geophysics is the oldest exploration method, and depends upon measuring accurately the anomalies of the local geomagnetic field produced by variations in the intensity of magnetization in rock formations which is related to the distribution of magnetic minerals within the rocks over which the field was measured. Magnetic prospecting may be carried out on land, from aircraft, and from ships, each involving a different technique and suitable instrumentation. The choice of the prospecting method depends on the nature of the survey in question and its objectives.

KASHIM IBRAHIM LIBRARY

The study presented in this thesis is based on data derived from the aeromagnetic survey of parts of the country carried out for GSN. The magnetometer most commonly employed in modern airborne work is the proton magnetometer. This instrument depends for its action on the phenomenon that the magnetic moments of protons (hydrogen nuclei) in say, a bottle of water or kerosene, can gyrate around the earth's magnetic flux density vector under certain conditions and the speed of their gyration provides a measure of the flux density of the field in which they gyrate. The proton magnetometer measures only the magnitude of the earth's total magnetic flux density but does not give its direction. Such measurements are therefore called total intensity measurements. In this case, we

are interested in the component of the total intensity anomaly in the direction of the total field vector which is a linear combination of the vertical component (Z) and the horizontal component (H).

Because of the enormous areas which have been surveyed worldwide by the airborne magnetometer, aeromagnetic interpretation has become almost a subject in itself. The use of the airborne magnetometer is keyed to two important factors, cost and speed. Firstly on account of high speed of operations, an aerial survey is many times cheaper than an equivalent ground survey, provided the area surveyed is sufficiently large. Secondly measurements can be made over mountains, jungles, swamps, lakes, glaciers and other terrains, which may be inaccessible or difficult for ground surveying parties.

Aeromagnetic surveys are used in mineral exploration. The direct detection of most mineral deposits is not possible with aeromagnetic surveys but the delineation of host environments favorable for mineral deposits is an important goal. They are an aid to geological mapping. The location and continuity of the magnetic features guide the geologist to key points on the ground where the rocks may be identified.

The airborne magnetometer is widely used in oil exploration to provide information on the depth to basement, revealing major tectonic features, possible faults and areas where there may be local relief on the basement surface. From these, the thickness of the overlying sediments can be

estimated and then the possibilities of the existence of certain deposits like hydrocarbons, can be assessed. Also deep crustal and upper mantle studies can be made from the results. In effect, many economically important discoveries can be either directly or indirectly be credited to the airborne magnetometer.

Data compilation, the major step in the entire process between measurement and interpretation, is an involved routine but can be automated with the aid of Doppler navigation and statistical techniques. Programs have been developed and are being applied for a gamut of mathematical filtration procedures such as polynomial surface fitting, correlation, derivatives, continuation, frequency analyses and power spectrum, etc. With these achievements, the method has become firmly established to the point that it is employed in most geophysical works, at least for reconnaissance purposes. Today, the magnetic method accounts for a major portion of the mining geophysical effort.

1.3 The Earth's Magnetic Field

Much speculation has been made as to the cause of the earth's magnetic field, and no completely satisfactory explanation has yet been given. A spherical harmonic analysis of the magnetic field observed at the surface of the earth shows that its source is predominantly internal. Superimposed on this field, however, is a rapidly varying external field giving rise to transient fluctuations. Unlike the secular variation, which is also of internal origin, these transient fluctuations produce no large enduring changes in the earth's

field. They give rise to a number of related upper atmospheric phenomena such as magnetic storms and aurora.

The possibility of permanent magnetization as the cause of the earth's magnetic field fails to account for other features of the earth's magnetic field, such as the close proximity of the magnetic and geographical poles and the high rate of change and westward drift of the non-dipole field. Also, the earth's field could not arise from the rotation of the earth, because the angular velocity of the earth is so small that the magnetization arising from such causes is negligible.

The dynamo theory of the earth's magnetic field which was due originally to Sir Joseph Lamor is held in high esteem. In 1919 he suggested that the magnetic field of the earth might be maintained by a mechanism analogous to that of a self-exciting dynamo.

The earth's core is a good conductor of electricity and a fluid in which motions can take place; i.e, it permits both mechanical motion and the flow of electric current, and the interaction of these could generate a self-sustaining magnetic field.

The dynamo theory suggests that the magnetic field is ultimately produced and maintained by an induction process, the magnetic energy being drawn from the kinetic energy of the fluid motions in the core (Jacob, 1967). A group of particles moving at different speeds in the fluid may pull laterally on

some magnetic lines of force, thus stretching, they will gain energy which is taken from the mechanical energy of the moving particles.

1.4 Crosscorrelation Function

Information on large scale tectonic trends may be derived by a wide variety of geological methods or by comprehensive geophysical surveys of the gravitational and magnetic fields. Analytical methods for determining the trend of tectonic features are often limited and are more subject to human bias. In this study, the fast Fourier transform is applied to the analysis of two-dimensional data. In particular, a cross correlation function, an empirical method has been used to obtain trend directions from aeromagnetic data over the study area (Agarwal and Kanasewich, 1971). Furthermore, some vital information can best be obtained from trend analysis. For example, Affleck (1963) determined anomaly trend and spacing patterns and related these to the intrabasement tectonic patterns.

1.5 Spectral Analysis

Spectral analysis refers primarily to the process of calculating and interpreting a spectrum. Hence, in the case of aeromagnetic data, the aim is to seek deeper understanding of the data, and of the systems which produce the data, for example the statistical structure of magnetization in the crust. It involves the analysis of two-dimensional data in the frequency or wave domain achieved through the Fourier transformation technique. The concept of Fourier transformation

is based on the Fourier series which expresses a time or space dependent signal of limited length as a summation of infinitely long series of sine and cosine waves of different wavelengths determined by the original time or space dependent signal.

The Fast Fourier Transform algorithm was first introduced in a new form by Cooley and Tukey (1965) and given in detail by Gentleman and Sande (1966). Since the exposition of this technique and the widespread introduction of digital computers, spectral analysis has been utilized in virtually every field of research. In this study, power spectral analysis was employed as did Spector and Grant (1970) and Fedi et al., (1997) to find the depth to magnetic sources.

1.6 Location of the Area

The Sokoto Basin of Northwestern Nigeria forms the southeastern sector of the Iullemmeden Basin. The Sokoto Basin is bound by latitudes 10.50^0-14.00^0 N and longitudes 3.50^0 - 6.50^0 E. The sedimentary basin consists predominantly of a gentle undulating plain with an average elevation varying from 250 to 400 m above sea level (Kogbe, 1979). This monotonous plain is occasionally interrupted by steepsided, flat-topped hills. A low escarpment which was named the Dange Scarp by earlier workers, is the most prominent feature in the basin. The area to the east of this escarpment consists predominantly of a gentle undulating, sandy plain, which extends south-westwards to the basement complex boundary. The escarpment itself has undergone intensive erosion. The edge is marked with a high drainage density indicating active stream dissection

resulting in deeply incised ravines with numerous mesas and outliers scattered on the plains to the east.

The drainage pattern in the area is dominated by the Sokoto River which flows southwards to join the River Niger. The main tributary of the Sokoto River is the Rima River, which joins it near Wamako. Usually, towards the end of the dry season, these rivers are almost completely dry. During the rains and early part of the dry season, springs are very common, but most of them dry up during the greater part of the dry season. There are very few lakes of importance in the northwestern Nigeria sedimentary basin. The three most important lakes are the Kalmayo, Kware and the Bodinga lakes.

1.7 Previous Geophysical Studies in the Study Area

The Geological Survey of Nigeria had since the 1930s carried out electrical resistivity, electromagnetic, and seismic refraction surveys in different parts of the basin. Some of these were done in collaboration with foreign governmental agencies such as the United States Agency for International Development (USAID) and recently the Japan International Cooperation Agency (JICA), to mention a few. The surveys are aimed at studying the aquifers of the basin with a view to selecting favorable sites for groundwater boreholes. The results of some of these surveys have been published either as Geological Survey of Nigeria Bulletins or as special publications (Raeburn and Tattam, 1965., Jones, 1948., Oteze, 1976., and JICA, 1989). The more recent surveys by the GSN have however remained largely unpublished. Unfortunately, none of

the numerous boreholes scattered over the basin is known to have reached the basement, and as such, depth to basement estimates have been by extrapolations.

The first comprehensive geophysical investigations in the region was the aeromagnetic mapping which was part of the nation wide airborne geophysical series carried out for the Geological Survey of Nigeria (GSN). Flying was completed in 1975, and contour maps of total magnetic field intensity were produced in 1976 on a large scale of 1:100,000 in half degree sheets for the Sokoto Basin area.

Ananaba (1983) carried out a reconnaissance remote sensing study over the entire area of the country north of 8^0 latitude using LANDSAT images. From the mosaic of LANDSAT images he compiled and analyzed two major indicator maps namely: drainage map and lineament map. The lineaments mapped were however not classified as faults, joints etc. and as such the LANDSAT study would require ground geological and geophysical follow up. A lineament density map was also compiled and on comparison with primary mineral map of Nigeria, revealed some remarkable correlation between the areas of high lineament density and areas of known primary mineral occurrence (Ananaba and Ajakaiye, 1987).

Uwah (1984) carried out a ground follow up radiometric survey of some radiometric anomalies delineated from the LANDSAT study mentioned above. This was confined to three locations with a total area of about 1 km^2 in the vicinity of

Dange village. These locations were considered to have the highest possibility of uranium mineralization in the Sokoto Basin. These high activity areas were observed to coincide with sedimentary sections with exposed compacted lateritic ironstones. The study concluded that the measured uranium concentrations were lower than the level normally regarded to be of economic importance.

Gravity measurements have been carried out on some major roads in this area between 1981 and 1982. In addition, there has been two other published accounts of gravimeter measurements in this area. Osazuwa (1985) established a primary gravity network for Nigeria of which five base stations were located in the basin.

Recently, Umego (1990) carried out a gravity survey over parts of the basin complemented by the analysis of aeromagnetic data over the basin area. He observed that the area shows an alignment of three linear belts of anomalous magnetic intensities. From the magnetic data, he produced the first depth to basement map of the basin using the Werner Deconvolution technique. The map reveals a generally shallow basement surface which dips gently towards the northwestern border with Niger Republic. The depth estimates are accurate to within 14 percent and this sets an upper limit of approximately 2.0 km as the maximum depth to the magnetic basement beneath the sediments in Sokoto Basin.

Ahmadu Bello University

magnetic analysis, Umego noted a significant difference in depth to basement estimates from both methods, the magnetic depth estimates being generally larger. For example, the maximum depth estimated by the gravity method was 1.0 km at one of the depressions while the magnetic method yielded a value of 1.4 km at the same location. At another location, comparisons showed estimates of 0.8 km and 1.6 km for the gravity and magnetic methods respectively. Several factors were suggested as being responsible for these differences. These include errors in density values for the gravity interpretation, the quality of the magnetic data which has been considerably filtered by contouring and redigitizing processes, differences in the geologic and magnetic basement, and the basic assumption of the Werner Deconvolution technique.

Sambo (1994) carried out an interpretation of the aeromagnetic anomalies over the Sokoto Basin by employing techniques based on spectral analysis. The results suggest the existence of two main source depths in the depth range considered under the area. The deeper source depth lies at a depth that varies between 0.3 km near the boundary with the basement complex and 1.85 km at the center of the basin. These deeper sources which represent the low frequency components of the spectrum are considered to reflect the depth to the basement. The shallow magnetic horizon represented by the high frequency components indicate either the near surface contributions or the noise effects.

472365

Sambo produced a generalized depth to magnetic basement

map from the depth results over the area. The map reveals generally a shallow basement surface deepest at the centre of the study area and decrease gradually towards the eastern and western boundaries. Also the depth to basement map reveals that the basement rocks in this region must have undergone at least two tectonic events which has resulted in the N-S structural features. The depth estimates according to Sambo (1994) are accurate to within 10% and this sets an upper limit of 1.85 km as the maximum depth to the magnetic basement in the Sokoto Basin.

1.8 Scope and Objectives of the Study

The present study involves statistical techniques, namely: the crosscorrelation function and spectral analysis of the aeromagnetic data from the Sokoto Basin. Before these analysis were carried out, the total magnetic field map was compiled and interpreted qualitatively. The total field map was further separated into the residual and regional components and interpreted. A study of the second vertical derivative map computed from the residual field of the area was carried out to enhance the identification of possible faults and faulted contacts between the different units and further correlate the magnetic field with the geologic units.

A two-dimensional analysis of the crosscorrelation function of the total field of the area under investigation was carried out. This aspect of the study was used to determine quantitatively the direction of the main trend of structures in the area.

KASHIM IBRAHIM LIBRARY

A two-dimensional spectral analysis of the residual field based on Fedi, et al. (1997) modification which is an improved version of the Spector and Grant (1970) method was carried out for the entire area. The objective was to determine the depth to the magnetic basement and also to investigate the lateral variation in the sedimentary thickness and structure under the basin.

CHAPTER TWO

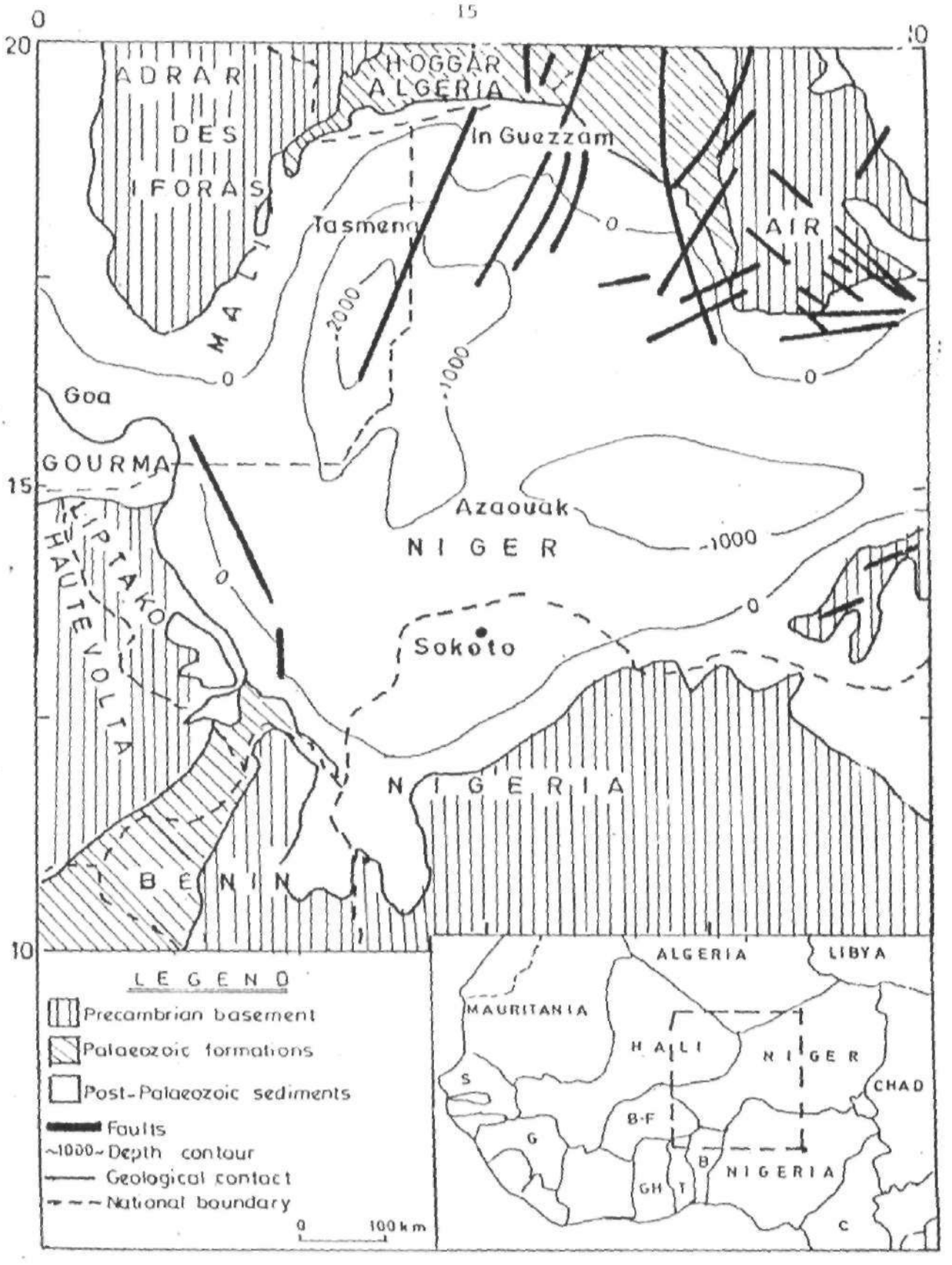
DETAILED GEOLOGY OF THE STUDY AREA

2.1 Introduction

The Sokoto Basin of Nigeria forms the southeastern sector of the Iullemmeden Basin - one of the young (mesozoic - tertiary) inland cratonic sedimentary basins of West Africa. The entire basin is believed to have developed by tectonic epeirogenic movements or stretching and rifting of tectonically stabilized crust during the Paleozoic (Kogbe, 1981 and Wright et al., 1985). Figure 2.1 shows the structural map of the Iullemmeden Basin and the position of Sokoto Basin while Figure 2.2 is a simplified geological map of Nigeria showing the boundary of the study area.

The geology of the sediments of the Sokoto Basin of northwestern Nigeria fits neatly into three major depositional episodes. The first episode occured during a continental period when the deposits of the Gundumi and Illo Formations were deposited unconformably on the Precambrian basement complex of migmatites, gneisses and metasediments. Northwestern Nigeria was part of an uplifted continental land mass far from the limits of the southern and northern seas.

The second episode began with the Maastrichtian trans-gression when the sea moved northwards from the Gulf of



Fig·2·1 :Structural map of the Iullemmeden Basin (After Kogbe, 1981)

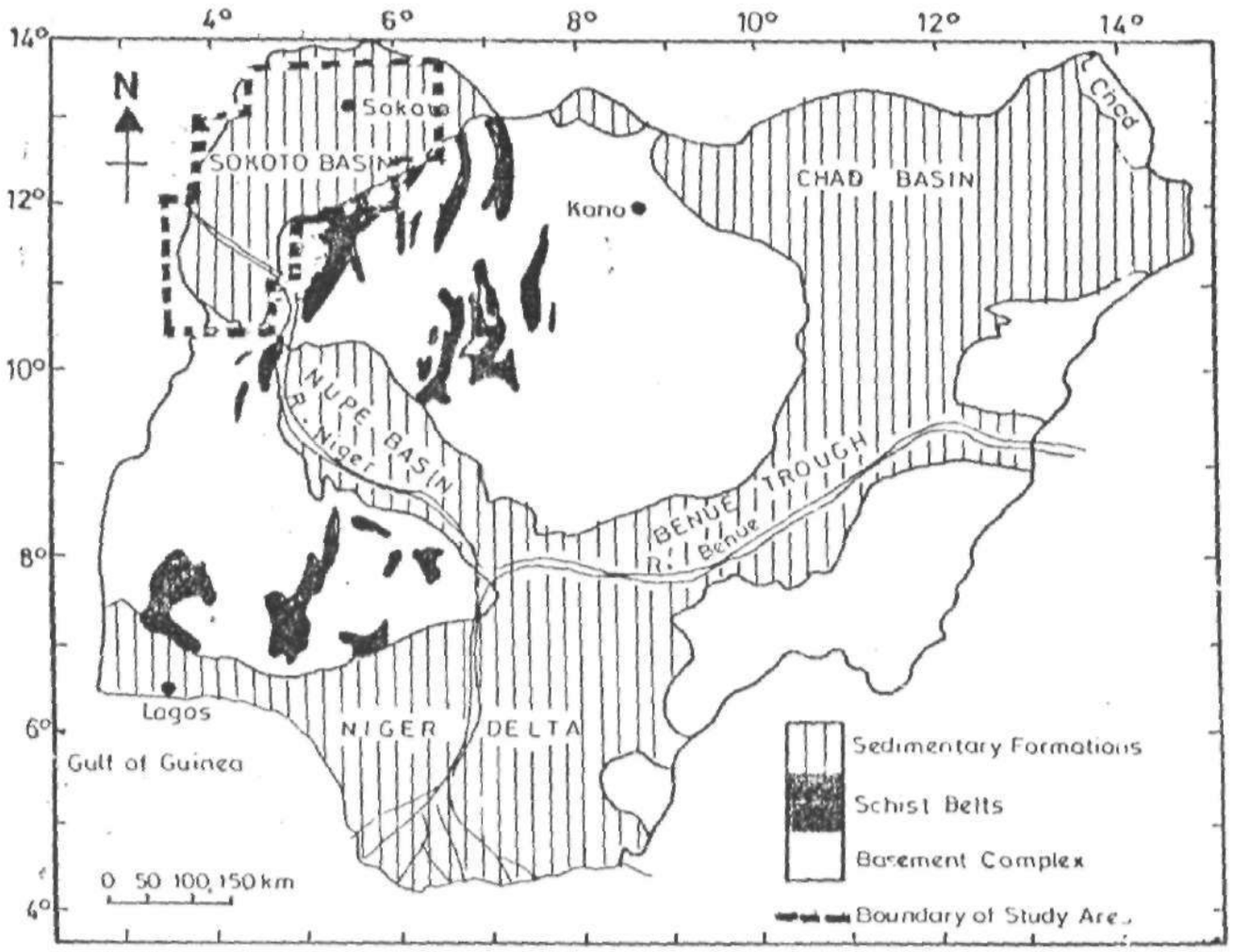


Fig.2-2 : Simplified geological map of Nigeria showing boundary of the study area

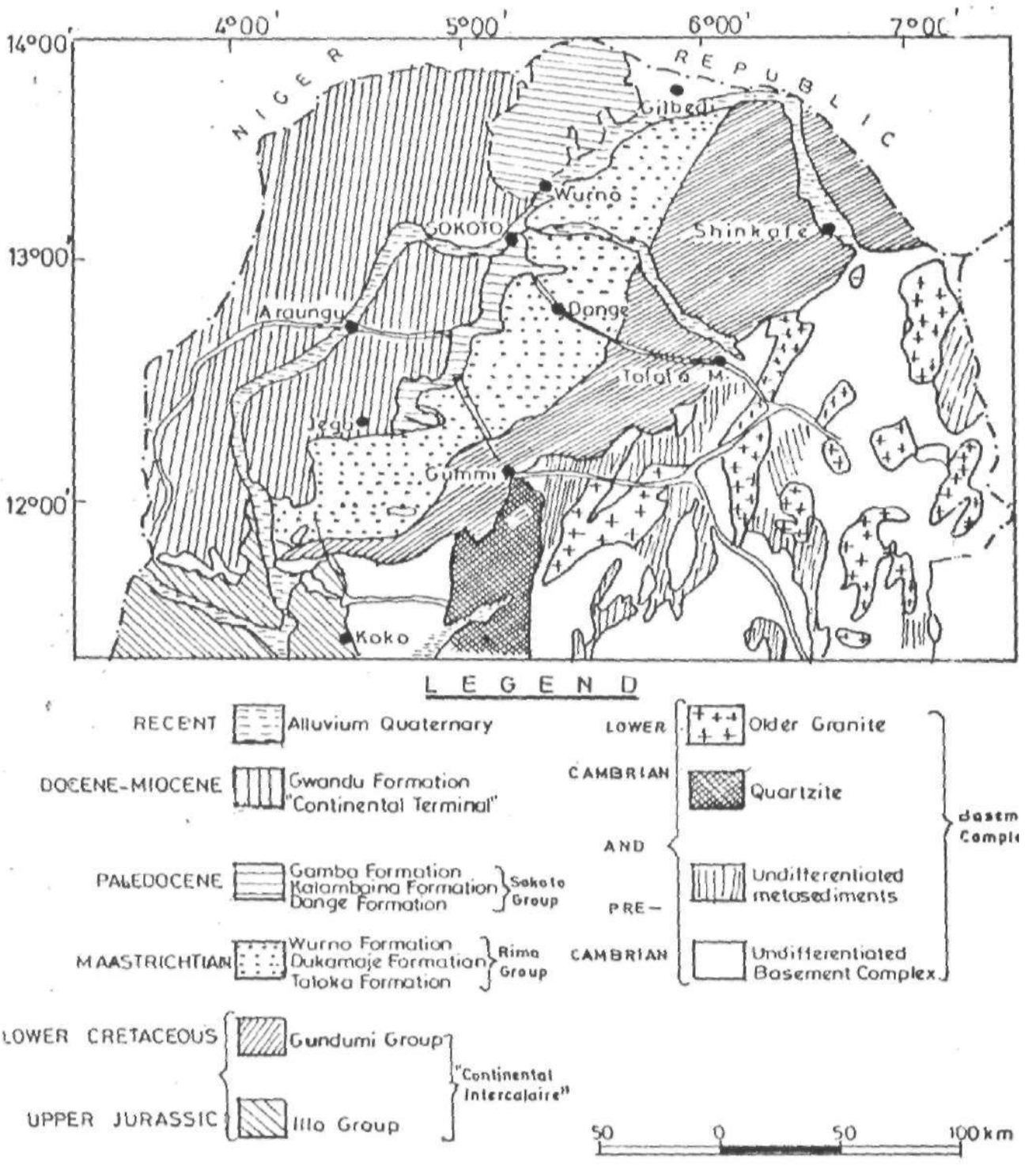
Guinea through the Mid-Niger Basin and southward from the Mediterranean through the Sahara. This transgression continued into the Paleocene. The Rima Group (Maastrichtian) and the Sokoto Group (Paleocene) were deposited during this period.

The third and final episode began during the early Eocene with the regression of the sea. Continental conditions prevailed again and continued till the present day. The Gwandu Formation of Eocene to Miocene age was laid down during this final episode. Figures 2.3 shows the geological map of the Sokoto Basin (Kogbe, 1981) and Table 2.1 shows the geological sequence in the Sokoto Basin.

2.2 The Basement Complex

The entire basin is underlain by the Basement Complex which includes all rocks older than the late Proterozoic (Mc Curry, 1976). The Nigerian Basement Complex lies within the Pan-African Mobile belt of West Africa and is believed to have a polytecto-metamorphic nature (McCurry, 1976., and Grant, 1978) and consequent metamorphism, migmatization and gneissification have extensively modified the original rocks. Three major rock successions are distinguishable (Odeyemi, 1988) and these are:

(a) A polycyclic crystalline complex of migmatites and gneisses which are the dominant rocks. The evolution of this complex is believed to have started during the Liberian Orogeny (2,800 ± 200ma).



Fig·2·3 ::Geological map of the Sokoto Basin (After Kogbe, 1981)

Table 2.1: Geological Sequence in the Sokoto Basin

(after Kogbe, 1981)

Age	Formation	Group	Environment
Quaternary	Sandy drifts	-----	Continental
Eocene-Miocene	laterites	"Continental" Formation	Continental
	----------unconformity----------		
Late Paleocene	Primary Oolitic Ironstone Gamba Formation Kalambaina Formation Dange Formation	Sokoto Group	Marine
	----------unconformity----------		
Maastrichtian	Wurno Formation Dukamaje Formation Taloka Formation	Rima Group	brackish water with brief marine intercalation
	----------unconformity----------		
Late Jurassic to earliest Cretaceous	Illo and Gundumi Formations	"Continental intercalaire" brief marine	Continental
	----------major unconformity----------		
Precambrian	**Basement**	**Complex**	

(b) The metasediments and metavolcanics which form the approximately N-S trending schist belts. The period of initiation of the sedimentary process leading to the deposition of these successions had until recently been assigned solely to the Pan-African Orogeny (600 ± 200ma). Recent work by Ogezi (1977), Grant (1978), Ajibade and Wright (1988), among others however indicate that part of these sediments may have been formed in the Kibaran (1,100 ± 200ma) times.

(c) The older Granite series which belong to late tectonic granite and granodiorites mark the intrusive phase (700 ± 500ma) of the Pan-African Orogeny in Nigeria. These granitoids intrude both the migmatite-gneiss complex and the Schist belts variably and are widespread in other parts of the Nigerian Basement and the Pan-African Province of West Africa.

2.3 Pre-Maastrichtian Deposits

In the Sokoto Basin, the Pre-Maastrichtian sediments are of fluviatile and lacustrine origin. They belong to the Gundumi and Illo Formations which extend northwards into the Niger Republic, where they are known as Gres du Tegama. These sediments belong to the upper part of the Continental Intercalaire which comprises a group of poorly fossiliferous sediments covering a very extensive area, bounded on the west by the crystalline basement rocks of the Niger Republic, and on the east by the quaternary sands of the Chad Basin.

The Gundumi Formation lies unconformably on the basement and consists of basal conglomerates, and gravels with sand and varicolored clays. The type locality of the formation is at

Dutsin Dambo. It is a fluviolacustrine deposit, overlying the basement unconformably; the contact with the basement is conglomeratic. The lithology is predominantly false-bedded, massive, feldspathic, clayey grits, clays, pebbly sand and conglomeratic in places. At Dutsin Dambo, the Gundumi sediments are capped by a hard, brittle, ironstone with quartz grains angular to sub-angular. Structures reminiscent of primary and cross-beddings are prominent. Outcrops of the Gundumi Formation are rare.

Essentially, the Illo Formation consists of non-marine sediments. Grits generally form the basal parts of the sections, but the conglomeratic base known to overlie the basement unconformably is seen at Libba (Kogbe and Lemoigne, 1976). The grits are crossbedded, and in most cases pebbly with lenses of clay and bands of ironstones which show relics of primary structures conformably with the bedding. The nodular and pisolitic clays are mostly restricted to the topographically high areas generally occupying the summit of the hills. The pisolitic overlie the nodular clay in most outcrops and generally are not continuous. They cannot, as such, be traced for long distances.

2.3.1 The Basal Conglomerates

An almost complete sequence of the Illo Formation is observed on a low-lying hill north of Libba. The nature of the basal conglomerates is well displayed in the quarry at Libba, where they are well exposed and hardened towards the contact with the underlying basement (Kogbe, 1979). The conglomerates

are of the quartz pebble type. Texturally they consists of quartz pebbles, which are of various shapes-oval to sub-rounded to rounded out-line and strongly cemented together. The cement as revealed by chemical analysis, is calc-silicic, and is most likely derived from the eroded underlying granitic and metamorphic terrain of the basement complex. The mineral found in Libba Quarry, and later identified as tourmaline, seems to support this.

2.3.2 Lateritic Ironstones

Laterites or lateritic ironstones deserve some consideration, because they occur extensively. The ferruginous sandstones have a wide occurrence within the grits, and contain a notable proportion of iron ore, as is evident in the slag heaps from local smelting. Occurrence as capping which is more widespread than the interbedded type, may be interpreted as having formed by decomposition of the rocks, that is as insoluble products of weathering. This offers a possible mode of formation, as clays are poorly permeable. By virtue of their position in the stratigraphic sequence, they occupy the flat summit of the topographically high areas, where they are well exposed to the atmosphere.

2.4 Maastrichtian Deposits

The second phase in the depositional history of the northwestern Nigerian Basin began during the Maastrichtian, when the Rima Group was deposited unconformably on Pre-Maastrichtian continental beds. The type sections of the three maastrichtian formations are at Taloka, Dukamaje and Wurno

Formations. This unconformity is well exposed at Wurno. Five lithologies are recognized at the Taloka Formation in the following order downwards (Kogbe, 1979):

(a) Grey, clayey siltstone

(b) White-grey siltstone alternating with brown siltstone

(c) Siltstone, whitish-grey alternating with purple siltstone

(d) Shaly siltstone

(e) Reddish brown siltstone

The lowest siltstone layer is reddish-brown, clayey, with some mudstone and poorly consolidated. This is overlain by the grey, light-brown shaly layer, which is semi-consolidated with some mudstone intercalations.

The Dukamaje Formation consists predominantly of shales with some limestones and mudstones. The shales contain numerous fragments of vertebrae and limb bones. A bone bed very richly fossiliferous lies near the base. Excellent exposures of the formation can be observed, and the most southerly exposure is at Wurno in a small outcrop near the village bordering the Dange Scarp. The Dukamaje Formation overlies the Taloka Formation conformably through the bone-bed with a sharp contact. The bone-bed is an excellent marker horizon in the field and was used as the index horizon for mapping at Taloka (Kogbe, 1972).

The Wurno Formation is very similar to the Taloka Formation already described. The sediments consist of pale colored, friable, fine-grained, sandstones, siltstones and intercalated mudstones. In boreholes, the sediments are dark in color due to the presence of carbonaceous material and finely divided iron sulphides. The loosely consolidated nature of the sediments make them very easily susceptible to weathering. The fine-grained, loosely cemented sandstones, siltstones and mudstones of the Wurno Formation are overlain unconformably by the Paleocene limestones, shales, clay-shales and calcareous shales of the Dange Formation.

2.5 Paleocene Deposits

This group consists of three formations, namely: Dange (oldest), Kalambaina and Gamba Formations.

The Dange Formation was erroneously dated as Eocene, but this error has been corrected by recent workers, and Paleocene age is now generally accepted for the Dange formation (Reyment, 1965., Kogbe, 1970). The formation consists of clayshales within bands of intercalated limestones near the base. The shales include bands of fibrous gypsum, plus a large number of irregularly shaped phosphatic nodules, which were probably derived from the abundant vertebrate fossil remains in formation. It is noteworthy that unlike the Dukamaje Formation with a distinct bone-bed at the base, the Dange Formation has no bone-bed. Although it is very richly fossiliferous, the vertebrate fossils are not concentrated in a particular horizon, but occur at random throughout the formation.

The Kalambaina Formation consists of a white marine, clayey limestone and shale. The type section of the formation is at the Quarry of the Cement Factory of Northern Nigeria. The thickness of the formation is quite variable, because of the subsurface dissolution of the limestone. The formation is rich in invertebrate fossils; mainly echinoids, corals, nautilus, lamellibranch and gastropods. Foraminifera and ostracods have been described from the formation (Reyment, 1965 and Peters, 1976).

The Gamba Formation consists of grey laminated shale overlying the calcareous Kalambaina Formation. The shale appears to be folded due to the removal by solution of the underlying beds. Except when overlain by the Gwandu Formation, the formation is covered by a mantle of loose sand and laterite. The type locality is at Gamba village near Sokoto while the type section is the Quarry of the Cement Factory of Northern Nigeria. (Kogbe, 1972).

The Continental Terminal is represented in the Sokoto Basin by the Gwandu Formation. Throughout the sedimentary basin, the tertiary marine sediments of the Sokoto Group are overlain disconformably by a thick series of deposits consisting predominantly of red and mottled massive clays, with sand stone intercalations. These sediments belong to the Gwandu Formation, with the type section and type area in the Gwandu Emirate. Rock exposures are rare on the plain, but numerous on the hillsides.

2.6 Faults and Folds

The Basement Complex and its supracrustal cover of Younger Metasediments of the Sokoto Basin were subjected to two phases of tight isoclinal folding during the Pan-African, which are responsible for the N-S trend common over much of Nigeria (McCurry, 1976). A series of transcurrent faults have been observed to affect the basement rocks adjoining the basin.

Wright (1968) and Ball (1980) have both identified a system of NE-SW and NW-SE conjugate pair of fractures which exist everywhere within the Pan African Mobile Belt. Wright (1976) suggested that these fracture system represent important lines of weakness in the continental crust and could be loci of economic mineralization. Ball (1980) attributes this conjugate strike-slip system to brittle deformation during the latter part of the Pan African Orogeny. The sediments in the basin were not subjected to any remarkable degree of faulting as only some WSW-ENE trending faults have been observed in the vicinities of Dange and Gilbedi villages (Kogbe, 1981).

2.7 Economic Geology

The most important economic minerals in the basin are the industrial minerals consisting of clays, ironstones and laterites, gypsum, limestone and gravels. Other minerals include lignite, radioactive minerals and salts. The latter minerals have been discovered only in small amounts and have no immediate economic application. Nevertheless, with the development of the economy and further exploration, coupled with advancement in mining, these minerals may prove to be of

interest; particularly when the more accessible occurrences are exhausted.

Clay deposits are abundant in the basin. A section of kaolinitic clay is found in the Illo, Dange, Kalambaina and Gwandu Formations. It could, however be possible to exploit most of the Illo and Gwandu Formation clays as the basic raw materials for a ceramic industry, whereas the clays or shales of the Sokoto Group of sediments are already being utilized in the Sokoto Cement Factory.

Two horizons of gypsiferous shales are known in the Sokoto Basin in the Dukamaje and Dange Formations. The presence of gypsum in shales of the Rima Valley was first reported by Falconer (1911) who assigned the whole sediments to the Eocene. In recent years, the establishment of a cement factory both in Malbaza (Niger Republic) and in Sokoto has produced a market for local gypsum, which is extracted in the form of local pitting by the inhabitants of the Rima Valley Heaps of iron slag are found in various parts of the basin. They indicate the existence of a smelting industry which has now been abandoned.

The fact that more than 90 % of the total road mileage in Nigeria consist of earth gravel roads, confirms the economic significance of the lateritic ironstones and ferruginised sandstones as construction materials in the country. Limestone is found in the Dukamaje, Dange and Kalambaina Formations. The limestone of the Kalambaina Formation was investigated by the Geological Survey of Nigeria (Jones, 1948) and a reserve of

over 100 million tons were assessed. The limestone is at present exploited by the Cement Company of Northern Nigeria.

CHAPTER THREE

DATA SOURCE AND PREPARATION

3.1 Introduction

Digital aeromagnetic data over the area of study was obtained from twenty half degree by half degree aeromagnetic map sheets of the Geological Survey of Nigeria (GSN) survey series (Umego, 1990). The nominal flight altitude was 152.3 m above terrain while the nominal flight line spacing and tie line spacings were 2 km and 20 km respectively.

A two-dimensional interpolation of the data was carried out to obtain data points on a regular grid for further analysis. The data was then interpolated on 51 X 51 grid obtaining 2601 equally spaced data points for each map. These maps were later merged to give the supermaps of the study area.

3.2 Regional-Residual Separation

There are two general types of magnetic anomalies present in any total field intensity map, namely; regional and residual anomalies. The regional field is of considerable magnetic relief. This component of the observed field changes systematically, resulting in a smooth surface. It is the component of the field with a low curvature or that which occupies the low frequency end of the field spectrum. From normal considerations of magnetization of basement rocks, it can be shown that the regional component must be caused in large part, by variations of magnetization within the basement. The residual field on the other hand may change in an irregular

or non systematic way, resulting in small highs and lows. This component could be due to smaller magnetization contrasts within the basement or to relief of the basement surface. Obviously, there is a great amount of uncertainty, as there is no clear-cut distinction between the two types of anomalies, particularly in the intermediate types (Nettleton, 1954).

In effect, the total field map is split into two parts, the regional and the residual field maps. The residual focuses attention on stronger features of small internal extent which are obscured by strong regional effects in the original map while the regional is related to variations in magnetization within the basement. Whatever the cause of differentiation, it is essential that methods be made available for the separation of the smaller anomalies from the more prominent anomalies.

3.2.1 Polynomial Fitting Method

With the increasing speed and capacities of the present day computers, the hitherto complicated mathematical procedure of surface fitting has largely become a routine operation. Polynomial fitting is a purely analytical method in which matching of the regional by a polynomial surface of low order exposes the residual features as random errors. This method is highly flexible and can be applied to both regularly and irregularly spaced data. A common practice in polynomial fitting is to use the least-squares technique (Oldham and Sutherland, 1955; Grant, 1957; Skeels, 1967; Dobrin, 1976).

This method presupposes that the residual field has a

normal Gaussian distribution. However, in field data many points do not fit this presumed Gaussian model. These deviatory field points cause a distortion of the regional field fitted to the data by the least squares method (Ojo and Kangkolo, 1997). In this study, the influence of the deviatory field points was suppressed by using robust estimation.

The expression for the regional surface over the study area is given by:

$$T = 7882.667 - 20.22722X - 13.26797Y$$

where T is the total magnetic field in nanotesla (nT), X and Y are the coordinates of the grid in kilometers (km) which describe the position of the data points with respect to the origin of the two axis of the data array. A value of 25000 nT must be added to all map data to obtain the actual total field values.

The estimated regional component was then subtracted from the measured field values to obtain the residual component which was then subjected to further analysis.

3.3 The Second Vertical Derivative

The second vertical derivative of the field was calculated from the residual magnetic field of the study area. Because of their resolving power, second vertical derivatives are useful in interpreting magnetic anomalies. There are many formulas published for the application of this procedure, but it is well

known that the results are essentially dependent upon grid size rather than the particular formula selected (Henderson and Zietz 1949)

The second vertical derivative function measures the curvature of the magnetic field and emphasizes the effects of sharp local anomalies at the expense of the broader regional features. The effect of near surface structures are more sensitive to abrupt changes, the anomalies of such structures are more enhanced by this function than those deep seated structures which usually have smoothly varying effects on the surface and hence less curvature. This property of the second vertical derivative is therefore used in delineating geologic boundaries especially in areas of surface cover.

Because of its high resolution, Vacquier et al., (1951) used second derivatives in conjunction with prismatic models to estimate depths to the basement from total intensity anomalies. Second vertical derivatives disclose more prominently the presence of magnetic rocks in sediments than is possible with the observed field (Henderson and Zietz 1949).

These derivatives are also useful in the analytical continuation of magnetic fields towards sources, although such uses are limited in accuracy both the data and the method of computing.

3.3.1 Basic Mathematical Theory of the Second Vertical Derivative

The use of the second vertical derivative can be understood by noting that the magnetic potential (V) satisfies Laplace's equation in the space above the earth's surface. Suppose ΔV is the anomaly in the magnetic potential, at all points of free space it satisfies the Laplace's equation:

$$\nabla^2(\Delta V) = 0 \qquad \ldots\ldots\ldots\ldots\ldots\ldots\ldots \qquad (3.1)$$

The component of the total-intensity anomaly ΔT in the direction of the earth's normal field (assumed invariant over the area) is given by:

$$\Delta T = \frac{\partial(\Delta V)}{\partial t} \qquad \ldots\ldots\ldots\ldots\ldots\ldots\ldots\ldots\ldots \qquad (3.2)$$

where t is the unit vector in the direction of the earth's undisturbed field. The equation (3.2) is valid as long as $\Delta T << T_o$ where T_o is the magnitude of the total field. Operating on each side of equation (3.2) with

$$\nabla^2 \equiv \frac{\partial^2}{\partial x^2} + \frac{\partial^2}{\partial y^2} + \frac{\partial^2}{\partial z^2} \qquad \ldots\ldots\ldots\ldots\ldots\ldots\ldots \qquad (3.3)$$

in consequence of equation (3.1) we have

$$\nabla^2(\Delta T) = \frac{\partial^2(\Delta T)}{\partial x^2} + \frac{\partial^2(\Delta T)}{\partial y^2} + \frac{\partial^2(\Delta T)}{\partial z^2} = 0 \qquad \ldots\ldots\ldots\ldots\ldots \qquad (3.4)$$

Therefore ΔT, on the bases assumed, satisfies the Laplaces equation.

By expressing equation (3.3) in the form of equation (3.4)

$$\frac{\partial^2(\Delta T)}{\partial Z^2} = -\left(\frac{\partial^2(\Delta T)}{\partial X^2} + \frac{\partial^2(\Delta T)}{\partial Y^2}\right) \qquad \ldots\ldots\ldots\ldots\ldots\ldots \quad (3.5)$$

it is seen that the second vertical derivative (left-hand side) is a measure of the curvature of the field.

CHAPTER FOUR

THEORITICAL BACKGROUND OF QUANTITATIVE TECHNIQUES USED

4.1 Introduction

Attempts have been made in the past to obtain significant trends of mapped data. Affleck (1963) carried out a statistical study on selected portions of magnetic data for trend determination. However, his method of trend determination was arbitrary and subject to individual bias. Hall (1964) carried out similar trend analysis and in his study, he analyzed various magnetic profiles by means of one-dimensional autocorrelation and crosscorrelation functions. Horton et al. (1964) determined trends with a two-dimensional autocorrelation function. The dominant trends obtained in their analysis were clearly observed, but the interpretation of the connecting positive and negative features was ambiguous, since these are derived by joining the positive or negative values in one quadrant with their symmetrical values in the other quadrants. Kangkolo (1996) used the crosscorrelation function as done in this study to determine the main trend of structures over the Mamfe Basin of Nigeria and Cameroon.

4.2 Crosscorrelation Function Technique

For a more automated trend analysis of magnetic data, the crosscorrelation function is used (Agarwal and Kanasewich, 1971). The crosscorrelation function is a measure of the similarity between two different sets of sampled data. One set of sampled data is displaced by varying amounts relative to the other and corresponding values of the two sets are multiplied

together and the products summed to give the value of the crosscorrelation (Sheriff and Geldart, 1983). The crosscorrelation of the field in different but overlapping areas is calculated.

The crosscorrelation coefficients C_{rs} for two sets of sampled data X and Y is given by:

$$C_{r,s} = \frac{\frac{N^2}{(N-r)(N-s)} \sum_{j=0}^{N-r-1} \sum_{k=0}^{N-s-1} X_{j,k} Y_{j+r,k+s}}{\sqrt{\sum_{j=0}^{N-1} \sum_{k=0}^{N-1} X^2_{j,k} \sum_{j=0}^{N-1} \sum_{k=0}^{N-1} Y^2_{j,k}}} \quad \ldots\ldots\ldots\ldots \quad (4.1)$$

where $X_{j,k}$, $Y_{j,k}$ are two sets of sampled data, N is the total number of data points on each sample set,

r,s = 0, $\pm$1, $\pm$2, ..., $\pm$m; and m = maximum lag

The crosscorrelation is obtained with two different sets of sampled data. The same matrix of values have been used for both functions, except that one of them is modified by surrounding the core with a null field. Let $X_{j,k}$ be the sampled values for a two-dimensional function and let $Y_{j,k}$ be chosen in such a way that

$$Y_{j,k} = X_{j,k} \quad \text{for } j \text{ , } k \leq n' \quad (n' \leq n)$$

$$= 0 \quad \text{otherwise} \qquad \ldots\ldots\ldots\ldots \quad (4.2)$$

where the positive integers n' and n are defined as shown in Figure 4.1(a) with origin (0,0).

The magnetic field map is considered as consisting of a test map and a sample map. The sample map is defined as the N^2

complete set of values $X_{j,k}$ while the test map is defined as the N^2_H nonzero values of the central core of $Y_{j,k}$ as shown in Figure 4(b). The values on the test map are identical to the central core of data placed in $X_{j,k}$. The concept of introducing a null field all around $Y_{j,k}$ makes it possible to obtain the correlation coefficient for the sample set without limitations imposed by the symmetry properties of an auto-correlation function.

The number of nonzero multiplications and additions in each correlation coefficient is identical, because the test map is embedded in an infinite field of null values. Therefore, the factor N/(N-r)(N-s) is unnecessary, and indeed undesirable. On removing this factor, the $C_{r,s}$ values are given in the various (r,s) regions as follows:

- for positive r and positive s

$$C_{r,-s} = \frac{\sum_{i=1}^{N-r} \sum_{j=s+1}^{N} X_{i,j} Y_{i+r,j-s}}{\sqrt{\sum_{i=1}^{N} \sum_{j=1}^{N} X^2_{i,j} \sum_{i=1}^{N} \sum_{j=1}^{N} Y^2_{j,k}}} \quad \ldots\ldots\ldots\ldots\ldots \quad (4.3(c))$$

with r,s = 0, 1, 2, ... m

- for negative r and negative s

note that $C_{-r,-s} = C_{r,s}$ ..... (4.3(b))

with r,s = 0, 1, 2, ... m

- for positive r and negative s

$$C_{r,s} = \frac{\sum_{i=1}^{N-r} \sum_{j=1}^{N-s} X_{i,j} Y_{i+r,j+s}}{\sqrt{\sum_{i=1}^{N} \sum_{j=1}^{N} X^2_{j,k} \sum_{i=1}^{N} \sum_{j=1}^{N} Y^2_{j,k}}} \quad \ldots\ldots\ldots\ldots\ldots \quad (4.3(a))$$

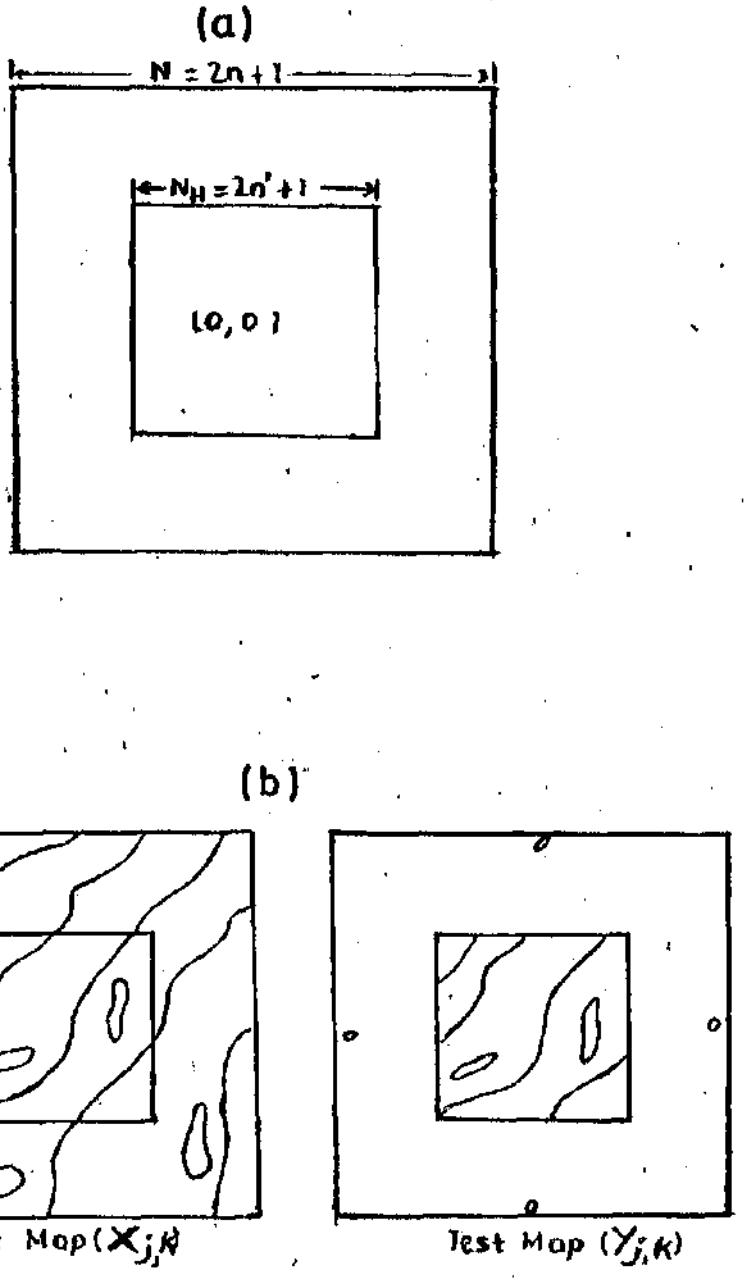


Fig.4.1: (a) Conventions for choosing $X_{j,k}$ from $Y_{j,k}$

(b) Schematic diagram from the sample sets $X_{j,k}$ and $Y_{j,k}$ used in the crosscorrelation technique

with r,s = 0, 1, 2,....., m

- for negative r and positive s

$$C_{-r,s} = \frac{\sum_{i=r+1}^{N} \sum_{j=1}^{N-s} X_{i,j} Y_{i-r,j+s}}{\sqrt{\sum_{i=1}^{N} \sum_{j=1}^{N} X^2_{i,j} \sum_{i=1}^{N} \sum_{j=1}^{N} Y^2_{i,j}}} \quad \ldots\ldots\ldots\ldots \quad (4.3(d))$$

with r,s = 0, 1, 2, ..., m.

Wherever the data sets are nearly the same, that is the data set has a high correlation, a large coefficient is obtained. When the data sets are unlike, some of the products will be positive and some negative and hence the coefficient will be small. Therefore a series of consecutive high coefficients should be indicative of a similar pattern which propagates in any direction in the original data. From the crosscorrelation coefficients, which vary systematically between +1 and -1 (or from -100 % to +100 %), it is possible to obtain the trend directions and an estimate of the average magnitude of the correlation over the sampled map.

4.3 Spectral Analysis Of Aromagnetic Fields

4.3.1 Introduction

Potential field data such as aeromagnetic data can be represented by one or two-dimensional Fourier series consisting of various frequencies which characterize the anomalies. The amplitude and phase relationship among these frequencies constitute what is known as a "complex line spectrum" (Negi et al., 1982). Spectral analysis is not unique to aeromagnetic

method alone but to other geophysical methods as well. As the computational power of digital computers has increased, so the range of problems, to which spectral analysis has been applied, has expanded. This technique is at present often used for the estimation of the depth of magnetic bodies in the earth's crust (e.g Bhattacharyya and Raychaudhuri, 1967; Naidu, 1970a; Spector and Grant, 1970; Garcia-Abdeslem and Ness, 1994; Fedi, et al. 1997).

4.3.2 Fast Fourier Analysis of Two-Dimensional Aeromagnetic Data

With the widespread introduction of the digital computers, fast Fourier analysis has become a standard technique for analyzing aeromagnetic data. The Fast Fourier Transform algorithm transforms a function into its Fourier components (amplitude, phase angles and frequencies). The main advantage of the transform is saving of computer time and storage capacity. It provides better accuracy than the standard Fourier transform. Using this algorithm, Naidu (1969), and many others have analyzed one or two-dimensional aeromagnetic data.

The residual total intensity values of a map can be represented by a double Fourier series expansion,

$$\Delta T_{x,y} = \sum_{n=0}^{N} \sum_{m=-M}^{M} P^{n}_{m} \cos\left[\left(\frac{2\pi}{L}\right)(nx+my)\right] + Q^{n}_{m} \sin\left[\left(\frac{2\pi}{L}\right)(nx+my)\right] \quad (4.4)$$

where L = length of the map in square form, P_n^m and Q_n^m = Fourier amplitudes and N,M are the number of grid points along

the x,y directions.

In order to represent the residual data in the above form, we have to obtain the two-dimensional Fourier transform of the data. The Fourier transform of two-dimensional data is obtained by first Fourier transforming columns (or rows) and next rows (or columns) (Naidu, 1970b). This can be shown as follows:

$$X(u,v) = \sum_{m=0}^{M} \sum_{n=0}^{N} X(m,n) \exp(-i(um+vn))$$

$$= \sum_{m=0}^{M} [\sum_{n=0}^{N} \exp(-ivn)] \exp(-ium)$$

$$= \sum_{m=0}^{M} X(m,n) \exp(-ium) \qquad \ldots\ldots\ldots\ldots\ldots \qquad (4.5)$$

where X(m,v) is a Fourier transform of the mth column and M,N are the dimensions of the data matrix. The normalized power or energy spectrum of the two-dimensional aeromagnetic data is;

$$S(u,v) = \frac{1}{NxM} |X(u,v)|^2 \qquad \ldots\ldots\ldots\ldots\ldots\ldots \qquad (4.6)$$

In general, and for this study in particular, M = N. The number of sample points is chosen according to the relation $N = 2^k$, for Fast Fourier Transform (FFT) analysis, where k is an integer constant. Since the FFT requires the input data in complex form, we have to place zeros in the imaginary part with

real data.

4.3.3 Data Treatment

Spectral analysis of aeromagnetic data involves the consideration of some pertinent problems that must be overcome or reduced in order to enable the retrieval of a true spectrum for interpretation. Some of these problems include the approximate depth to the magnetic sources of interest, the flight line spacing, the aliasing and truncation effects (Bath, 1974).

The digitization sampling interval Δt defines the highest resolvable frequency in the spectral calculation. This means that the shortest period which can be detected is $2\Delta t$, or that the highest resolvable frequency is $1/2\Delta t$. This frequency limit for the calculated spectrum is referred to as the Nyquist frequency or the folding frequency. The Nyquist frequency is the lowest frequency which is its own alias, that is the limit of both the sequence of frequencies and of the sequence of their aliases. The Nyquist frequency is equal to one-half the sampling frequency.

$$f_{nq} = \frac{1}{2}\,\frac{1}{\Delta t} \qquad \ldots\ldots\ldots\ldots\ldots\ldots\ldots \qquad (4.7)$$

where Δt = sampling frequency

Aliasing is a phenomenon which occurs when spectral components with frequencies higher than the Nyquist frequency contaminate spectral components with frequencies lower than the

Nyquist frequency. Aliasing implies naturally a falsification of the spectrum of affected frequencies below the Nyquist frequency. Aliasing was effectively reduced by interpolating the data at small grid intervals in this study.

The longest wavelength for which the Fourier transform can be calculated is the total length of the map. But the spectrum of the map only contains depth information down to a depth of length/2π (Shuey et al., 1977). If the source bodies have bottoms deeper than the length of the map, the spectral peak occurs at a frequency lower than the fundamental frequency for the map and cannot be resolved by spectral analysis.

The implication of using a finite data window in spectral analysis is that a true spectrum cannot be recovered from the data because of the truncation effects. Truncation effects result in the amplitude and phase characteristics of the resulting spectrum being distorted. The shape of the data window determines the degree of distortion in the computed spectrum. The rectangular time window and the corresponding spectral window are shown in Figure 4.2(a).

The data window in the frequency domain has the effect of broadening spectral lines and introducing a series of spurious peaks called side lobes. This is highly undesirable particularly in the neighborhood of a spectral peak (Naidu, 1969). Bingham et al. (1967) suggested a way of reducing the ill effect of side lobes. This requires the usage of a window function which does not abruptly go to zero. However this

results in a wider main lobe instead of the expected high concentration to the central (main) lobe and small or insignificant side lobes. To keep the spectral distortion close to a minimum, the cosine-tapered rectangular window was used in this study. This data window remains fairly flat but tapers off near the two ends of the record (see Figure 4.2(b)). The tapering eliminates the high frequencies erroneously introduced by the sharp truncation in the rectangular data window.

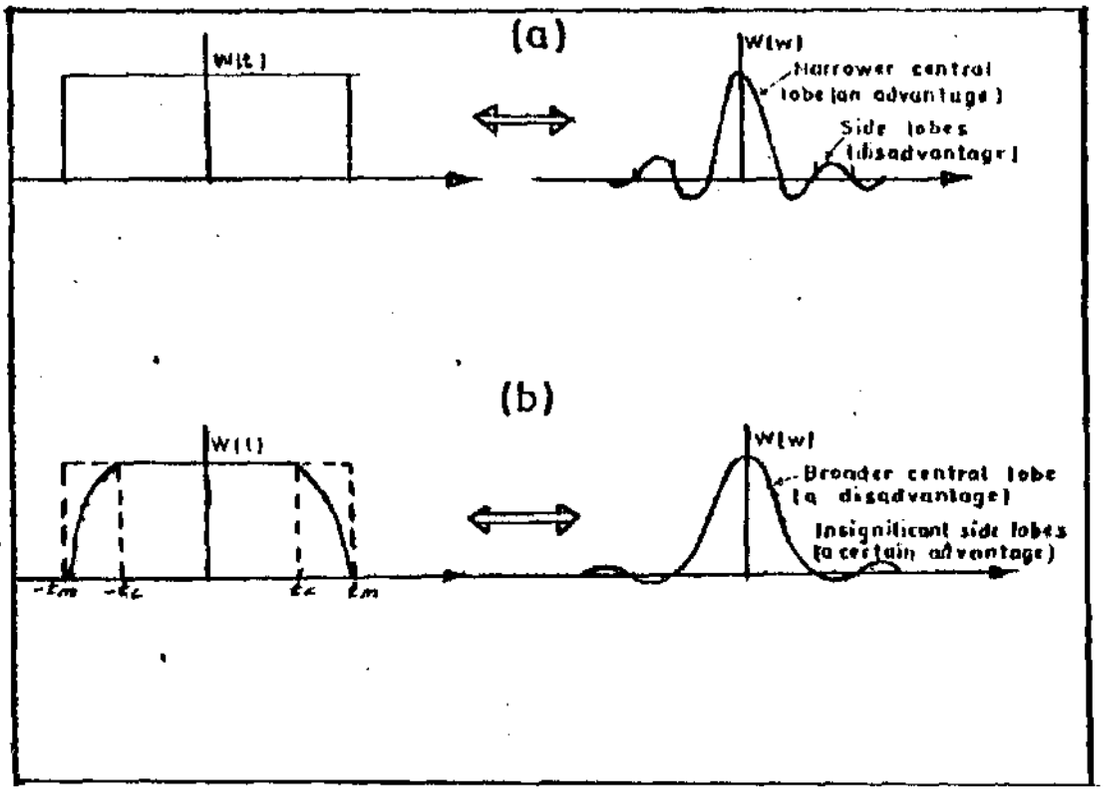


Fig.4.2: (a) Rectangular data window and the corresponding spectral window

(b) A cosine-bell data window and the corresponding spectral window

An excellent taper consists of a pair of cosine bells defined as follows (see Figure 4.2(b) above)

$$W_{(t)} = \frac{1}{2}\left[1 + \frac{\cos\pi\,(t_c - t)}{t_c - t_m}\right] \quad for\ -t_m \le t \le -t_c$$

$$= 1, \quad for\ -t_c \le t \le t_c$$

$$= \frac{1}{2}\left[1 + \frac{\cos\pi\,(t - t_c)}{t_m - t_c}\right], \quad for\ t_c < t < t_m \qquad \ldots\ldots\ldots\ldots (4.8)$$

The procedure for smoothing the shape of the data window through the application of the cosine taper was based on the basic formulas of equation (4.8) above.

4.3.4 An Improved Estimation of the Source Depth From Magnetic Spectra

The map of the magnetic field intensity over an area, after the removal of the main geomagnetic component, is assumed to consist of the superposition of a large number of individual anomalies which appear to be derived from block-type sources corresponding to various geological units. (Grant and West, 1965).

Spector and Grant (1970) considered an ensemble of rectangular, vertical-sided parallelepipeds, characterized by a joint uniform frequency distribution for the depth, width, length, depth extent, magnetization and direction cosines of the magnetization (L,M,N) and of the geomagnetic vector (l,m,n).

The spectral expression for a single parallelepiped (Bhattacharyya, 1966), in polar frequency coordinates is;

$$E_{1(\rho,\theta)} = \left(\frac{\mu_0}{2}\right)^2 K^2 \exp(-2h\rho)\,(1-\exp(-t\rho))^2 S^2(\rho,\theta)\,R^2_T(\theta)\,R^2_K(\theta) \quad (4.9)$$

μ_o = permeability of free space.

ρ = $(u^2 + v^2)$ magnitude of the frequency vector.

u and v are frequency components.

θ = tan u/v direction of the frequency vector.

k = magnetic moment per unit depth.

h = depth to the top of the prism.

S = factor for the horizontal size of the prism.

R_T = factor for geomagnetic field direction.

R_K = factor for magnetization direction of the prism.

Spector and Grant used the statistical mechanics postulate that the mathematical expectation of an ensemble power density function is equal to the ensemble average. The ensemble power spectrum at the magnetic pole (E) is;

$$E(\rho) = \left(\frac{\mu_0}{2}\right)^2 \bar{K}^2 C(\rho,\bar{a},\bar{b})\,T(\rho,\bar{t})\,H(\rho,\bar{h}) \quad \ldots\ldots\ldots\ldots \quad (4.10)$$

where $\bar{h}$, $\bar{a}$, $\bar{b}$, $\bar{t}$, $\bar{k}$, refer to the parameter average values of the ensemble and a and b are the average body dimensions. C is the azimuthal average.

$$C(\rho,\bar{a},\bar{b}) = \frac{1}{\pi}\int_0^{\pi} \langle S^2(\rho,\theta,a,b)\rangle d\theta \qquad \ldots\ldots\ldots\ldots \quad (4.11)$$

where $< S^2(\rho,\theta,a,b) >$ is the expected value of S^2 over the range of allowed widths and lengths, $< >$ is the expected value and

$$\bar{k}^2 = < k^2 > \qquad \ldots\ldots\ldots\ldots\ldots \quad (4.12)$$

$$T(\rho,\bar{t}) = \langle (1-\exp(-t\rho))^2 \rangle$$

$$= \frac{1-[(3-\exp(-2\bar{t}\rho)(1-\exp(-2\bar{t}\rho)]}{4t\rho} \qquad \ldots\ldots\ldots\ldots \quad (4.13)$$

$$H(\rho,\bar{h}) = \langle (\exp(-h\rho))^2 \rangle$$

$$= \exp(-2\bar{h}\rho)\,\frac{\sinh(2\rho\Delta h)}{2\rho\Delta h} \qquad \ldots\ldots\ldots\ldots \quad (4.14)$$

The depth factor for this ensemble of anomalies is practically equal to exp $(-2\bar{h}\rho)$ for depth variations $\Delta h < 0.5\,\bar{h}$, as suggested by Spector and Grant. The spectral factors $\bar{k}$, T, and C in equation (4.10) can be grouped conveniently into a single form as;

$$M = \bar{k}^2 TC \qquad \ldots\ldots\ldots\ldots\ldots\ldots\ldots \quad (4.15)$$

Hence equation (4.10) becomes;

$$E(\rho) = \left(\frac{\mu_0}{2}\right)^2 M(\rho,\bar{k},\bar{a},\bar{b},\bar{t})\,H(\rho,\bar{h}) \qquad \ldots\ldots\ldots\ldots \quad (4.16)$$

In most cases when $\bar{t}$, $\bar{a}$, and $\bar{b}$ are not too small, equation (4.16) is approximated as;

$$E(\rho) = (\frac{\mu_0}{2})^2 K^2 \rho^{-2.9} H(\rho, \bar{h}) \qquad \ldots\ldots\ldots\ldots \qquad (4.17)$$

at $\bar{h} = 0$, we find

$$E_0(\rho) \propto \rho \exp(-2.9) \qquad \ldots\ldots\ldots\ldots\ldots \qquad (4.18)$$

where 2.9 is the power law exponent.

Spector and Grant (1970) noted that the factor C in equation (4.15) increases the spectrum decay rate, and they infer for it an exponential form towards the larger wave numbers. Fedi et al. (1997) showed that the factor C has conversely a power law form as shown above. Consequently spectral depth estimation by the method of Spector and Grant, without spectral decay correction, consistently overestimates depths. To substantially improve our ability to estimate the depth $\bar{h}$ by the method of Spector and Grant, the power spectrum should be divided by the correcting factor $\rho^{2.9}$ before estimates of $\bar{h}$ could be taken.

To determine the depth, the logarithm of the energy values (In(E')) is plotted against frequency ρ (rad/km) on a linear scale, where $E' = E(\rho)\ \rho^{2.9}$ and $E(\rho)$ is the power spectrum. The linear segments of the plot groups points due to anomalies caused by bodies occurring within a particular depth. The mean depth of burial of the ensemble is given by;

$$\bar{h} = -\frac{M}{2} \qquad \ldots\ldots\ldots\ldots\ldots\ldots \qquad (4.19)$$

where M is the slope of the best fitting straight line through a reasonable number of points. When the frequency unit is in cycles per km, the corresponding relation will be;

$$\bar{h} = -\frac{M}{4\pi} \qquad \ldots\ldots\ldots\ldots\ldots\ldots\ldots\ldots \qquad (4.20)$$

CHAPTER FIVE

RESULTS AND INTERPRETATION

5.1 Introduction

The immediate purpose of magnetic surveys is to detect rocks or minerals possessing unusual magnetic properties, which reveal themselves by causing anomalies in the intensity of the earth's magnetic field. A magnetic map, in itself, is of little value unless it has been interpreted and used to discover geological structure. Generally, the interpretation can be divided into three basic groups, namely: qualitative analysis, profile analysis, and map analysis (Reford and Sumner, 1964).

Qualitative analysis involves a close study of magnetic contour map. This map is compared with the geological map of the same area and correlations and trends are noted. Magnetic maps show integrated magnetic effects of all bodies within several kilometers of the surface, but geological maps only show surface geology.

Profile analysis involves the estimation of parameters from magnetic data along profiles. In oil surveys, the basement depths are computed, in mineral surveys, susceptibilities and dips are more important. Susceptibility contrasts can be estimated from the anomaly magnitudes.

Map analysis involves the separation of total intensity map into regional and residual components, construction of vertical derivatives or curvature of the magnetic field. It

also permits the use of two-dimensional Fourier transform to obtain wave number spectrum; allows the use of digital filter theory to design and use high, low, and band pass filters for multiple analysis such as isolation of anomaly, downward and upward continuation.

5.2 Qualitative Interpretation

5.2.1 Total Field Magnetic Map

In the Sokoto Basin, the aeromagnetic anomalies consist of several short wavelength local anomalies superimposed upon larger and broader anomalies. The combined effect of these anomalies and the regional gradient of the geomagnetic field produce the observed total field map as seen in Figure 5.1. A value of 25,000 nT must be added to the values indicated on the contours to obtain the actual field values. The field values on the map range from 760 nT to 8010 nT.

Unfortunately, the individual contours and anomalies are too small to be distinguished due to the scale of reduction, but the pattern of anomalous zones is clear.

A critical study of the prominent magnetic anomalies manifested on the total field map can be considered in small groups numbered [1], [2], [3], [4], [5] and [6].

It is generally observed that the total field values are higher in the southwest section of the map. This could be due to the concentration of metamorphic and igneous rocks like quartzite and granite respectively with greater susceptibility

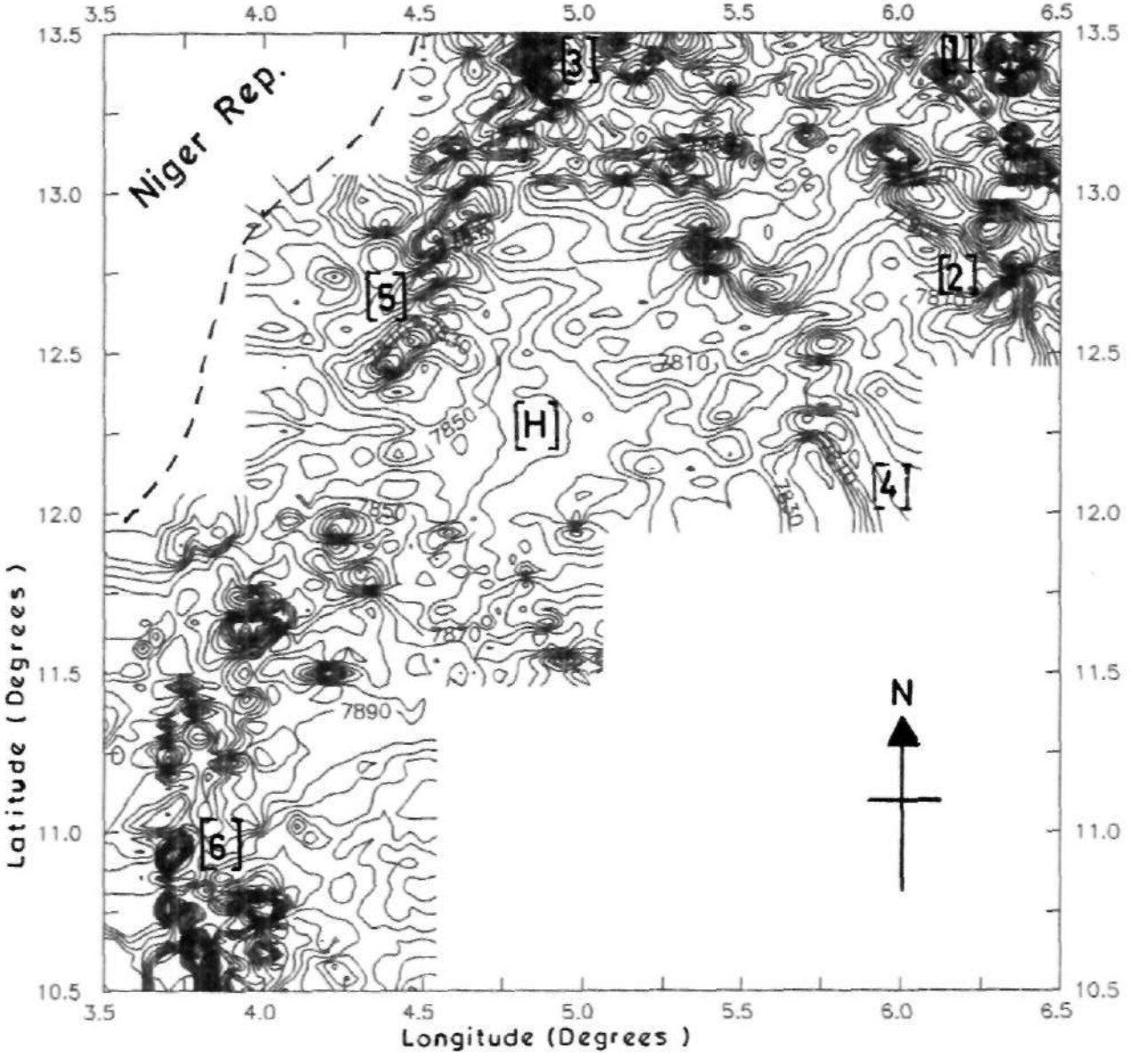


Fig 5.1: Total Field Magnetic Map of the Basin(Contour interval is 10nT)

ranges. The central portion of the total field map marked [H] has low amplitude long wavelength anomalies. The low gradient magnetic field evident over much of this region partly reflects the uniform magnetic properties of the underlying rocks in this area, probably within the crystalline Pre-Cambrian basement. It also confirms the fact that the magnetic sources are from deeply seated structures in this portion.

There are several magnetic highs and lows in the total field magnetic map which do not manifest any surface expression on the basin. Most of the anomalies are short wavelength with circular contours. The anomalies observed are largely due to extensive igneous intrusions probably buried at relatively shallow depths within the sediments or possibly to the presence of the shallow Pre-Cambrian basement rocks. This assertion is made because sedimentary rocks are usually so weakly magnetized and of such configuration that the do not produce anomalies of measurable size at normal distances between source and instrument for surveys of this type (Affleck, 1963).

5.2.2 Anomaly Alignments

A close observation of the total magnetic field map (Fig. 5.1) reveals the alignment of prominent anomaly groups in approximately three linear patterns as follows:
[1] and [2]; [3] and [4]; [3], [5] and [6].

The orientation of these linear patterns is conspicuous and respectively in the N-S direction, NW-SE direction, and

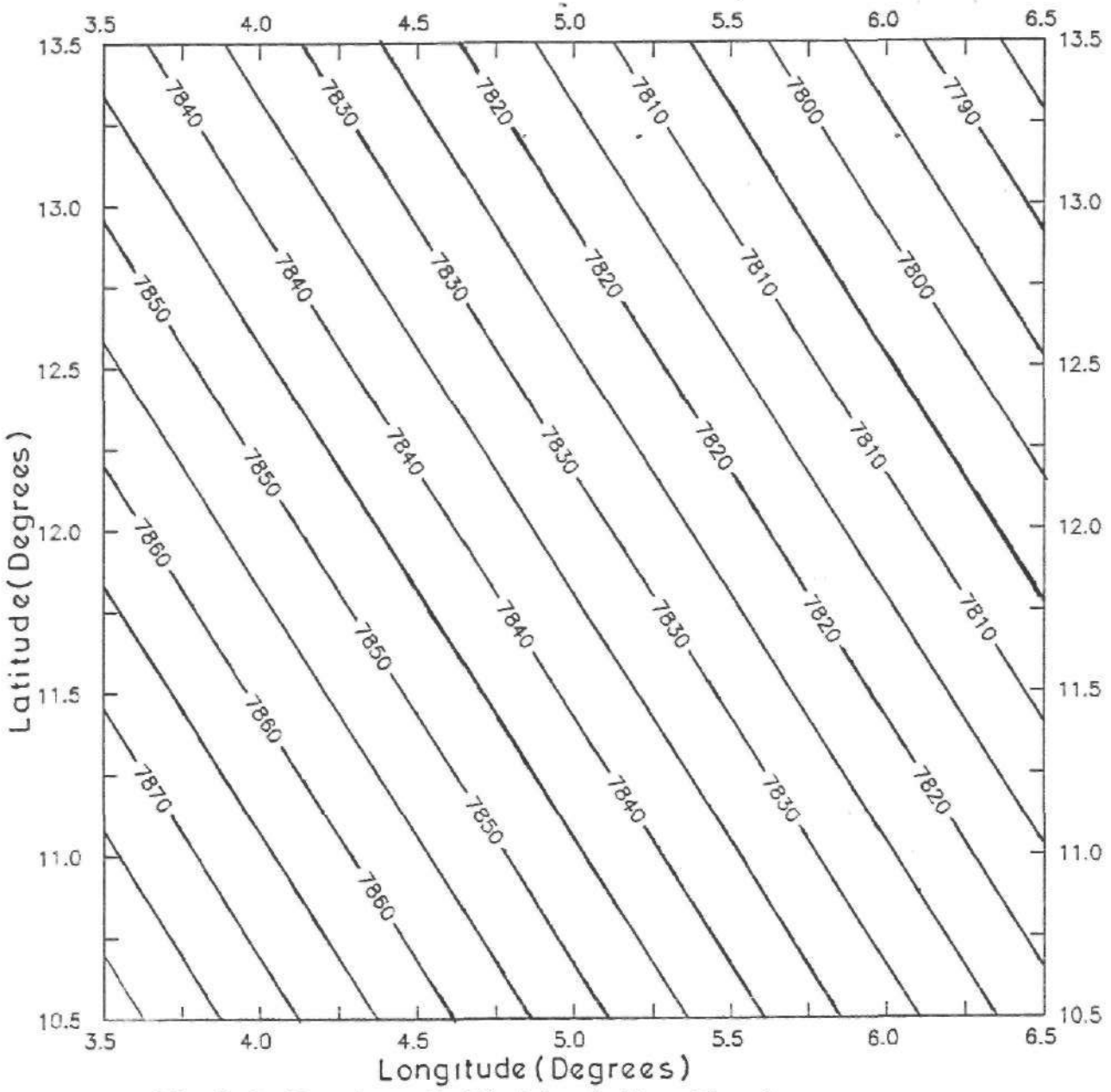
NNE-SSW direction. However, the anomaly alignment [3], [5] and [6] is not continuous at the central portion of the study area indicating a break in the subsurface magnetic structures. Generally, known fault and structural lineaments correlate closely with anomaly systems. It is suggested that the anomaly trend system is related to systematic tectonic lineaments which could be manifested as faults, fractures etc. These patterns fit with the orientation of some palaeostructures and lineament swarms in Nigeria and adjacent countries (Buser, 1966).

Figure 5.2 shows the regional magnetic field dipping in the NE-SW direction. The gradient of the field is 0.11nT/km. A possible explanation of the low gradient of the field is that the regional is due to fairly deep seated structures leading to fairly moderate variation of the regional field over the area.

5.3 The Residual Magnetic Map and Surface Geology

Residual maps are used extensively by geophysicists to bring into focus features which tend to be obscured by the broad features of the field. The residual field map shown in Figure 5.3 for the entire basin indicates mostly weak anomalies in the range of 10 nT to 60 nT and a few negative anomalies in the east of the central portion of the map. It is not surprising that there is no apparent correlation between the various sedimentary groups and the anomalies, as sediments are known to be non-magnetic. However, there is a magnetic low over the Dange Scarp which is the most prominent structural feature in the basin, centered around longitude 5.40^0 and latitude 12.80^0.

KASHIM IBRAHIM LIBRARY



Fig·5·2: Regional Field of the Basin

One remarkable observation worth noting, is the very close resemblance of the contours of the residual field map and the total field map. This is partly suggestive that the anomalies observed in this basin are largely due to extensive igneous intrusions buried within the shallow basement rocks. The deep seated structures are possibly not well separated from the local features and hence the dominance of the so-called intermediate features (Nettleton, 1954). Also, the fact that the residual anomalies in this basin change little from anomalies of the observed field, probably indicates that the basin is in the flat saddle of the regional magnetic field (Allingham, 1966).

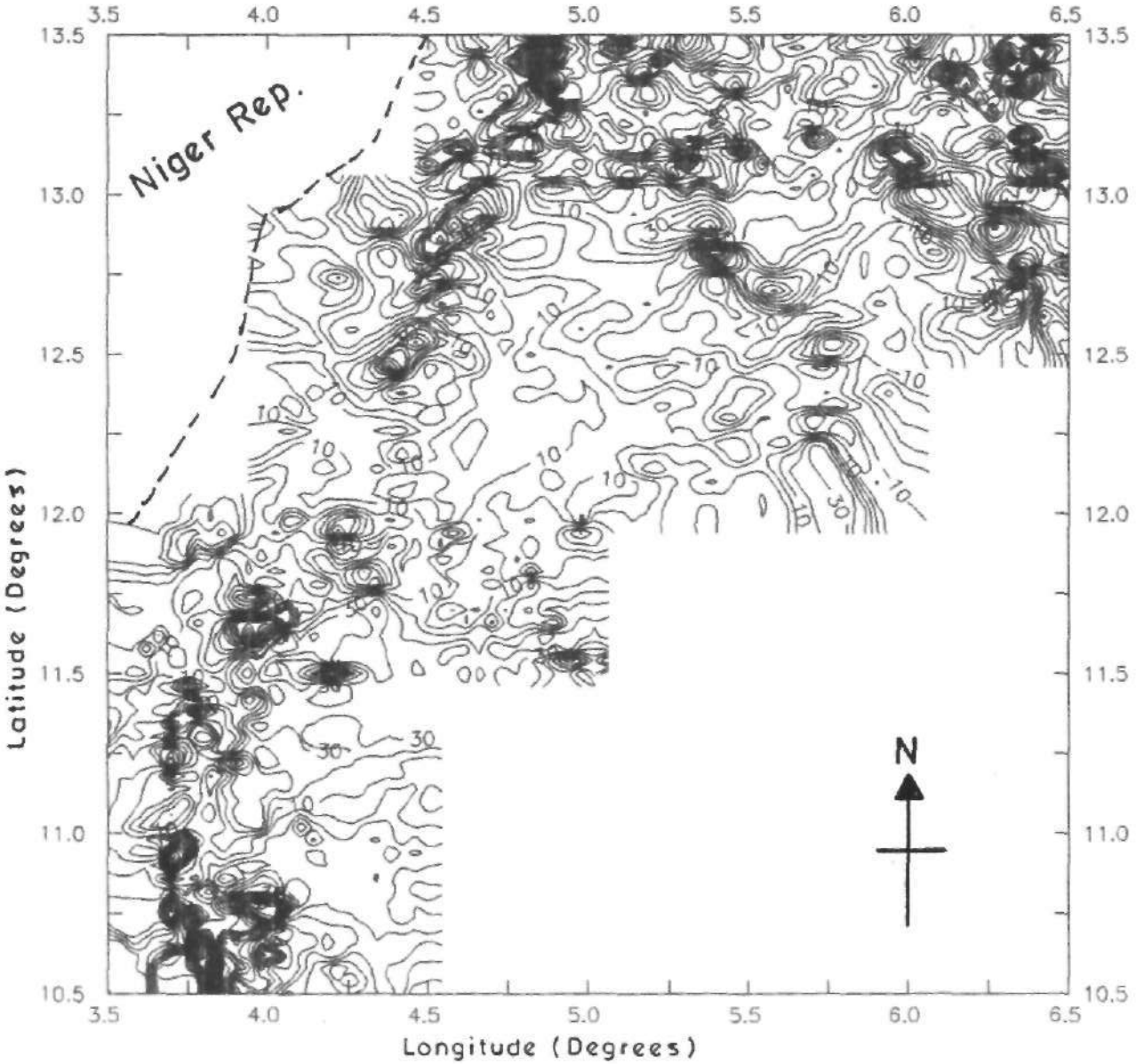


Fig.5.3: Residual Field of the Basin (Contour interval is 10 nT)

5.4 Application And Results Of The Second Vertical Derivative

The residual magnetic field of the study area was used to compute the values of the second vertical derivative. Smoothing was first carried out on the residual field by upward continuation before generating the second vertical derivative.

Figure 5.4 shows the structurally significant zero contours of the second vertical derivative. These contours delineate geologic boundaries in the subsurface structures.

Careful observation of the map shows that the high density zero contour portions represent near surface structures or anomalous zones in the residual magnetic map. Between latitude 12.50^0 and 13.00^0 N across the study area, the zero contours are elongated in the E-W direction but are widely spaced in the central portion. This is an indication of discontinuity in the subsurface magnetic rocks. In the southern section of the map between latitude 11.00^0 to 12.50^0 N, the elongation of the zero contours is in the E-W and NE-SW directions. However, these elongated zero contours are not without breaks, again confirming magnetic trends that are not continuous. The portions with high density zero contours depict highly intruded sections of the basin.

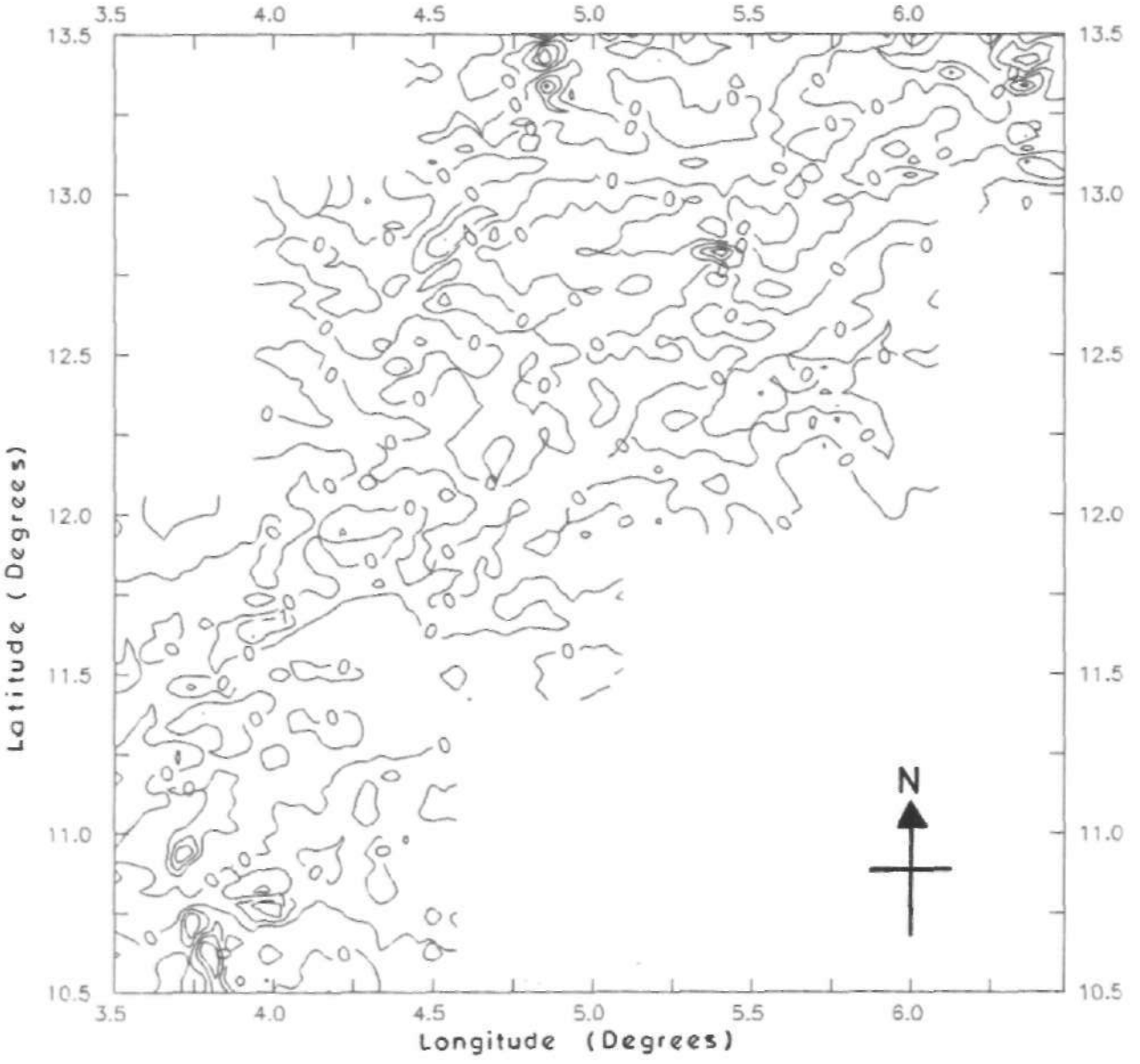


Fig.5.4:Second Vertical Derivative of the Basin

5.5 Qualitative Interpretation

5.5.1 Application Of Crosscorrelation

The study area was analyzed in twenty sections representing the twenty maps. Each of these sections consists of a square grid with 51 data points on each side (N = 51). The grid spacing is approximately 1.08 km and a maximum lap of 8 (m = 8) was chosen for the calculation of the coefficients.

In the process of calculating the crosscorrelation coefficients, the main field value for each map is computed and then subtracted from the field value of each data point. This involves the usage of equations (4.3) to (4.6). This has no effect on the trend directions obtained and results in easy comparison between the maps (Kangkolo, 1996).

Analysis of trend systems is simple. By definition a trend represents only the large scale fluctuations: all the small scale oscillations are removed (Affleck, 1963). The trend is the angle measured clockwise from geodetic north to the axis of the structure.

5.5.2 Results of Crosscorrelation

Figure 5.6(a) shows the coefficient map for section M009. The contour values of the coefficients are expressed as percentages. A high degree of correlation (75 %) in the data values can be observed. The main trend is ENE-WSW in the direction N 74^0 E. The coefficient map for section M010 is shown in Figure 5.6(b) above. We can notice a moderately high degree of correlation (68 %) over the data values. The main

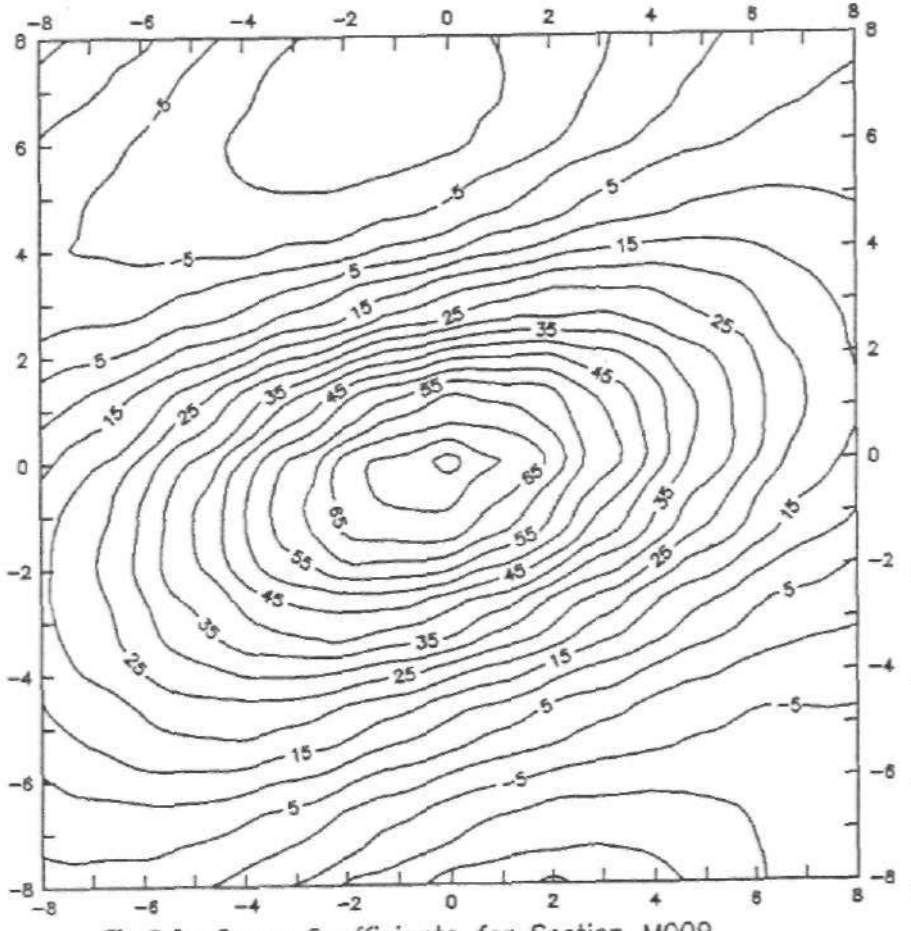


Fig.5.6a: Cross Coefficients for Section M009

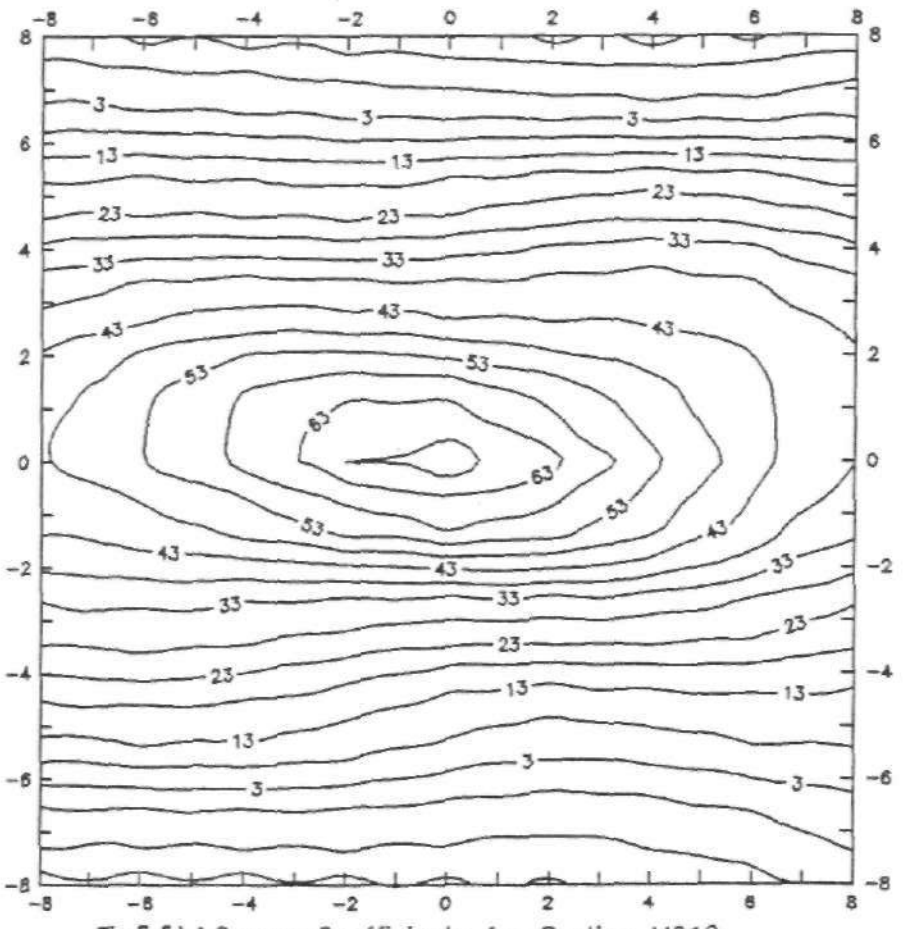


Fig.5.6b: Crosss Coefficients for Section M010

trend is WNW-ESE (almost E-W), in the direction N 92^0 E. The coefficient map for section M116 is shown in Figure 5.7a with a moderately high degree of correlation (68 %) in the data values. It is worth noting that this is the only section in the study area where the structure trends NNE-SSW (almost N-S) in the direction N 3^0 E. Figure 5.7b shows the coefficient map for section M117 with a very low degree of correlation (46 %) in the data values. The main trend is ENE-WSW in the direction N 67^0 E. The remaining crosscoefficient maps can be observed under Appendix 2.

Figure 5.8 shows the sheet layout of the study area indicating the direction of the main trend for each section. Table 5.1 summarizes the main trend, its direction and the correlation coefficient for each section while Table 5.2 shows the latitude and longitude extensions for each section.

Generally, a moderately high degree of correlation is observed in the northern section of the basin while a low correlation is common in the southwest section.

Unfortunately, the rugged or irregular nature of the area of study could not permit the evaluation of the cross coefficients for the supermap of the total field of the basin. However, it is conspicuous that most of the structures in the various sections are trending ENE-WSW and a few in E-W direction.

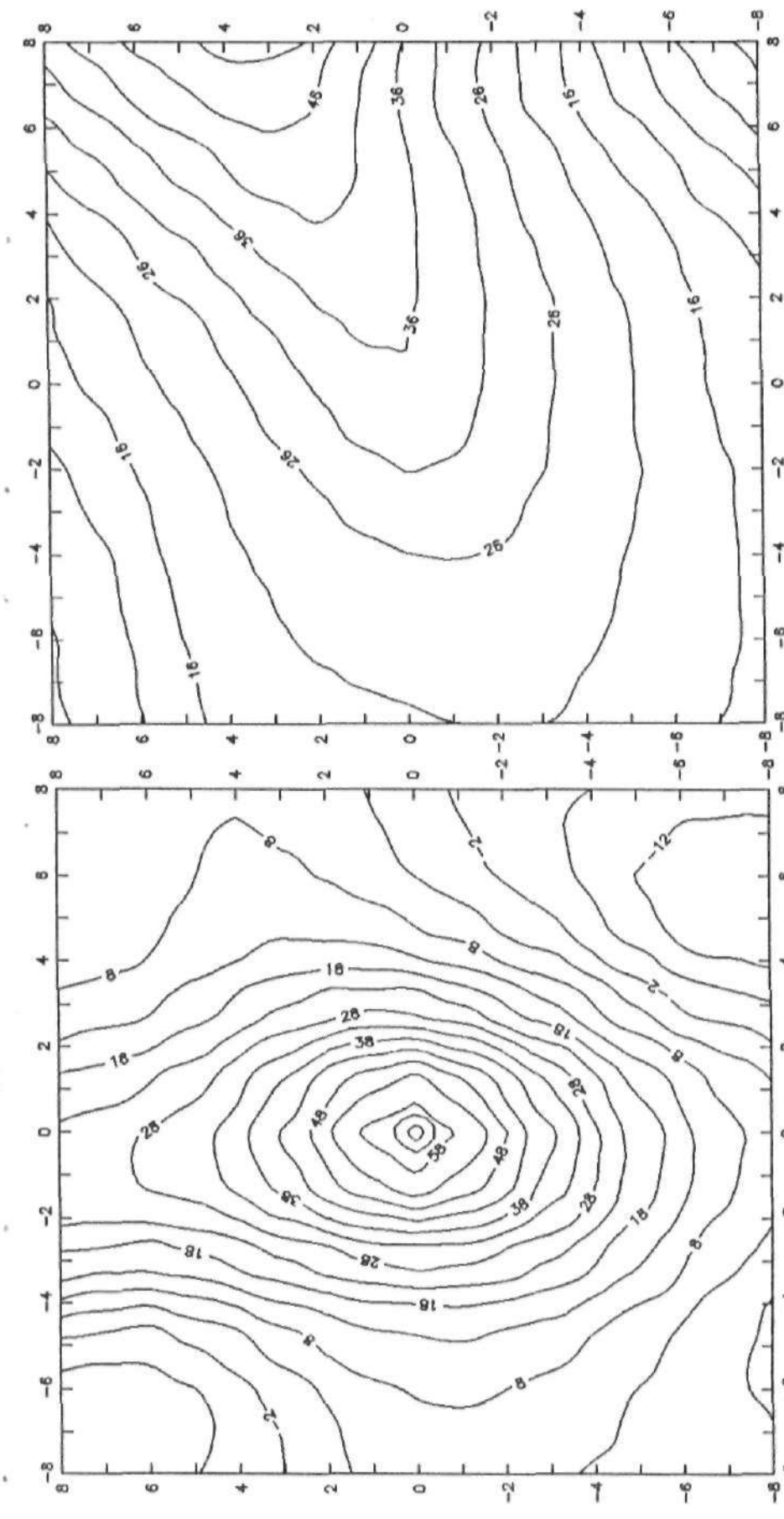


Fig.5.7a : Cross Coefficients for Section M116

Fig.5.7b: Cross Coefficients for Section M117

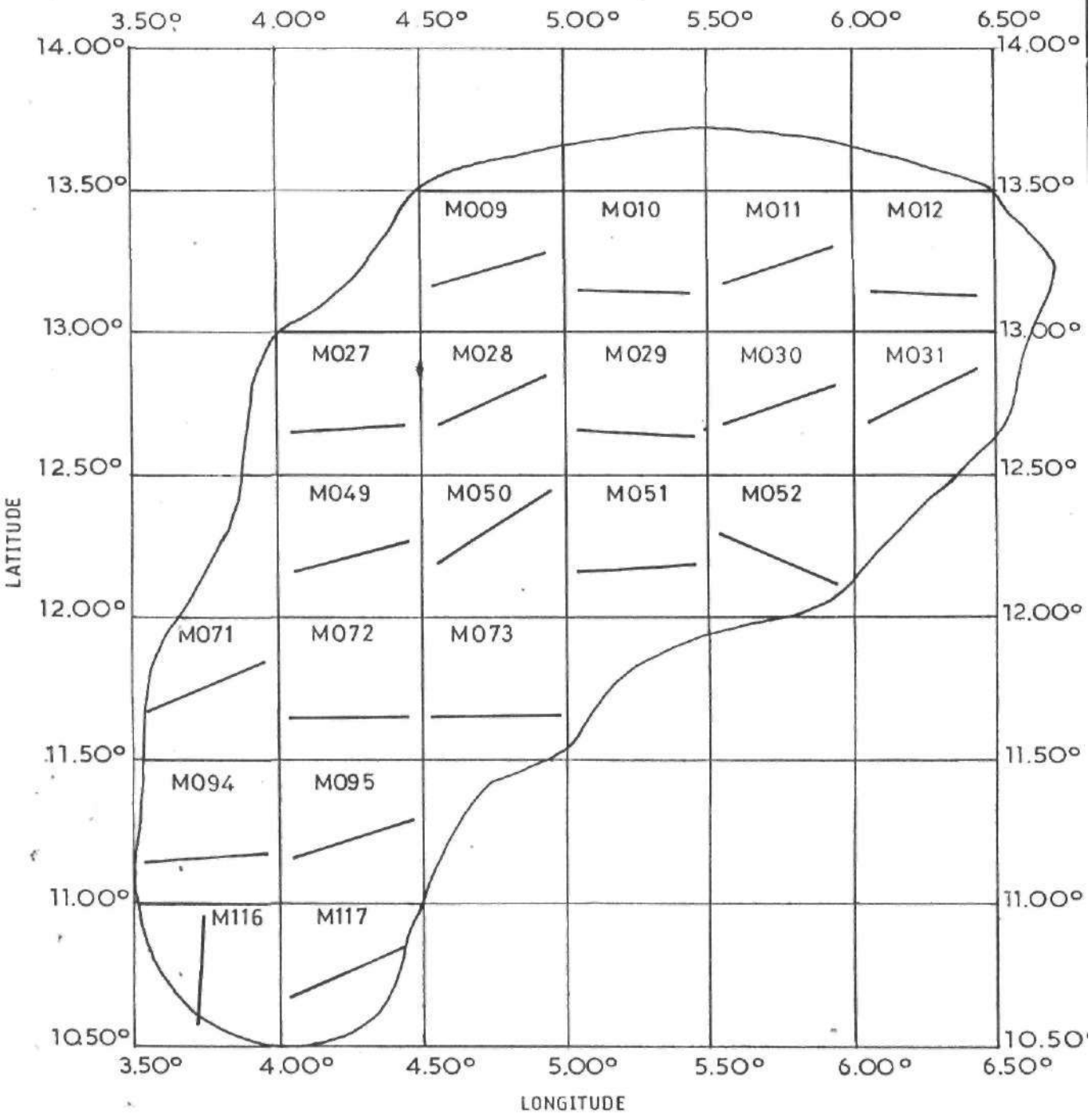


Fig. 5.8: Sheet layout of Sokoto Basin showing the direction of the main trend for each section.

Table 5.1 Direction of the Main Trend and the Correlation Coefficient for Each Section.

Section	Main Trend	Direction	Correlation Coefficient.
M009	ENE-WSW	N 74^0 E	75 %
M010	WNE-ESE	N 92^0 E	68 %
M011	ENE-WSW	N 71^0 E	63 %
M012	WNW-ESE	N 93^0 E	70 %
M027	ENE-WSW	N 87^0 E	56 %
M028	ENE-WSW	N 66^0 E	56 %
M029	WNW-ESE	N 93^0 E	83 %
M030	ENE-WSW	N 71^0 E	60 %
M031	ENE-WSW	N 64^0 E	75 %
M049	ENE-WSW	N 76^0 E	51 %
M050	ENE-WSW	N 63^0 E	52 %
M051	ENE-WSW	N 88^0 E	57 %
M052	WNW-ESE	N 114^0 E	76 %
M071	ENE-WSW	N 67^0 E	63 %
M072	E-W	N 90^0 E	64 %
M073	E-W	N 90^0 E	57 %
M094	ENE-WSW	N 85^0 E	72 %
M095	ENE-WSW	N 72^0 E	44 %
M116	NNE-SSW	N 3^0 E	68 %
M117	ENE-WSW	N 67^0 E	46 %

Table 5.2 Latitude and Longitude Extensions for Each Section

Section	Latitude Extension	Longitude Extension
M009	13.00^0 - 13.50^0	4.50^0 - 5.00^0
M010	13.00^0 - 13.50^0	5.00^0 - 5.50^0
M011	13.00^0 - 13.50^0	5.50^0 - 6.00^0
M012	13.00^0 - 13.50^0	6.00^0 - 6.50^0
M027	12.50^0 - 13.00^0	4.00^0 - 4.50^0
M028	12.50^0 - 13.00^0	4.50^0 - 5.00^0
M029	12.50^0 - 13.00^0	5.00^0 - 5.50^0
M030	12.50^0 - 13.00^0	5.50^0 - 6.00^0
M031	12.50^0 - 13.00^0	6.00^0 - 6.50^0
M049	12.00^0 - 12.50^0	4.00^0 - 4.50^0
M050	12.00^0 - 12.50^0	4.50^0 - 5.00^0
M051	12.00^0 - 12.50^0	5.00^0 - 5.50^0
M052	12.00^0 - 12.50^0	5.50^0 - 6.00^0
M071	11.50^0 - 12.00^0	3.50^0 - 4.00^0
M072	11.50^0 - 12.00^0	4.00^0 - 4.50^0
M073	11.50^0 - 12.00^0	4.50^0 - 5.00^0
M094	11.00^0 - 11.50^0	3.50^0 - 4.00^0
M095	11.00^0 - 11.50^0	4.00^0 - 4.50^0
M116	10.50^0 - 11.00^0	3.50^0 - 4.00^0
M117	10.50^0 - 11.00^0	4.00^0 - 4.50^0

It is interesting to point out the fact that the trends obtained by crosscorrelation completely agrees with the delineation of the geologic boundaries of the subsurface structures using the second vertical derivative. In both methods as can be observed in Figure 5.8 and Figure 5.4, the structures are trending mostly in the ENE-WSW and E-W directions. A very unique case in the two Figures mentioned above can be observed in section M116 where trend is in the N-S direction in both cases. It is suggested that tectonic processes must have drastically altered the subsurface structures in this portion of the study area.

It is worth noting that the anomaly alignment as observed in the total field map should not necessarily mean the trend of the anomalies as observed from the cross-correlation function and the second vertical derivative.

5.6 Application of Power Spectral Analysis

The study area was divided into forty eight blocks overlapping with each other. Each of these blocks covers a square area of about 55 km x 55 km, representing a square grid of 51 x 51 residual field points. However, to meet the conditions of fast Fourier transform (FFT), these points were zero-padded to a 64 x 64 grid which was then cosine-tapered before the evaluation of the power spectrum. The Fourier transform of the data for each block was obtained by first Fourier transforming columns (or rows) and next rows (or columns) as explained section 4.3.2.

After the evaluation of the slopes, equation 4.19 was used to calculate the depth to the causative layers from the elevation height of the aircraft. It should be recalled that the data for this study was collected from a survey altitude of approximately 153 m above the terrain. In order to reduce the spectral depths to the ground surface, which is our datum surface, the flight elevation was subtracted from the depth estimates obtained from the spectral plots (Nwogbo, 1987)

It is however important to remember that spectral depths are generally average depths and individual depth estimates may have values which differ significantly from the actual depths at the selected points.

5.6.1 Results of Power Spectral Analysis

Graphs showing the logarithms of spectral energies against frequencies obtained from four of the blocks are shown in Figures 5.9 and 5.10 below. Most of the plots yielded two segments as observed in the spectral plots in Figures 5.9(a) and 5.9(b) for blocks 5 and 6 respectively. However Figures 5.10(a) and 5.10(b) reveal the only three-layer cases as seen in blocks 11 and 12 respectively.The remaining graphs can be observed under Appendix 3. Table 5.3 shows the location of the blocks indicated by the longitude and latitude values of X1, X2 and Y1, Y2 respectively in degrees. D1, D2 and D3 represent increasing depths in kilometres to magnetic sources.

The two line segments observed in the spectral plots indicate that the different gradients are produced by an

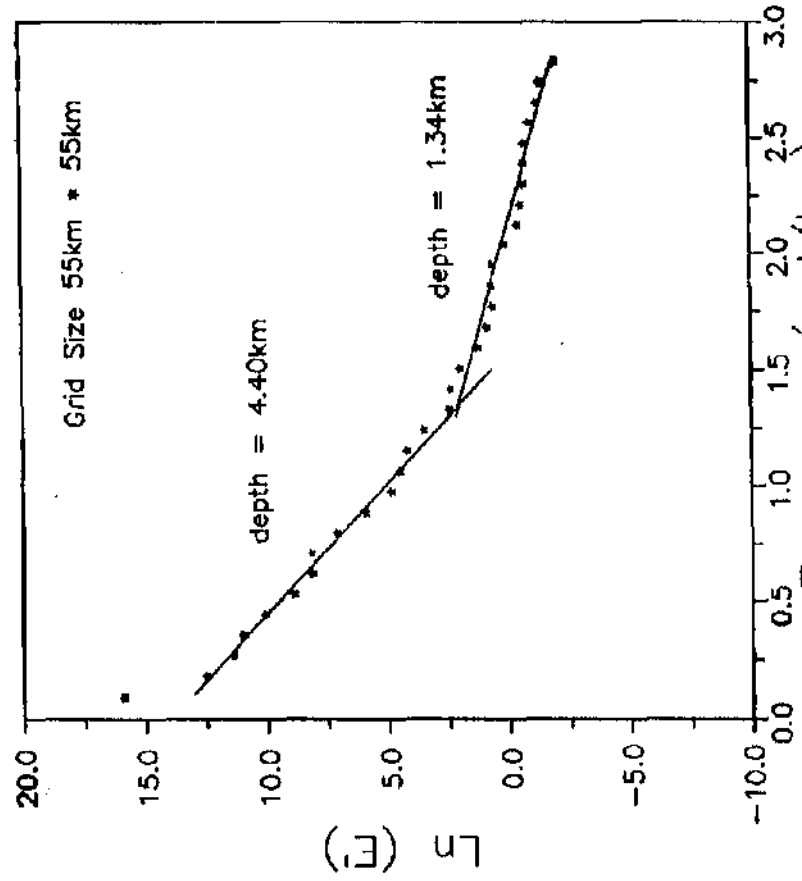


Fig5.9b: Power Spectrum Analysis for Block 6

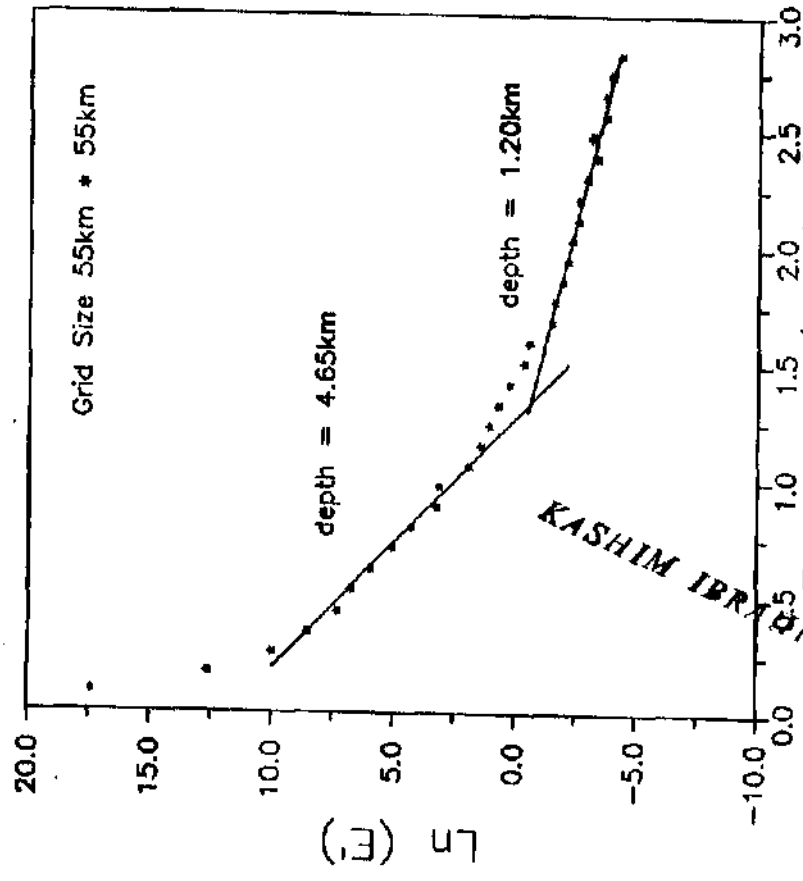


Fig.5.9a: Power Spectrum Analysis for Block 5

KASHIM IBRAHIM LIBRARY

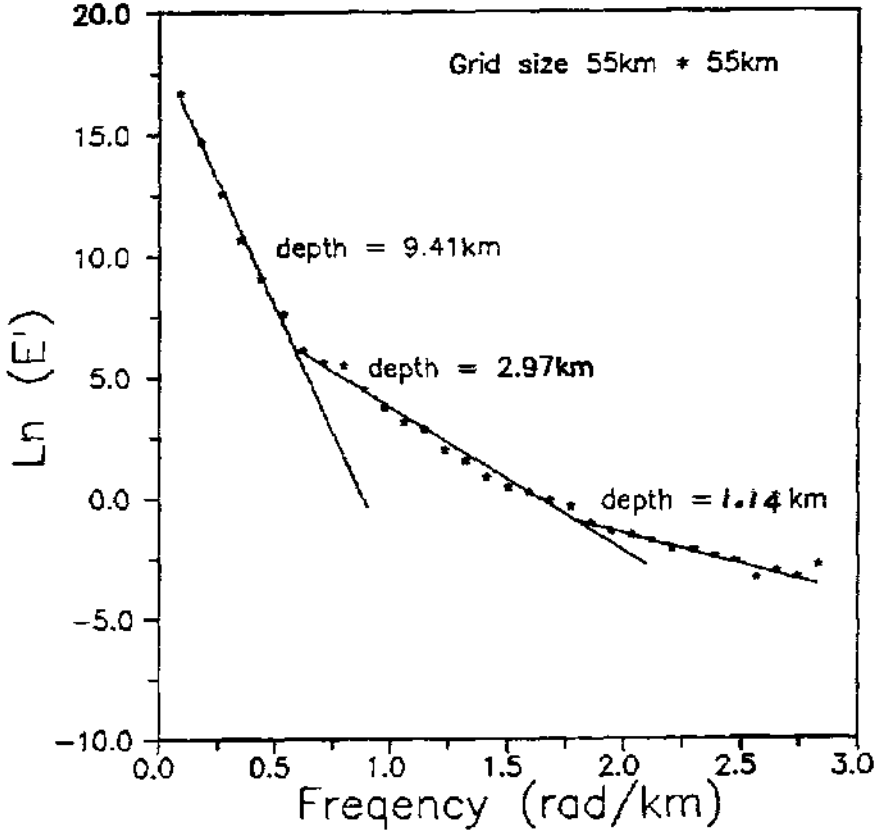


Fig.5.10a Power Spectrum Analysis for Block 11

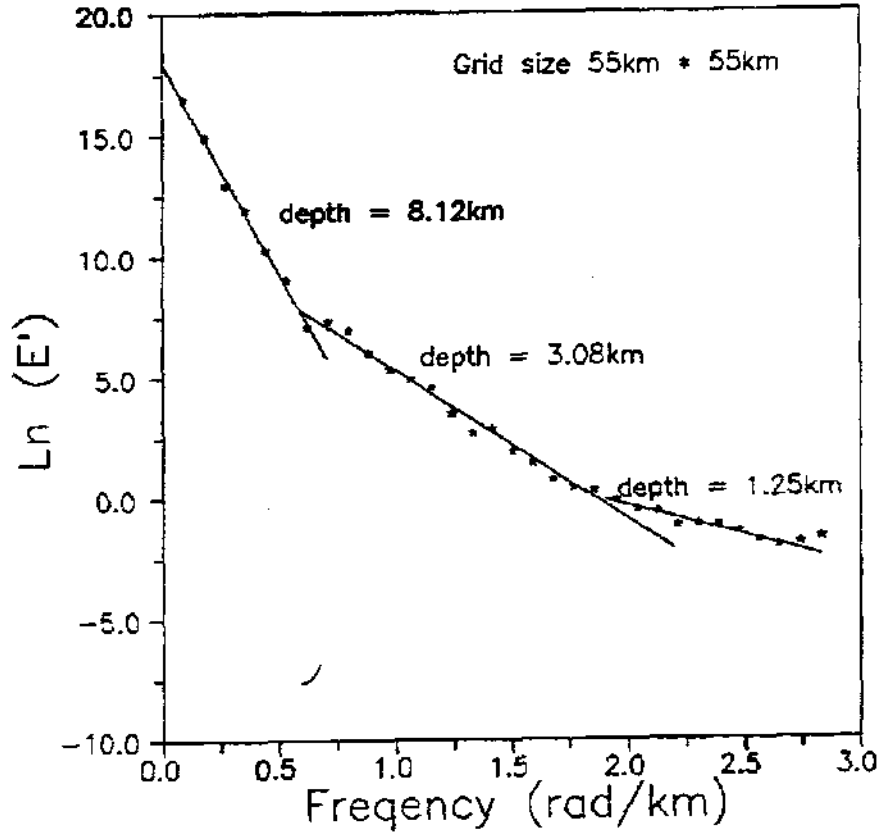


Fig.5.10b. Power Spectrum Analysis for Block 12

Table 5.3 Locations and Identification Numbers for the Blocks with their respective Depths.

Block no.	X1 (^{0})	X2 (^{0})	Y1 (^{0})	Y2 (^{0})	D1 (Km)	D2 (Km)	D3 (Km)
01	3.50	4.00	10.50	11.00	0.989	4.421	.....
02	3.76	4.26	10.50	11.00	1.782	5.835	.....
03	4.00	4.50	10.50	11.00	1.841	5.569	.....
04	3.50	4.00	10.76	11.26	1.780	4.793	.....
05	4.00	4.50	10.76	11.26	1.051	4.494	.....
06	3.50	4.00	11.00	11.50	1.166	4.250	.....
07	3.76	4.26	11.00	11.50	1.175	3.670	.....
08	4.00	4.50	11.00	11.50	1.294	4.169	.....
09	3.50	4.00	11.26	11.76	1.414	3.327	.....
10	4.00	4.50	11.26	11.76	1.267	3.652	.....
11	3.50	4.00	11.50	12.00	1.134	2.818	8.347
12	3.76	4.26	11.50	12.00	1.101	2.927	7.967
13	4.00	4.50	11.50	12.00	0.968	2.201	.....
14	4.26	4.76	11.50	12.00	1.770	6.910	.....
15	4.50	5.00	11.50	12.00	1.785	5.947	.....
16	4.00	4.50	11.76	12.26	1.196	5.044	.....
17	4.50	5.00	11.76	12.26	1.821	3.921	.....
18	4.00	4.50	12.00	12.50	1.353	3.627	.....
19	4.26	4.76	12.00	12.50	1.235	3.956	.....
20	4.50	5.00	12.00	12.50	1.265	3.575	.....
21	4.76	5.26	12.00	12.50	1.265	4.449	.....
22	5.00	5.50	12.00	12.50	1.173	4.166	.....
23	5.26	5.76	12.00	12.50	1.021	2.995	.....
24	5.50	6.00	12.00	12.50	1.295	6.585	.....
25	4.00	4.50	12.26	12.76	2.166	4.058	.....
26	4.50	5.00	12.26	12.76	1.478	3.885	.....
27	5.00	5.50	12.26	12.76	1.222	4.096	.....
28	5.50	6.00	12.26	12.76	1.842	4.777	.....
29	4.00	4.50	12.50	13.00	2.248	5.005	.....
30	4.26	4.76	12.50	13.00	1.042	4.107	.....
31	4.50	5.00	12.50	13.00	1.087	3.984	.....
32	4.76	5.26	12.50	13.00	1.109	4.652	.....
33	5.00	5.50	12.50	13.00	1.951	6.425	.....
34	5.26	5.76	12.50	13.00	1.719	5.884	.....
35	5.50	6.00	12.50	13.00	1.496	4.897	.....
36	5.76	6.26	12.50	13.00	1.098	2.739	8.357
37	6.00	6.50	12.50	13.00	1.349	6.928	.....
38	4.50	5.00	12.76	13.26	0.928	3.820	.....
39	5.00	5.50	12.76	13.26	1.245	2.676	.....
40	5.50	6.00	12.76	13.26	0.882	3.386	.....
41	6.00	6.50	12.76	13.26	1.379	6.855	.....
42	4.50	5.00	13.00	13.50	1.192	4.884	.....
43	4.76	5.26	13.00	13.50	1.366	4.411	.....
44	5.00	5.50	13.00	13.50	1.353	3.616	.....
45	5.26	5.76	13.00	13.50	1.220	3.436	.....
46	5.50	6.00	13.00	13.50	1.189	3.318	.....
47	5.76	6.26	13.00	13.50	1.557	2.686	.....
48	6.00	6.50	13.00	13.50	0.946	4.362	.....

arrangement of magnetic sources at two different depths. Thus the power spectrum of a double ensemble consists of two parts - the first, which relates to deeper sources, is at the small wave numbers (low frequency) and decays rapidly; and the second which arises from a shallower ensemble of sources, dominates the short wavelength (high frequency) end of the spectrum.

Considering that the area of study is sedimentary, the high frequency end of the spectrum for each block originates from magnetic sources from the shallow basement and hence the slope of this segment relates to the depth to magnetic basement. The spectral depths corresponding to the first segment in the low frequency region for each of these blocks may therefore relate to magnetic sources lying within the basement.

No single ensemble of sources was observed, and only very few blocks show three ensemble cases. By long odds, the most common occurrence is where just two sets of sources are discernible in the spectrum (Spector and Grant, 1970). They are easily recognized by a marked change that takes place in the spectral decay rate. It is however important to note that the removal of the power-law effect has eliminated the presence of false slopes (Fedi et al., 1997).

5.6.2 Discussion of the Depth to Magnetic Basement Map

Figure 5.11 shows a generalized depth to basement map with various depths to the basement posted at the centers of the

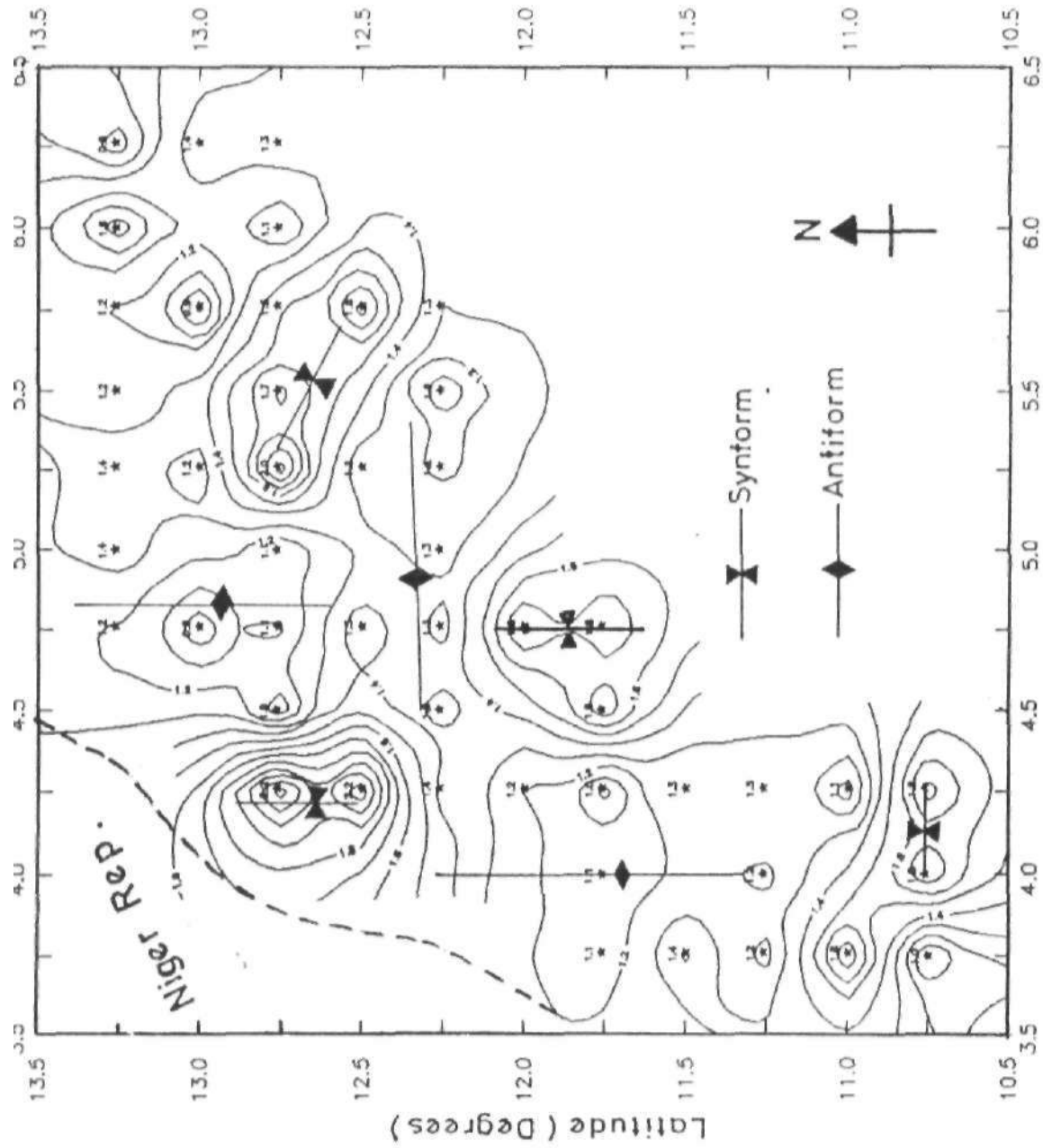


Fig.5.11: Generalised Depth to the Magnetic Basement Map (Contour interval is 0·1km)

overlapping blocks while Figure 5.12 shows the depth to the second layer of the study area.

The depths to the magnetic basement (D1) range from 0.9km to 2.2 km with an average of 1.4 km, while the second layer depths varies from 2.2 km to 6.9 km with an average of 4.3 km. The third layer was discerned only in a few blocks. These depths can be observed in the last three columns of Table 5.3.

The depth to basement map indicates that the magnetic basement beneath the sediments in the basin is generally shallow and of low relief. The highest depth of 2.2 km is recorded in the northwest section of the study area near the boundary with Niger Republic. The lowest depth of 0.9 km is recorded in the northeast section near the basement complex region.

The depth to basement map reveals four synforms centered respectively at longitude 4.75^0 E and latitude 11.75^0 N, longitude 5.25^0 E and latitude 12.75^0 N, longitude 4.75^0 E and latitude 11.80^0 N and longitude 4.25^0 E and latitude 10.75^0.N. Interspaced between these basement lows (synforms) are basement highs (antiforms) in the form of ridges which have gentle slopes. Generally in the southwest of the basin, the ridge

trends roughly N-S and terminates with another ridge trending E-W. In the northeast section of the study area, a ridge trending in the N-S direction separates the two depressions in the northwest and northeast of the basin. Some of these depressions contain very thick sediments which could be probable sources for ground water exploration. The electrical resistivity method can be used to confirm this assertion.

The series of ridges and troughs suggest that the subsurface basement rocks must have undergone gentle folding. This could be indicative that the basement rocks must have been gently deformed or altered into a series of antiforms and synforms with axis trending in various directions as described above.

The total magnetic field map and the residual field map of the study area each correlates very well with the depth to basement map. The four depressions depict the areas represented by a low gradient magnetic field, while the basement highs or antiforms correspond to the short wavelength anomalous zones on the residual field map. This is however the expectation because short wavelength anomalies are highlighted by shallow magnetic sources while long wavelength anomalies reveal deeper magnetic sources.

Considering that the average temperature gradient of 1° c per 30 m in the Niger Delta is applicable here and the general conditions for hydrocarbon accumulation are favorable, then the least thickness of sediments to reach the threshold temperature

of 115° c for the commencement of oil formation from organic remains would be 2.3 km approximately (Wright et al. (1985)). The fact that this study has proven a maximum depth of 2.2 km, implies that the prospect of hydrocarbon accumulation may not be completely ruled out.

CHAPTER SIX

GENERAL DISCUSSIONS AND CONCLUSIONS

6.1 Improved Method of Depth Estimation

The Spector and Grant (1970) method for the estimation of depths to individual magnetic bodies (or zones) has enjoyed a wide and continued popularity over the past 30 years. It relates average depths to magnetic sources to the rate of decay of the magnetic power spectra.

For the purpose of analyzing aeromagnetic maps, the map of the magnetic field intensity over an area, after the removal of the main geomagnetic field, is assumed to consist of the superposition of a large number of individual anomalies, most of them overlapping, which are caused by several ensemble of blocks of various dimensions and magnetization. The method, then assumes a uniform distribution of parameters for an ensemble of magnetized block, and leads to a depth dependent exponential decay (Spector and Grant, 1970)

Fedi et al. (1997), showed that also inherent in the Spector and Grant model, is a power-law rate of decay that is independent of depth. For most cases, except for extreme depths and small block sizes, the observed power spectrum should be corrected for a power-law decay rate. For the two-ensemble case as well, correction by the power-law should yield better depth estimations in the power spectrum.

A slope change in the power spectrum can be caused either

by a two-ensemble effect or by an inherent power law effect in the single ensemble case (Fedi et al., 1997). The removal of the power-law effect can help solve this ambiguity.

The Spector and Grant method, without spectral decay correction, consistently overestimates depths. The rate of decay of the spectrum is hence determined by two parameters, the exponent of the power-law ($-\beta$) and the average depth $\bar{h}$. A power-law of about 2.9 arises from an ensemble of blocks uniformly distributed. To substantially improve our ability to estimate the depth, the power spectrum should be divided by the correcting factor $\rho^{2.9}$ before applying the Spector and Grant method. (Fedi et al., 1997).

6.2 Summary of the Results

Quantitative study of the structural trends in the total field map reveals an alignment of prominent anomaly groups in approximately linear patterns. These linear patterns are oriented in the N-S, NNE-SSW and NW-SE directions. The contours of both the residual field and the observed total field are similar.

The residual magnetic field of the study area was then used for the computation of the second vertical derivative map. Particularly, the zero contours of the second vertical derivative map were used for the delineation of geologic or magnetic boundaries of subsurface structures. The elongation of the zero contours are mostly oriented in the E-W and the NE-SW directions. However some of these elongations are broken off at

short distances in some sections of the area.

The method of crosscorrelation was used to quantitatively determine the main trend in the magnetic field for the twenty sections covering the area of study. The main trend for most sections is in the ENE-WSW direction and a few in the E-W direction. Only section M116 in the extreme southwest of the study area indicates a N-S trend. A moderately high degree of correlation over the data values is noted in the northern half of the study area as opposed to the southwest section where a low degree of correlation is common.

Spectral analysis of the residual magnetic field over 48 overlapping blocks covering the study area reveal that the thickness of the sedimentary formations overlying the basement complex range from 0.9 km to 2.2 km. The topography of the basement surface shows a general trend from shallow in the northeast and southwest sections to deep in the northwest section of the area. The magnetic basement map depicts a series of ridges and troughs over the area with four depressions.

KASHIM IBRAHIM LIBRARY

6.3 Deductions and Comments

The anomaly closures in the observed total field map are made up of magnetic minima and maxima. The structures in the basement giving rise to the alignment of major anomaly groups are likely having the same orientation.

It is suggested that these magnetic lineations could be

fracture zones which show up on the total field map as distortions in what otherwise appears to be a regular anomaly pattern. Zones of crushed rock may show up as minima in magnetic intensity, rather than maxima, that is negative anomalies in relation to surrounding rock. The explanation is that tectonic processes often destroy the properties of what was once fresh magnetic rock. Even when the rocks of an area are weakly magnetic, it may be possible to delineate sufficiently wide fracture zones from small magnetic anomalies.

It is also possible that these magnetic lineations oriented in the N-S, NNE-SSW, NW-SE could represent faults or contacts of rocks of different lithologies. Recognition of faulting is important in mineral exploration. In some major fault zones, the magnetic minerals have been altered to non-magnetic assemblages by meteoric waters.

Wright (1968) and Ball (1980) have both identified a system of NE-SW and NW-SE conjugate pairs of fractures which exist everywhere within the Pan African Mobile Belt. They suggested that these fracture systems represent important lines of weakness in the continental crust and could be loci of economic mineralization.

A series of transcurrent faults have been observed to affect the basement rocks adjoining the study area (Mc Curry, 1976). Kogbe (1981) reported a WSW-ENE trending fault in the vicinity of Gilbedi Village. Hence, some of the magnetic lineations observed in the total field map could represent

faults that have not yet been mapped by geologists.

A moderately high degree of correlation in the crosscoefficient maps was observed in the northern section of the study area. This implies that there are fewer intrusive bodies in the formation, while a low degree in the southwest section indicates a greater number of intrusions. This is in agreement with the results from the zero contours of the second vertical derivative.

Earlier workers had reported similar magnetic lineations in the environs of the study area. Some intensive investigations to establish structural trends was carried out by Buser (1966). He established the existence of paleostructures in his study that covers Nigeria and adjacent countries. The origin of paleostructures are shown to be due to the interaction of three main geophysical forces like geomagnetism, gravitation and rotation. The paleostructures have directed events like tectonic movements, sedimentation, metamorphism, intrusions, mineralization, volcanism and drainage. He identified these structures in a NNE-SSW direction. It is possible that because of the influence of these paleostructures, some of the major tectonic features in the study area have trends in approximately NNE-SSW direction as observed in the total field magnetic map.

In their interpretation of aeromagnetic data across the central crystalline shield area of Nigeria, Ajakaiye et al. (1985) identified that the NE-SW trending anomalies are the

dominant magnetic features of most of this shield area. They pointed out that this concentration of magnetic lineaments appears to be connected with the occurrences of Younger Granites since almost all of the known Younger Granite complexes lie within the region dominated by these trends.

Generally, any extensive magnetic survey will contain anomalies whose pattern is not random. Certain similarities in both trends and spacings appear in all surveys. Usually one or two dominant trends are seen, and distance between adjacent anomaly axis are fairly constant.

Affleck (1963) has found by statistical analysis, part of which involved a portion of the Canadian shield, that there is a marked similarity in the magnetization of rocks all over the earth. His conclusions reveal a preferred anomaly orientation of N-S, E-W, NW-SE and NE-SW, which he suggests may be related to the rotational motion of the earth. These facts all suggest very strongly that the anomaly trend systems are indeed related to systematic lineaments and to rotational and tidal forces.

Results from the power spectral analysis of the residual field show two distinct slopes for almost all the blocks. The first segment of the spectral plots could be attributed to magnetic sources within the basement. These could probably be caused by intrabasement features such as faults and fractures that have already been identified. It is suggested that these faults could be responsible for the existence of depressions as revealed by the depth to basement map of the study area. The

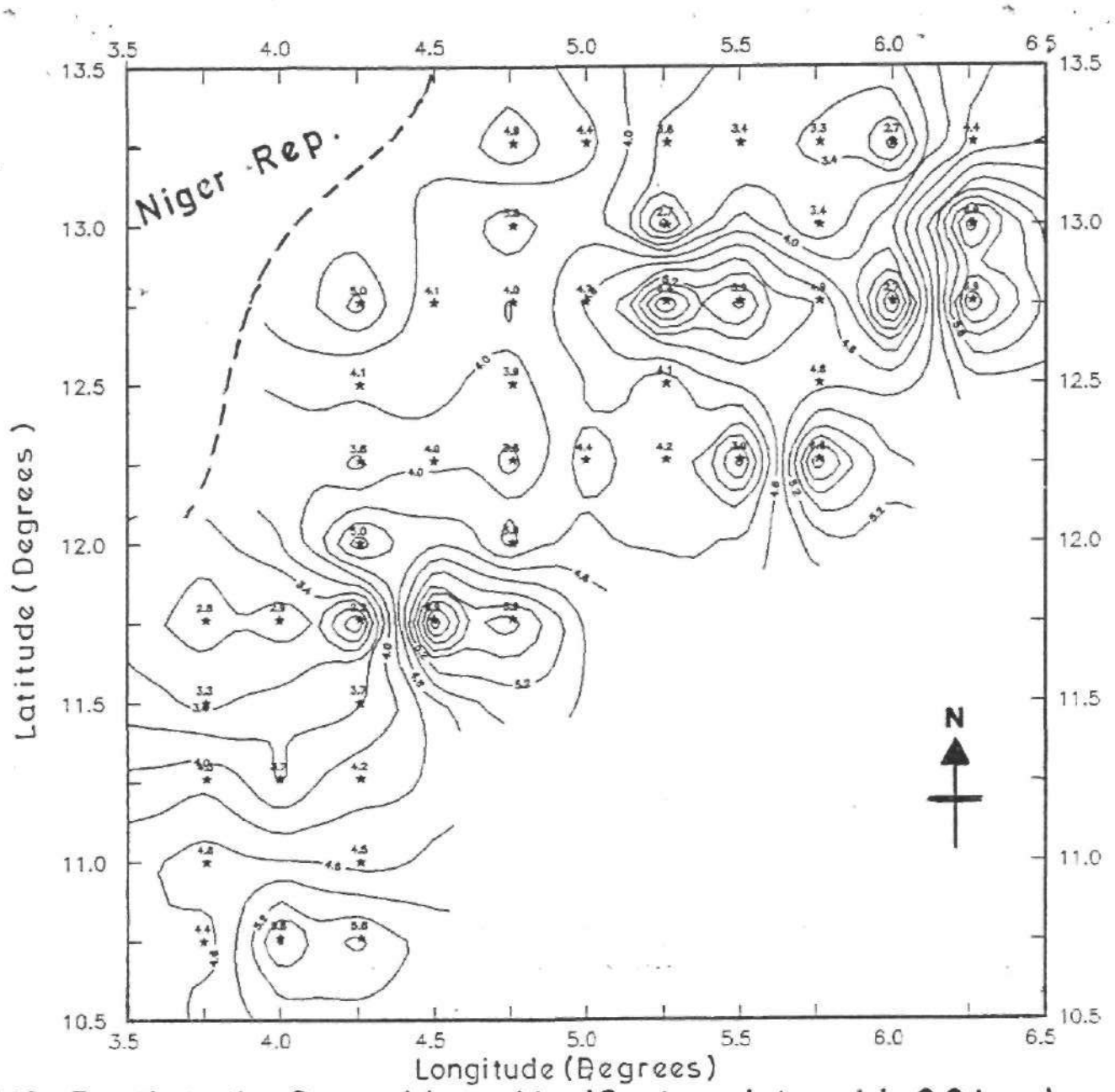


Fig.5.12: Depth to the Second Layer Map (Contour interval is 0.2 km)

second segment arises from shallower ensemble and is attributed to magnetic sources on the surface of the basement complex that is suprabasement features. In the few three-ensemble cases, the first segment is probably due to deeply buried magnetic sources which are not distributed evenly in the basin, while the second and third segments are due to uniformly distributed magnetic sources within the basement and on the basement surface respectively.

The depth to basement reveals that the basement surface presents a successive pattern of troughs and crests. The crests or antiforms strike generally in the N-S and E-W directions. This probably confirms the earlier report that the Basement Complex and its supracrustal cover of the Younger Metasediments of the basin were subjected to two phases of tight isoclinal folding during the Pan-African, which are responsible for the N-S trending common over much of Nigeria (Mc Curry, 1976).

An attempt was made to compare the results of depth estimates obtained from this study with those of the previous workers. However, one should bear in mind that this study did not completely cover the entire basin. This study, reveals depth ranges from 0.9 km to 2.2 km, depicting the magnitude of the undulations of the basement topography. Generally, the topography of the basement surface dips in the northwest direction attaining a maximum depth of 2.2 km near the boundary with Niger Republic. Kogbe (1979) reported that the deepest part of the basement in the basin is around the Gwandu Emirates located in the same northwestern portion of the study area.

Umego (1990) employed both the magnetic and gravity methods to estimate the depth to basement. Using the Wenner Deconvolution technique, he reported a depth variation from 1.2 km to 2 km. He produced the first depth to basement map which shows a generally shallow basement surface. It dips gently in a northwesterly direction reaching a maximum depth of 2 km at the northwest border with Niger Republic. His depth estimates from gravity analysis were however lower than those from the magnetic method.

Sambo (1994) using the magnetic method, employed techniques based on spectral analysis to estimate the depth to the magnetic basement in the study area. His depth estimates vary from 0.3 km near the boundary with the basement complex to 1.85 km at the centre of the basin. He produced a generalized depth to magnetic basement map which reveals generally a shallow basement surface deeepest at the centre of the basin with a magnitude of 1.85 km and decreases gradually towards the eastern and western boundaries.

In the exploration of sedimentary basins, aeromagnetic survey are often flown in the first stages for reconnaissance purposes. The prime purpose is to find the general structure of the basin and estimate the thickness of the sediments. It is a truism to say that without a magnetic anomaly, there cannot be a depth estimate (Reford and Sumner, 1964). The deeper the basement, the broader and fewer are the magnetic features, and the depth estimates will be fewer.

6.4 Limitations and Assumptions

Generally potential fields of any type are inherently ambiguous. In other words, theoretically, an infinite number of solutions may be obtained for the physical property distribution giving rise to a particular anomaly, be it magnetic, gravitational or electrical.

Confusion can arise when the petroleum geologist thinks in terms of a basement that is not formed of magnetic rocks. For instance, quartzite or slightly metamorphosed rocks may form an economic basement far above the igneous rocks which affect the magnetic field. Most of the magnetic anomalies may come from the basement surface, but some will be caused by bodies which lie beneath it. The interpretation may then be ambiguous, but this ambiguity can only be resolved by other sources of information from the geology of the area. The most difficult ambiguities for earth scientists to tackle are the cases of weakly magnetic basement and magnetic layers within the sediments.

If the average values of the source parameters like thickness and magnetization are small, this will affect the slope of the power spectrum at low frequencies. Since the deep source effect is often restricted to a low frequency interval, faulty estimates are likely to arise. For these reasons, it is customary in the spectral approach used presently to neglect the first few points in the power spectrum as has been done in this study (Pal et al. 1978).

In the total magnetic field interpretation carried out in this study, the map represents the total picture available and no assumptions regarding strike and lateral extent of the source was made. However, it is worth remembering that no matter how careful the compilation, the contoured magnetic map cannot depict all the information shown on the original magnetometer records. Since the map methods use only selected points from the contoured map, each application will involve a further loss of detail. Computing a new map does not constitute an interpretation. It simply puts the original data into a new form, which may make the interpretation easier.

The various interpretations of the aeromagnetic field carried out have been based upon the premise that the magnetization of the rock is brought about solely by magnetic induction. This premise is often not true because many rocks are permanently magnetized. The permanent magnetization can have a direction significantly different from the present geomagnetic field (Green, 1960).

It suffices to state here that one of the constraints in this study was the small size of the computer core memory. This was as a result of the enormous amounts of data needed to compute the supermaps of the entire area of study. The author then resorted to a very difficult and tedious sampling process (decimation). A smaller sampling interval would have been desirable, since it enables us to study smaller anomalies which may be of economic significance.

6.5 Conclusions

The anomaly alignments in the observed total field comprising of magnetic minima and maxima is suggested to be caused by faults in the basin. Recognition of faulting is important in mineral exploration as these could be potential sources of economic mineralization.

The zero contours of the second vertical derivative map generally reveal trending magnetic discontinuities of sub-surface structures over the study area.

Results from the crosscoefficient maps indicate a general high degree of correlation over the data values in the northern section, implying a few intrusive bodies, while the low degree of correlation in the southwest section reveals a greater number of intrusions probably on the basement surface.

The thickest sedimentary deposit corresponding to 2.2 km was recorded in the northwest section with a minimum depth of 0.90 km in the northeast section. The average depth of all the 48 blocks is 1.3 km.

6.6 Recommendations

(1) More detailed geophysical and geological investigations employing more sophisticated but highly reliable methods should be carried out, that is, a detailed ground follow-up magnetic survey should be carried out along the short wavelength anomalous zones as revealed by the total field map as these could be potential sources of economic mineralization.

REFERENCES

Affleck, J. (1963). Magnetic Anomaly Trend and Spacing Patterns. Geophysics, 28 (3):279 - 395.

Agarwal, R.G. and Kanasewich, E.R.(1971). Automatic Trend Analysis and Interpretation of Potential Field Data. Geophysics, 36 (2): 339 - 348.

Ajakaiye, D.E. Hall, D.H. and Miller, T.W. (1985). Interpretation of aeromagnetic data across the central crystalline shield area of Nigeria. Geophysics. J.R. astr. Soc., 83: 503 - 517.

Ajibade, A.C. and Wright, J.B. (1988). Structural relationships in the schist belt of north-western Nigeria In: Oluyide, P.O. (Ed.) Precambrian Geology of Nigeria - Geological Surv. of Nigeria, Kaduna, pp. 103 - 109

Allingham, J.W., (1966). Aeromagnetic anomalies in the Bonne Terre area of the southeast Missouri mining district. Mining Geophysics, (SEG, Tulsa) 1:36 - 53.

Ananaba, S.E. (1983). Evaluation of Remote Sensing Application to Geophysical studies in Nigeria. Unpublished Ph.D Thesis, Ahmadu Bello University, Zaria, Nigeria.

Ananaba, S. E. and Ajakaiye, D.E., (1987). Evidence of tectonic control of mineralization in Nigeria from lineament density analysis. A Landsat Study. Int. J. Remote Sensing 8,10:1445 - 1453.

Ball, E. (1980). An example of very consistent brittle deformation over a wide intracontinental area:The late Pan - African fracture system of the Taureg and Nigerian Shield. Tectonophysics, 61:363 - 379.

Bath, M. (1974). Spectral Analysis in Geophysics. Elsevier Scientific Publishing Co. Amsterdam.

Bhattacharyya, B.K. (1966).Continuous spectrum of the total magnetic field anomaly due to a rectangular prismatic body, Geophysics, 31: 97 - 121.

Bhattacharyya, B.K. and Raychaudhuri, B., (1967).Aeromagnetic and geological interpretation of a section of the Appalachian Belt in Canada, Can. J. Earth Sci. 4: 1015 - 1037.

Bingham, C., Godfrey, M.D. and Tukey, J.W. (1967): Modern techniques of power spectrum estimation. IEEE Transactions on Audio and Electroacoustics, Vol. AU. 15 pp. 56 - 66.

Buser, H. (1966). Paleostructures of Nigeria and Adjacent Countries. Scheizerbart'sche Verlagsbuchhandlung, Stuttgart (1966).

Cooley, J.W. and Tukey, J.W. (1965). An Algorithm for the machine calculation of Complex Fourier Series. Mathematics of Computation, 19: 297 - 301.

Dobrin, B.D. (1976). Introduction to Geophysical Prospecting. Mc Graw - Hill Book Co. (3rd Ed). New York.

Falconer, J.D., (1911). The geology and geography of Nortwestern Nigeria. London (Mac Millan) Publishers.

Fedi, M., Quarta, T., and De Santis, A., (1997). Inherent power-law behavior of magnetic field power spectra from a spector and Grant ensemble. Geophysics, 62: 1143 - 1150.

Garcia-Abdeslem, J.G., and Ness, G.E., (1994). Inversion of the power spectrum from magnetic anomalies: Geophysics, 59: 391 - 401.

Gentleman, W.M. and Sande, G. (1966). Fast Fourier transforms for fun and profit. Proceedings of the Fall Joint Computer Conference, San Francisco. 563 - 578.

Grant, F., (1957). A problem in the analysis of geophysical data. Geophysics, 22 (2): 309 - 344.

Grant. F.S., and West. G.F., (1965). Interpretation theory in applied geophysics: McGraw - Hill Book Co. New York.

Grant, N.K. (1978). Structural distinction between a metasedimentary cover and an underlying basement in the 600 Ma. old Pan-African domain of northwestern Nigeria; West Africa. Bull. Soc. Am., 89: 50 - 58.

Green, R., (1960). Remanent Magnetization and the Interpretation of Magnetic Anomalies: Geophysical Prospecting. 8: 368 - 376

Hall, D.H. (1964). Magnetic and tectonic regionalization of Texada Island, British Columbia. Geophysics, 29: pp 565 - 581.

Henderson, R.G., and Zietz, I. (1949). The Computation of Second Vertical Derivative of Geomagnetic Fields. Mining Geophysics, (SEG, Tulsa): 606 - 614.

Horton, C.W., Hempkins, W.B and Hoffman, A.A.J. (1964). A Statistical Analysis of some Aeromagnetic maps from the Northern Canadian Shield. Geophysics, 24: 582 - 601.

Jacobs, J.A., (1967). The Earth's Magnetic Field. Mining Geophysics, 2: 424 - 436.

Japan International Cooperation Agency (J.I.C.A.) (1989). The study for groundwater development in Sokoto State: *Progress Report 2. pp 20 - 175.*

Jones, B., (1948). The Sedimentary rock of Sokoto Province. Bull. Geol. Survey of Nigeria, 18: 1 - 72.

Kangkolo, R., (1996). A detailed interpretation of the aeromagnetic field over the Mamfe Basin of Nigeria and Cameroon. Unpublished Ph.D. Thesis, Ahmadu Bello University, Zaria, Nigeria.

Kogbe, C. A., (1970). Preliminary notes on the geology of the Nigerian sector of the Iullemmeden Basin. Proc. Ist Conf. on African Geology. Ibadan.

_____, (1972). Preliminary study of the geology of the Nigerian sector of the Iullemmeden Basin. African Geology, Ibadan.

_____, (1979). Geology of the South Eastern (Sokoto) Sector of the Iullemmeden Basin. Bulletin Department of Geology Ahmadu Bello University Zaria, Nigeria. 2: No. 1.

_____, (1981). Cretaceous and Tertiary of the Iullemmeden Basin in Nigeria (West Africa) Cretaceous Research, 2: 129 - 186.

Kogbe,C.A. and Lemoigne, Y., (1976). Fossil wood from the Gundumi and Illo Formations (Continental Intercalaire) of northern Nigeria. Proc. 13th African Micropal. Coll., Ile - Ife, Nigeria.

Mc Curry, P., (1976). The geology of the precambrian to lower palaeozoic rocks of northern Nigeria - a review In: Kogbe, C.A. (e.d) Geology of Nigeria. Elizabeth Pub. Co. Lagos, Nigeria: 41 - 58.

Naidu, P.S. (1969). Estimation of spectrum and cross spectrum of aeromagnetic fields using fast digital Fourier transform, (FDFT) techniques. Geophysical Prospecting., 17: 344 - 361.

_____, (1970a). Fourier Transform of large scale aeromagnetic field using modified version of Fast Fourier transform, Pure appl. Geophys, 81: 17 - 25.

_____, (1970b). Statistical structure of aeromagnetic field, Geophysics, 35: 279 - 292.

Negi, J.G., Agrawal, P.K. and Rao, K.N.N. (1983). Three-Dimensional Model of the Koyna Area of Maharashtra State (India) based on the Spectral Analysis of Aeromagnetic Data. Geophysics, 48: 964 - 974.

Nettleton, L.L., (1954). Regionals, Residuals and Structure, Geophysics, 19 (1): 1 - 22.

Nwogbo, P.O. (1987). Spectral Analysis and Interpratation of Aeromagnetic Anomalies over the Upper Benue Trough, Nigeria. Unpublished M.Sc. Thesis, Ahmadu Bello University, Zaria, Nigeria.

Odeyemi, I.B (1988). Lithostratigraphy and structural relationships of the Upper Precambrian metasediments in Igarra area, Southwestern Nigeria. In: Oluyide, P.O. (Ed.) Precambrian Geology of Nigeria - Geological Survey Nigeria, Kaduna, pp. 111 - 125.

Ogezi, A.E.O. (1977). Geochemistry and geochronology of basement rock from north-western Nigeria. Unpublished Ph.D. Thesis, Leeds University.

Ojo, S.B., and Kangkolo, R. (1995). Shortcomings in the determination of regional fields by polynomial fitting: A simple solution. Journal of Applied Geophysics, 36: 205 - 212.

Oldham, C.H.G. and Sutherland, D.B., (1955). Orthogonal Polynomials: Their use in estimating the regional Effects. Geophysics, 20(2): 295 - 306.

Osazuwa, I.B., (1985) The establishment of a primary gravity network of Nigeria. Unpublished Ph.D Thesis, Ahmadu Bello University Zaria-Nigeria.

Oteze,G.E., (1976). The Hydrogeology of the N.W Nigerian Basin In: Ed. C.A Kogbe. Geology of Nigeria, 373-390. Ibadan.

Oyawoye, M.O. (1964). The geology of the Nigerian basement complex. J. Mining Geol. and Metals. Soc. 1: 87 - 102.

Pal, P.C., Khurana, K.K. and Unnikrishnan, P. (1978). Two examples of Spectral Approach to Source Depth Estimation in Gravity and Magnetics. PAGEOPH, 117: 772 - 783.

Peters, S., (1976). The marine maastrichtian and palaeocene sediments (of northwestern Nigeria). The Dukamaje Formation and the Sokoto Group. Geological Guide to some Nigerian Cretaceous Recent Localities: 7th African Micropal. Coll. Ille - Ife, Nigeria. pp. 75 - 87.

Raeburn, C., and Tattam, C.M. (1930). A preliminary note on sedimentary rocks of Sokoto Province. Bull Geol. Survey of Nigeria 13: 57 - 60.

Reford, M.S. and Sumner, J.S. (1964). Aeromagnetics: review article. Geophysics, 29: 482 - 516.

Reyment, R.A., (1965). Aspects of the Geology of Nigeria. Ibadan University Press.

Sambo, S.O., (1994). Spectral Analysis and interpretation of aeromagnetic anomalies over Sokoto Basin, Nigeria. Unpublished M.Sc. Thesis Ahmadu Bello University, Zaria, Nigeria.

Sheriff, R.E., and Geldart, L.P. (1983). Data - Processing and Interpretation. Exploration Seismology 2: 34pp. Cambridge University Press.

Shuey, R.T., Schellinger, D.K., Tripp, A.C., and Alley, L.B., (1977). Curie depth determination from aeromagnetic spectra. Geophys. J. Roy Astr. Soc., 37: 75 - 102.

Skeels, D.C. (1967). What is Residual Gravity? Geophysics, 32: 872 - 876.

Spector, A. and Grant, F.S. (1970). Statistical models for interpreting aeromagnetic data, Geophysics, 35: 293 - 302.

Umego, M.N. (1990). Structural interpretation of gravity and aeromagnetic anomalies over Sokoto Basin,Northern Nigeria. Unpublished Ph.D. Thesis, Ahmadu Bello University, Zaria, Nigeria.

Uwa, E.J. (1984). Investigation of radiometric anomalies by nuclear and other methods: A case study of the Sokoto Basin of Nigeria. Unpublished Ph.D Thesis. Ahmadu Bello University, Zaria, Nigeria.

Vacquier, V., Steenland, N.C., Henderson, R.G., and Zietz, I., (1951). Interpretation of aeromagnetic maps. Geol. Soc. America memoirs 47.

Wright, J.B., (1968). South Atlantic continental drift and the Benue Trough. Tectonophysics, 61: 363 - 379.

Wright, J.B., (1976). Fracture systems in Nigeria and initiation of fracture zones in the South Atlantic. Tectonophysics, 34: T43 - T47.

Wright, J.B., Hastings, D.A., Jones, W.B. and Williams, H.R. (1985). Geology and Mineral Resources of Africa. George allen and Urwin, London. 90 - 120.

APPENDIX 1

Fundamentals of Spectral Analysis

A periodic function f(x) of the independent variable x, the dimension of which is length, may be expressed as a Fourier series in the following way

$$f(x) = \frac{a_o}{2} + \sum_{n=1}^{\infty} (a_n \cos nwx + b_n \sin nwx) \quad \ldots\ldots\ldots\ldots\ldots \quad (1)$$

where w is the fundamental angular frequency given by $w = 2\pi / x$, x being the total length of x over which f(x) has been measured. The coefficients a_n and b_n are given by

$$a_n = \frac{2}{X} \int_{-\frac{X}{2}}^{\frac{X}{2}} f(x) \cos nwx \, dx \quad \ldots\ldots\ldots\ldots\ldots\ldots\ldots \quad (2)$$

$$b_n = \frac{2}{X} \int_{-\frac{X}{2}}^{\frac{X}{2}} f(x) \sin nwx \, dx \quad \ldots\ldots\ldots\ldots\ldots\ldots\ldots \quad (3)$$

Expressed in the exponential form, equation (1) may be written as,

$$f(x) = \sum_{n=-\infty}^{\infty} F(n) \exp(jnwx) \quad \ldots\ldots\ldots\ldots\ldots\ldots \quad (4)$$

$$F(n) = \frac{1}{X} \int_{-\frac{X}{2}}^{\frac{X}{2}} f(x) \exp(-jnwx)\, dx \quad \ldots\ldots\ldots\ldots\ldots \quad (5)$$

where F(n) is the complex line spectrum of f(x). When the period x is allowed to tend to infinity, the function f(x) begins to approach an aperiodic function or a transient function which contains all possible frequencies. In such a case the summation sign in the series in equation (4) is replaced by an integral and equation (4) reduces to

$$f(x) = \frac{1}{2\pi} \int_{-\infty}^{\infty} \exp(jwx)\, dw \int_{-\infty}^{\infty} f(\sigma) \exp(-jw\sigma)\, d\sigma \quad \ldots\ldots\ldots\ldots \quad (6$$

The reciprocal relations for f(x) in equation 4 may be written as

$$F(w) = \int_{-\infty}^{\infty} f(x) \exp(-jwx)\, dx \quad \ldots\ldots\ldots\ldots\ldots\ldots \quad (7)$$

$$f(x) = \frac{1}{2\pi} \int_{-\infty}^{\infty} F(w) \exp(jwx)\, dx \quad \ldots\ldots\ldots\ldots\ldots\ldots \quad (8)$$

From equation (8) it is evident that the aperiodic function f(x) may be thought of as a synthesis of an infinite

aggregate of sinosoids e^{jwx} of all angular frequencies w in the continuous infinite range $(-\infty , \infty)$ having a complex amplitude F(w) (Bhattacharyya, 1966). This function F(w) is a complex continuous spectrum of the aperiodic function f(x). The relations equation (7) and equation (8) may be written as the Fourier transforms.

When the theory of Fourier transforms is extended to the two dimensional case, equations (7) and (8) may be written as

$$G(u,v) = \int_{-\infty}^{\infty}\int_{-\infty}^{\infty} g(x,y)\, \exp\left(-j(ux+vy)\right) dxdy \quad \ldots\ldots\ldots\ldots \quad (9)$$

$$g(x,y) = \frac{1}{4\pi^2}\int_{-\infty}^{\infty}\int_{-\infty}^{\infty} G(u,v)\, \exp\left(j(ux+vy)\right) dudv \quad \ldots\ldots \quad (10)$$

where u and v are the angular frequencies in the x and y - directions, respectively.

G(u,v) is, in general, complex and contains information on the amplitude and phase relationships about all the frequencies that make up the two-dimensional function g(x,y). G(u,v), when broken up into its real and imaginary parts, is given by

$$G(u,v) = P(u,v) + jQ(u,v) \quad \ldots\ldots\ldots\ldots\ldots\ldots \quad (11)$$

The amplitude density spectrum, or simply amplitude spectrum, of G(u,v) is

$$A(u,v) = G(u,v) = \sqrt{(P^2+Q^2)} \qquad \ldots\ldots\ldots\ldots \qquad (12)$$

and its phase density spectrum, or simply phase spectrum, is

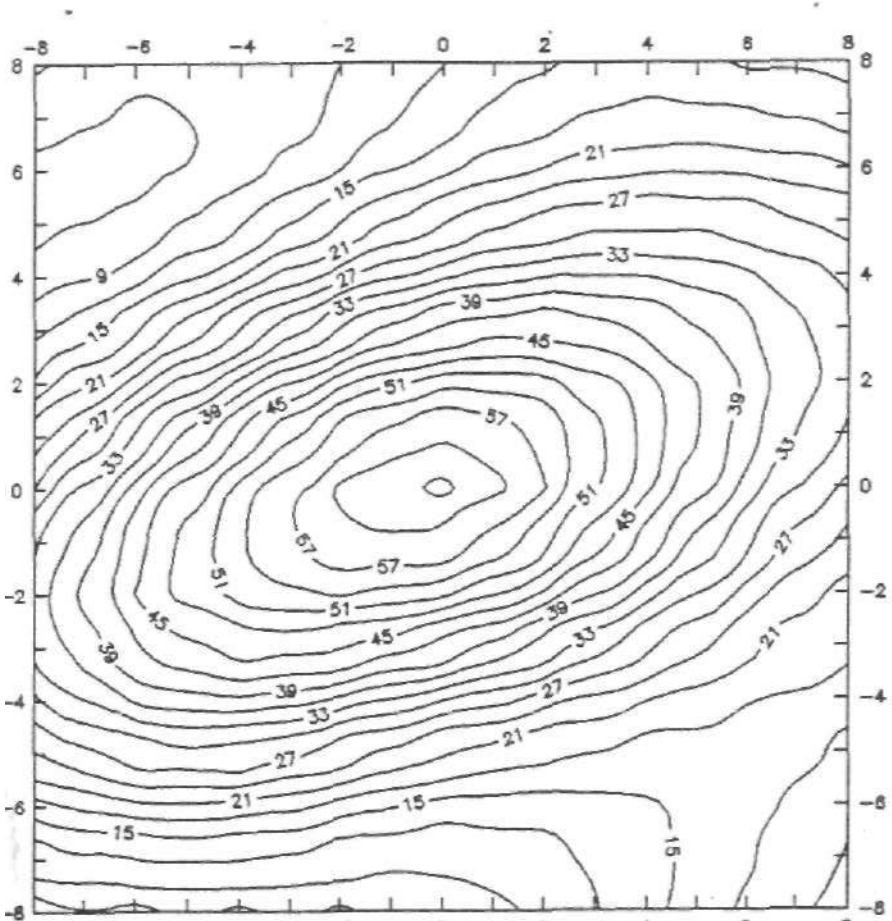
$$\theta(u,v) = \arctan\left(\frac{Q}{P}\right) \qquad \ldots\ldots\ldots\ldots\ldots\ldots\ldots \qquad (13)$$

The energy density spectrum, or simply the energy spectrum, is

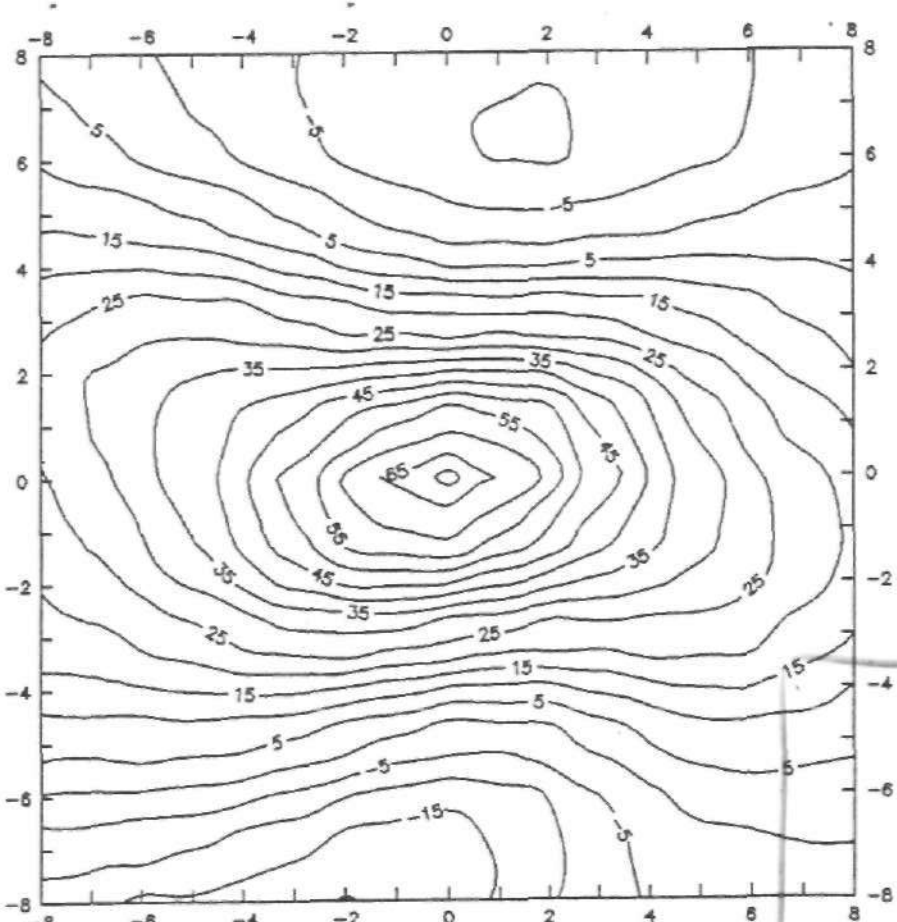
$$E(u,v) = [G(,v)]^2 = P^2+Q^2 \qquad \ldots\ldots\ldots\ldots \qquad (14)$$

APPENDIX 2

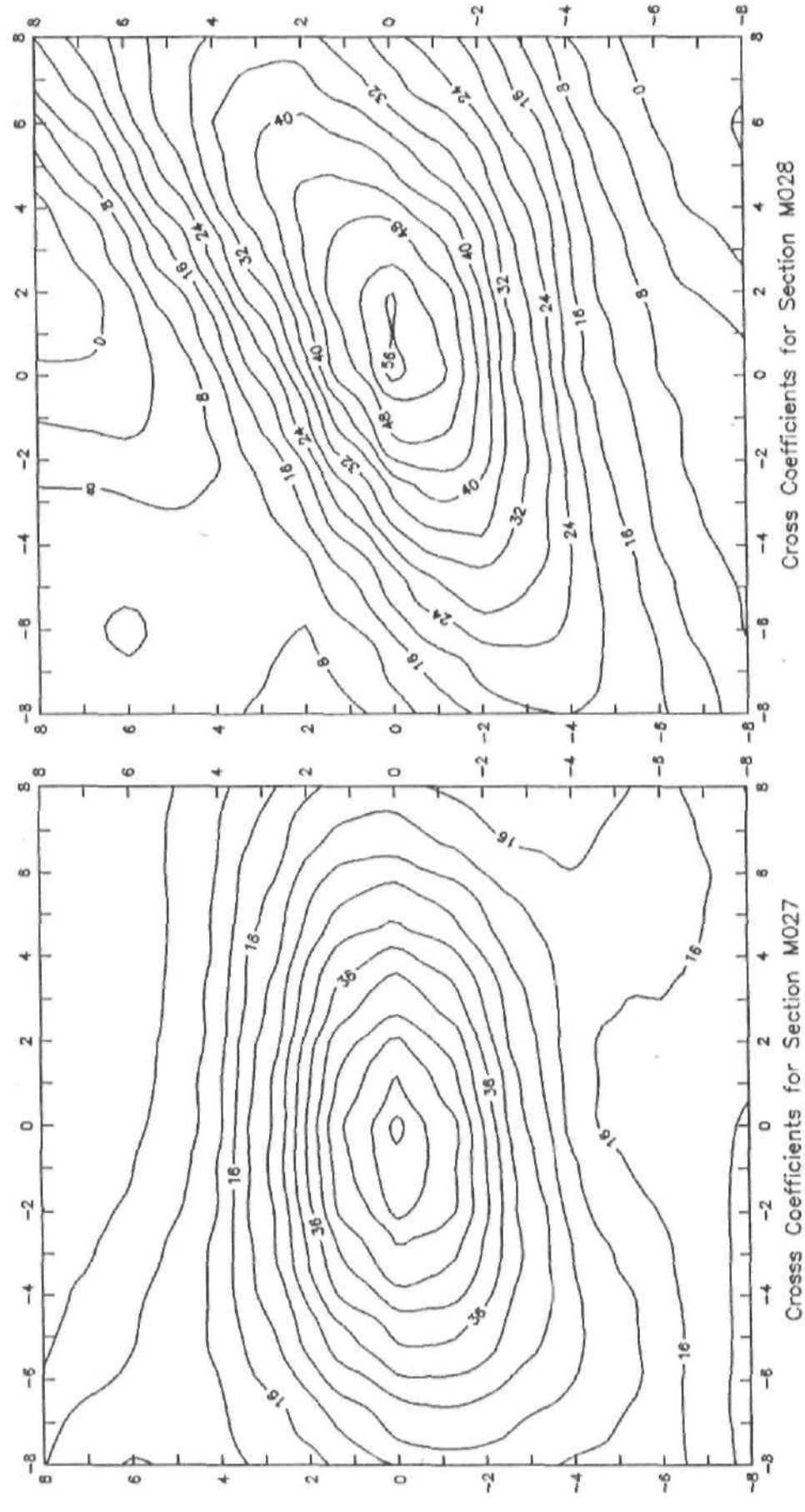
CROSSCORRELATION COEFFICIENT MAPS

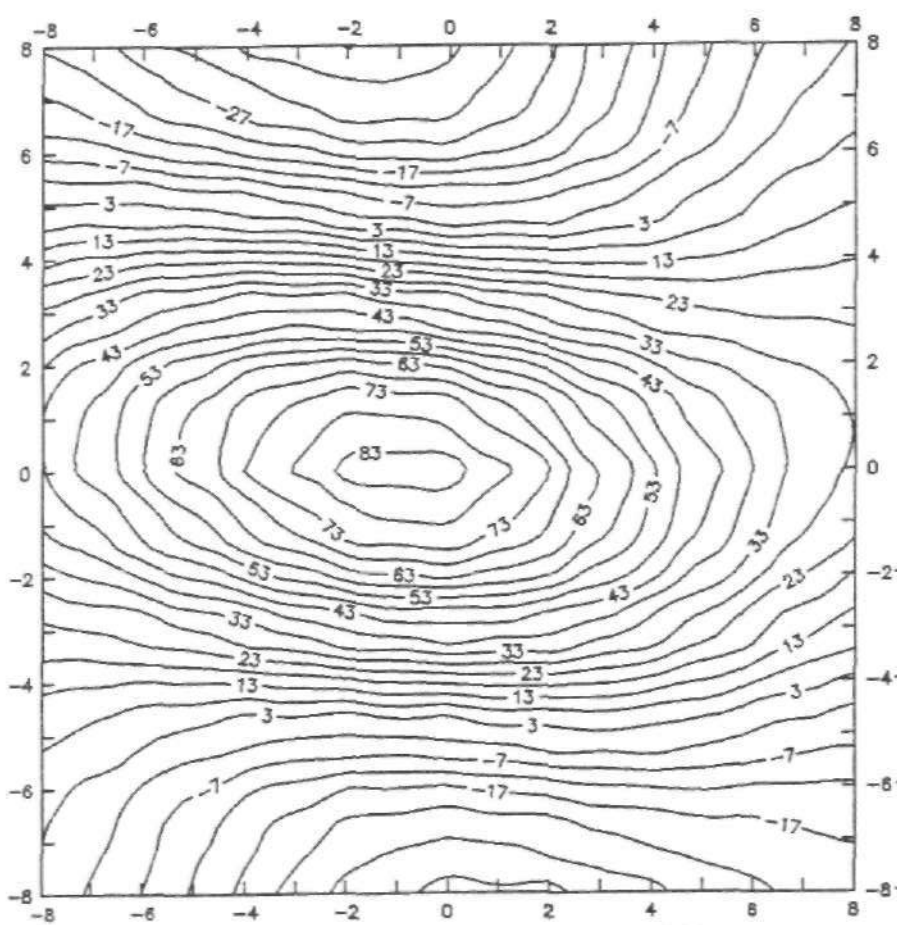


Cross Coefficients for Section M011

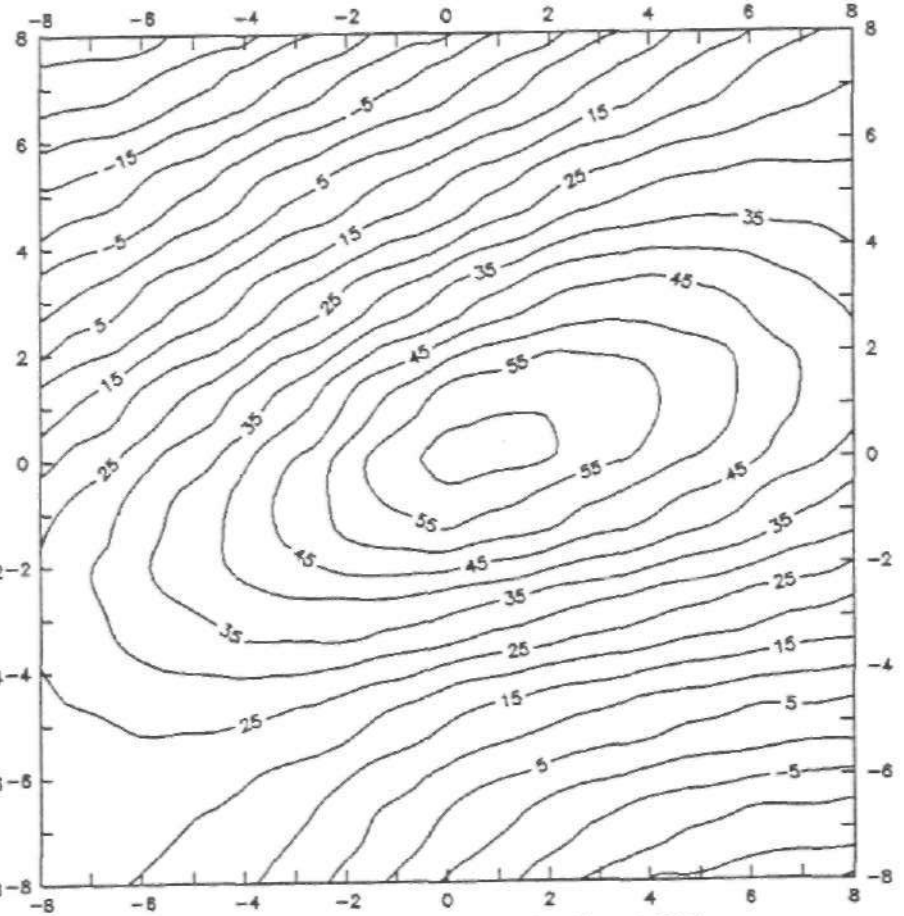


Cross Coefficients for Section M012

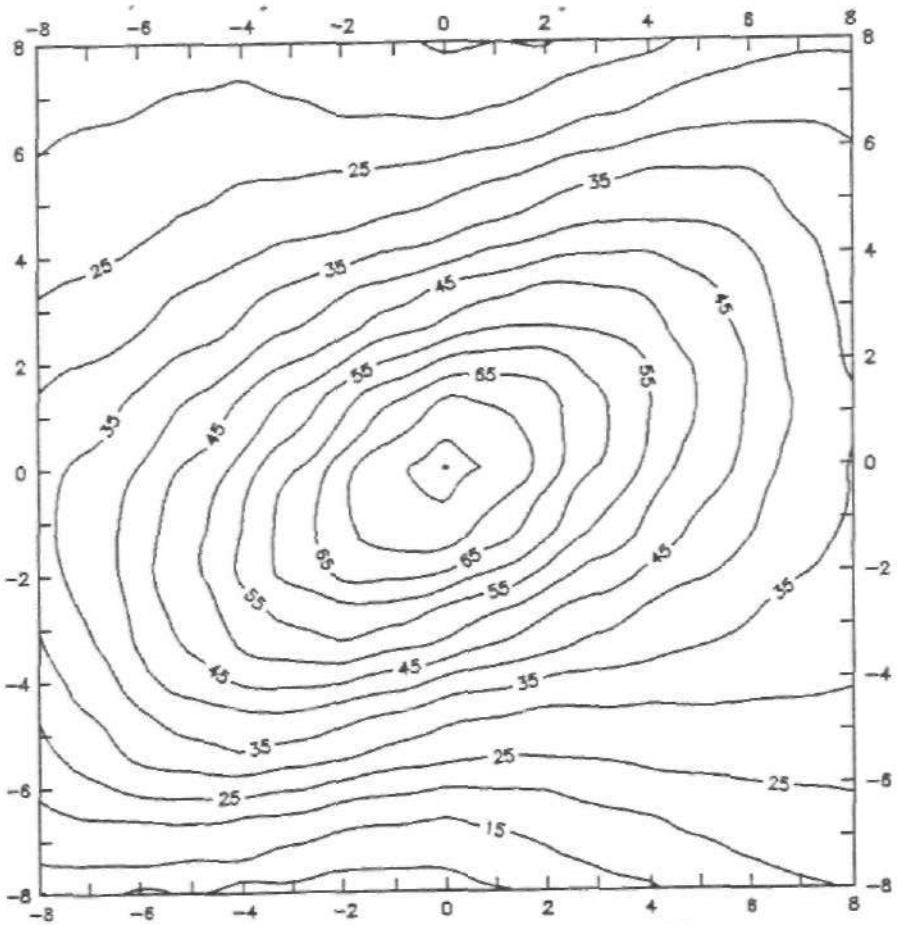

Cross Coefficients for Section M028
Crosss Coefficients for Section M027



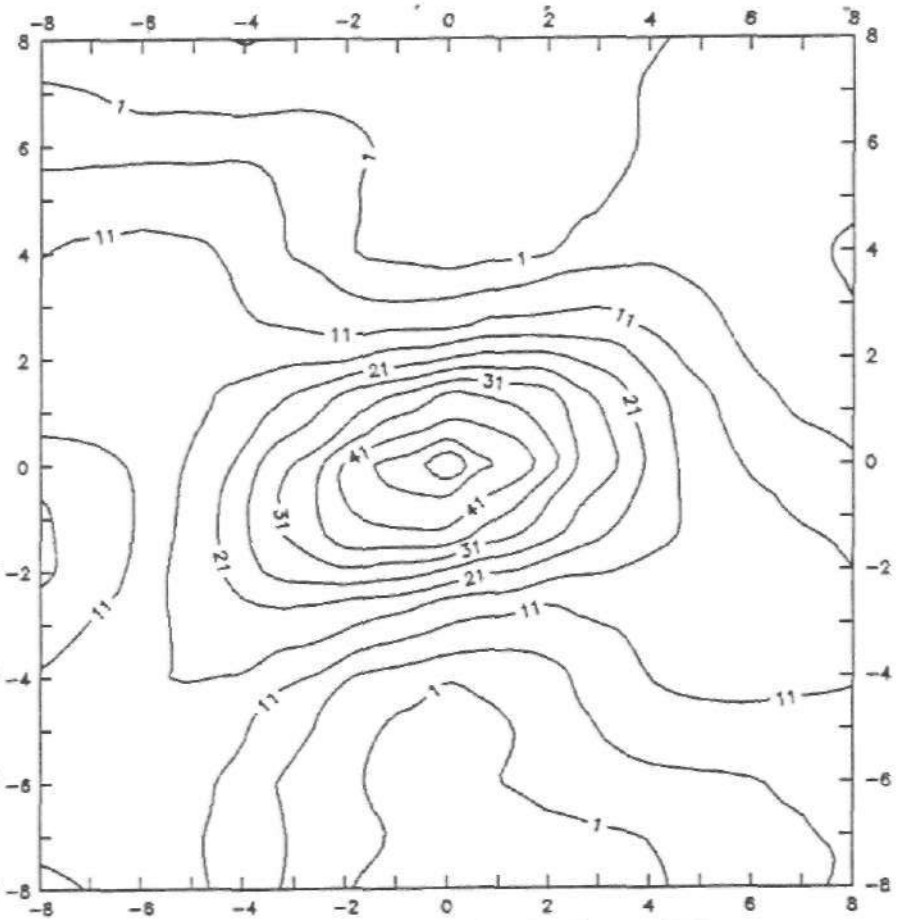
Cross Coefficients for Section M029



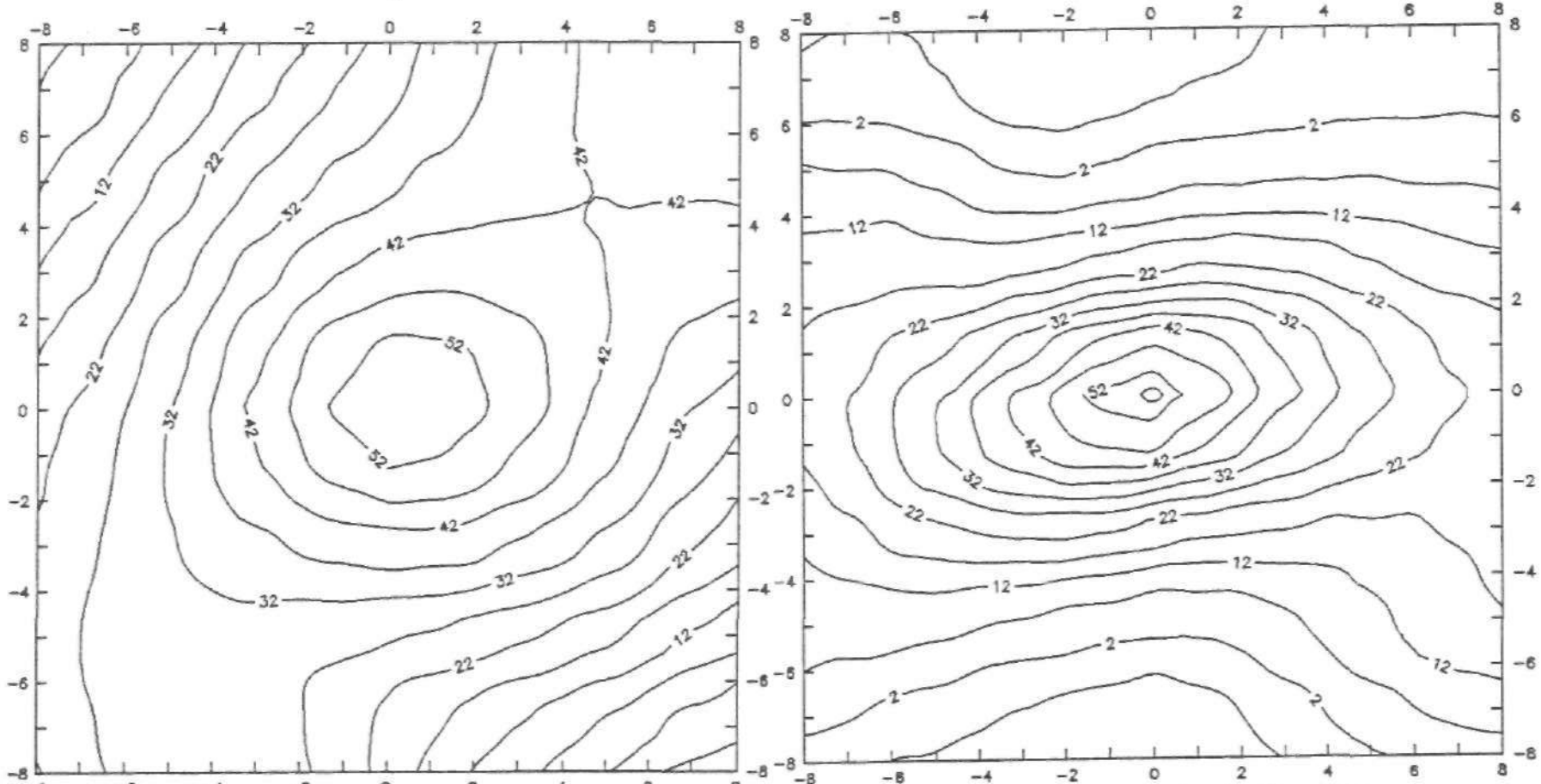
Cross Coefficients for Section M030

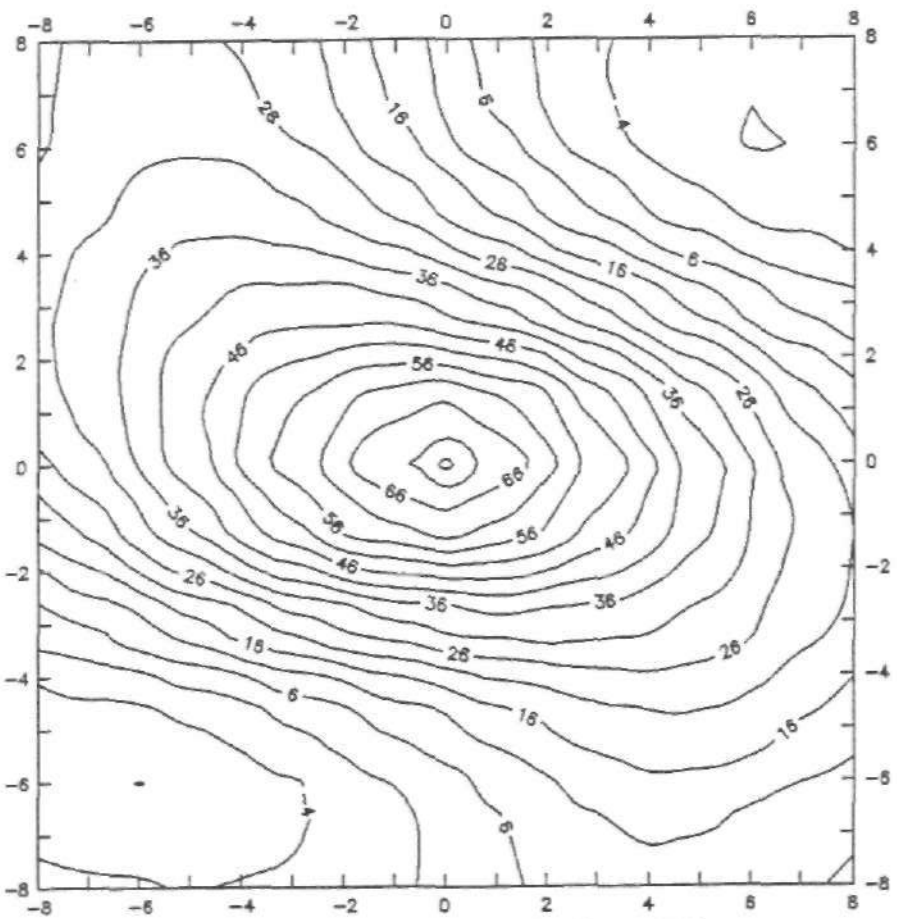


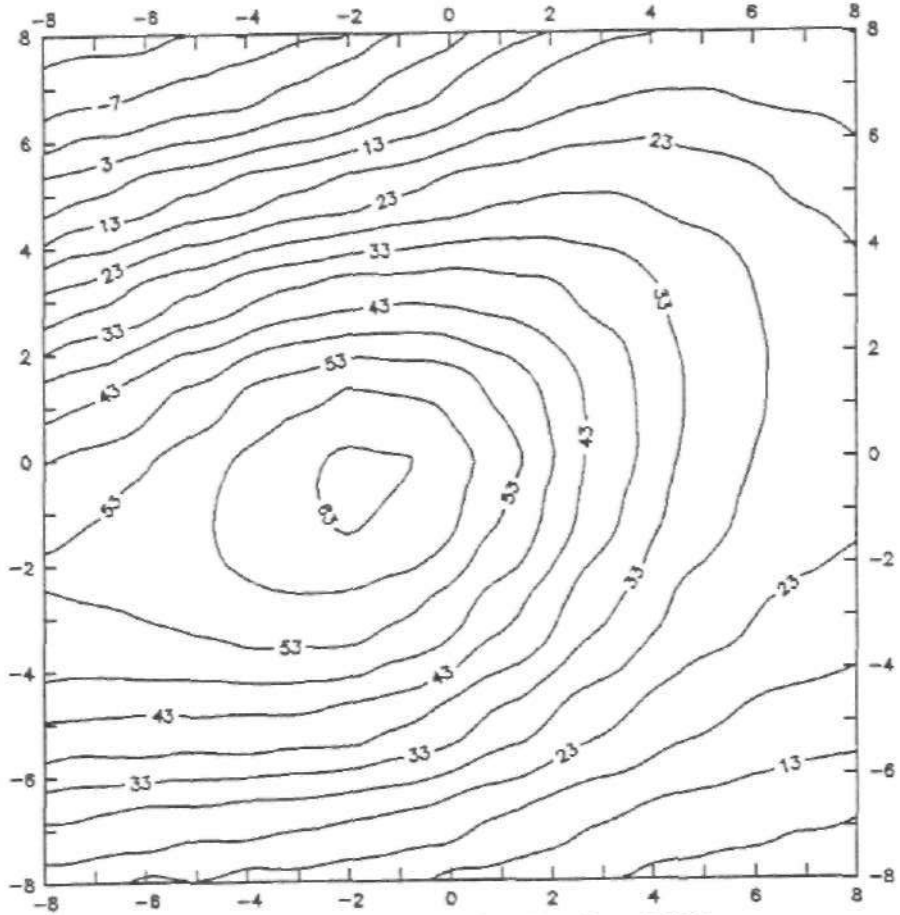
Cross Coefficients for Section M031

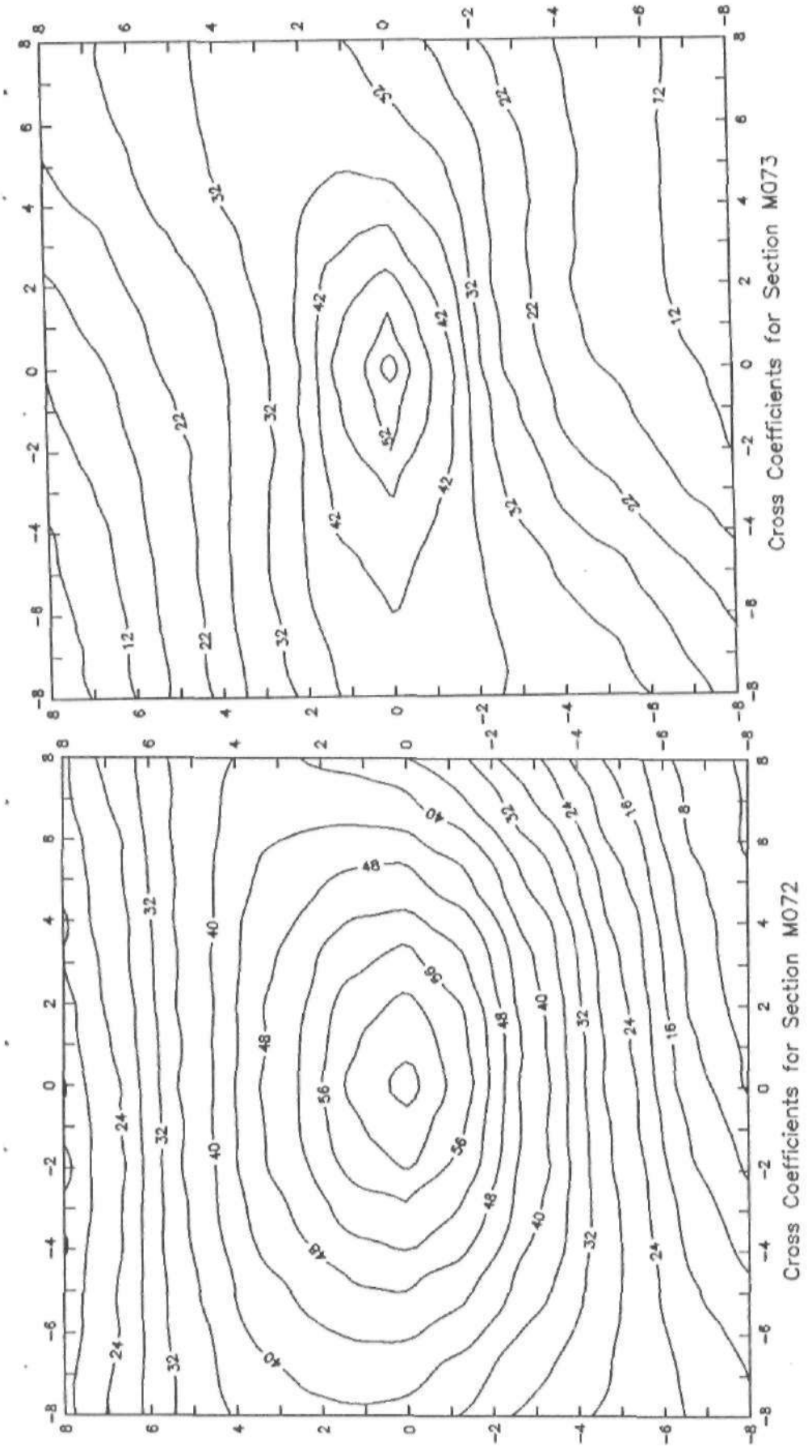


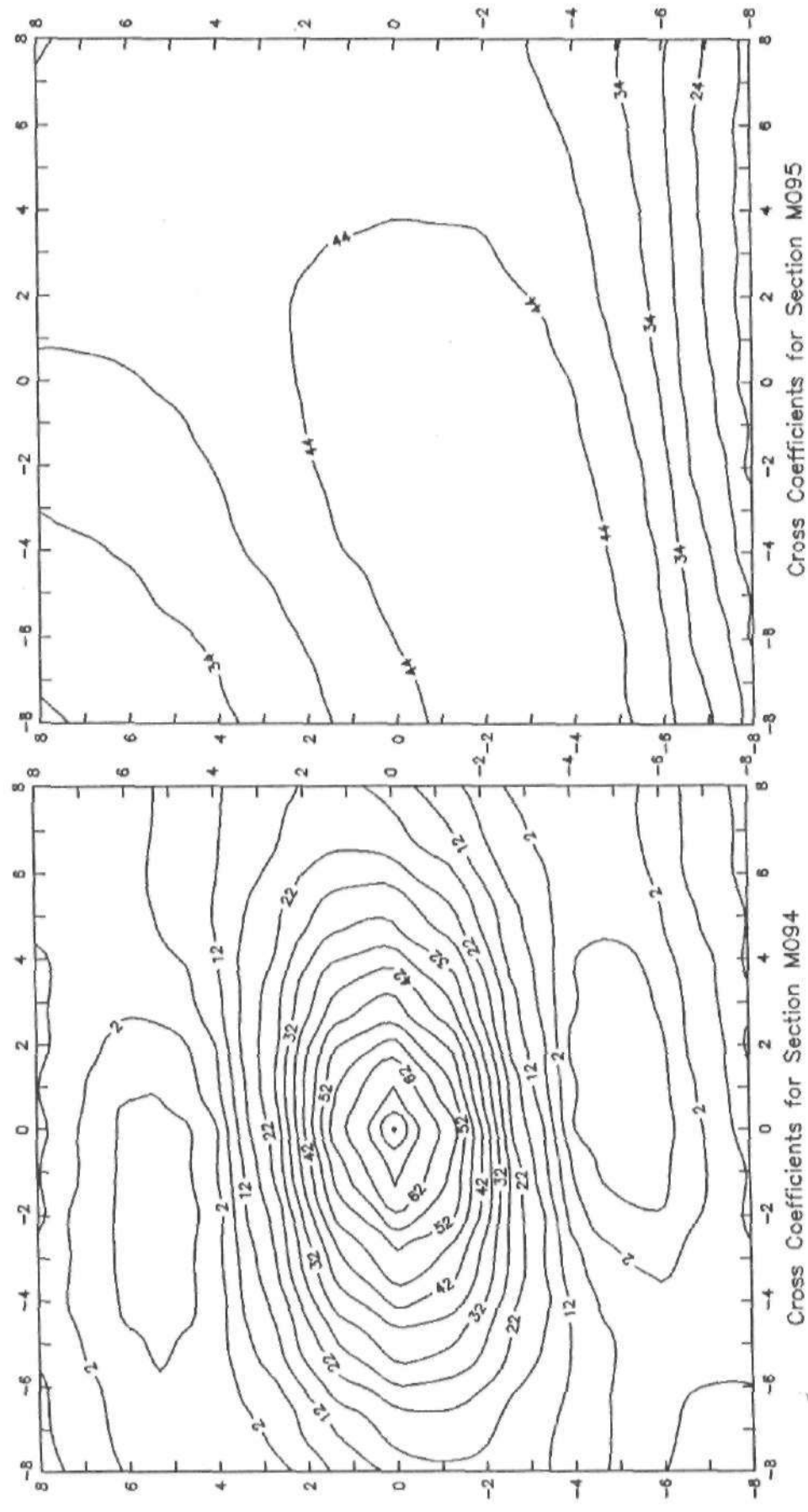
Cross Coefficients for Section m049


Cross Coefficients for Section M050
Cross Coefficients for Section M051


Cross Coefficients for Section M052

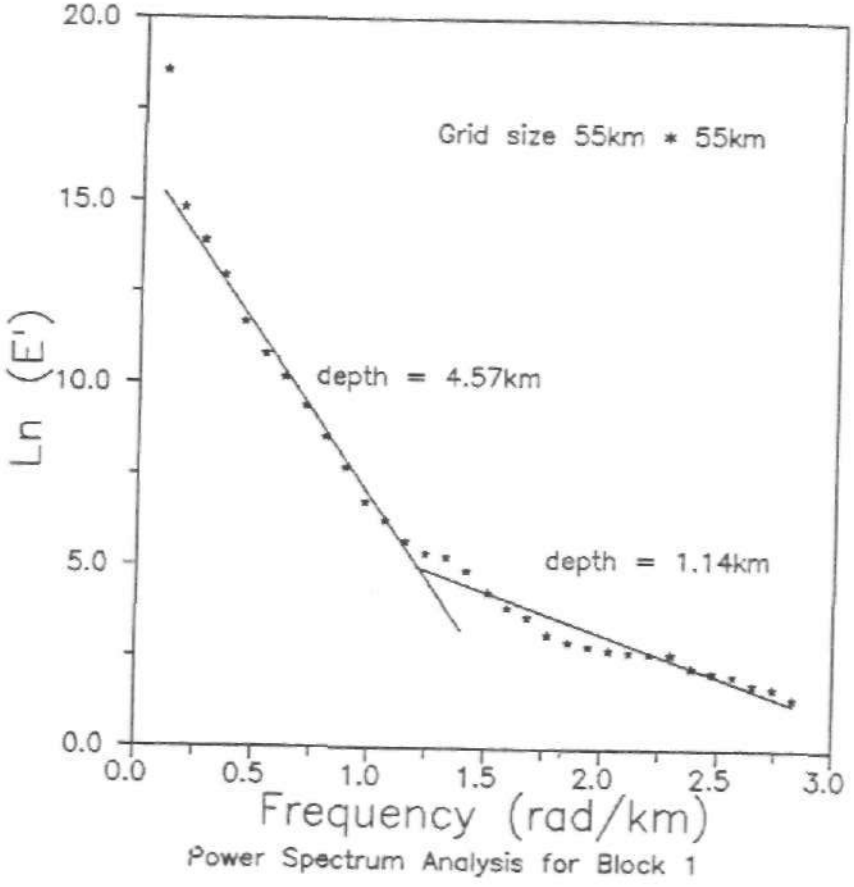

Cross Coefficients for Section M071


Cross Coefficients for Section M073
Cross Coefficients for Section M072

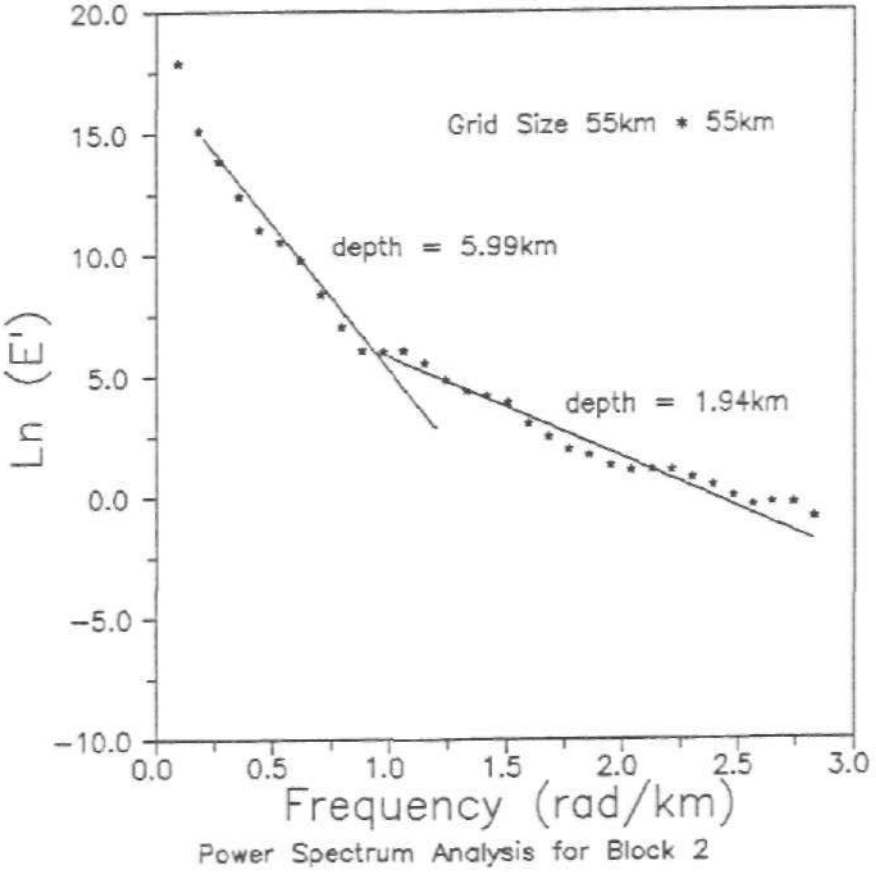

Cross Coefficients for Section M095
Cross Coefficients for Section M094

APPENDIX 3

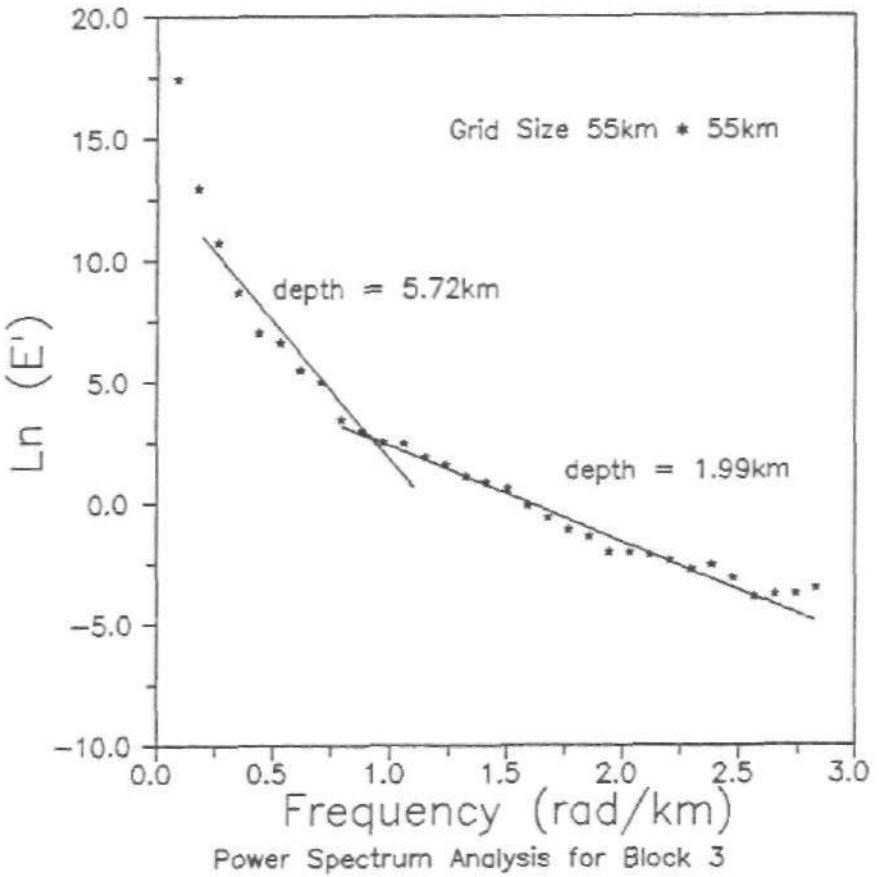
POWER SPECTRUM ANALYSIS



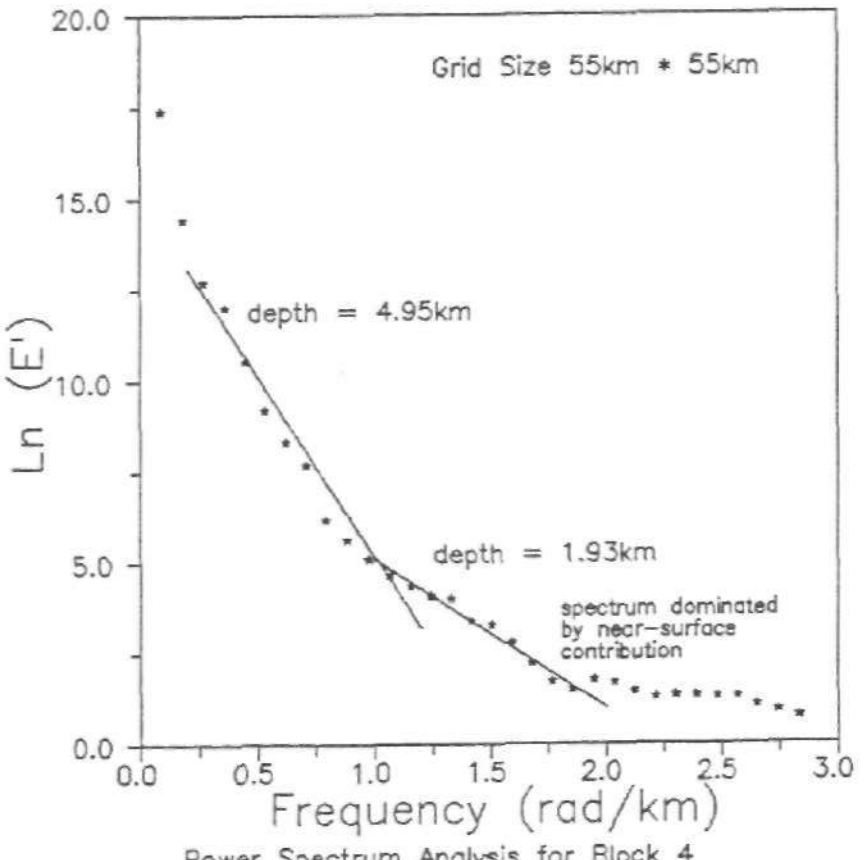
Power Spectrum Analysis for Block 1



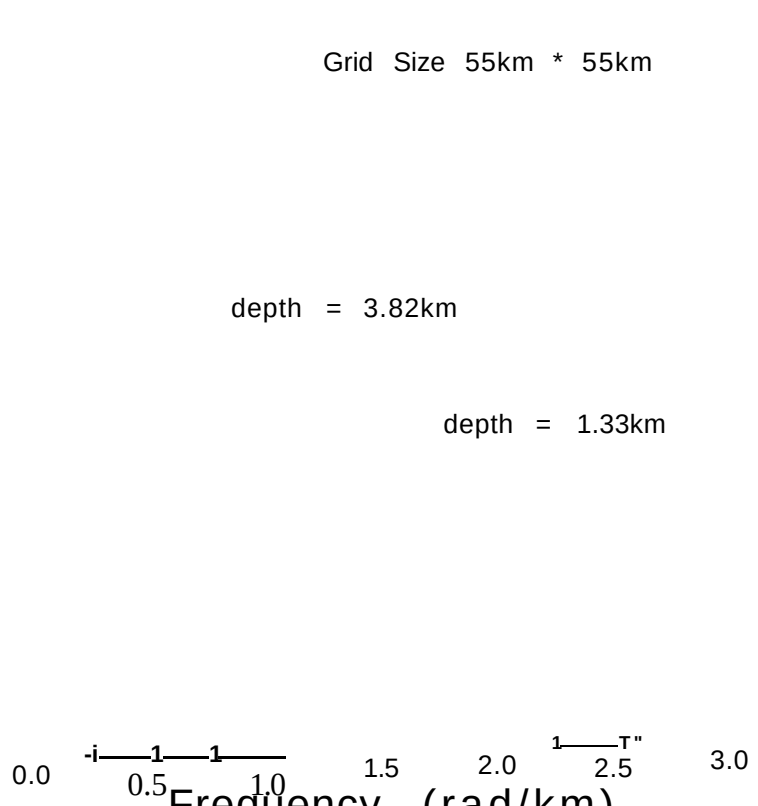
Power Spectrum Analysis for Block 2



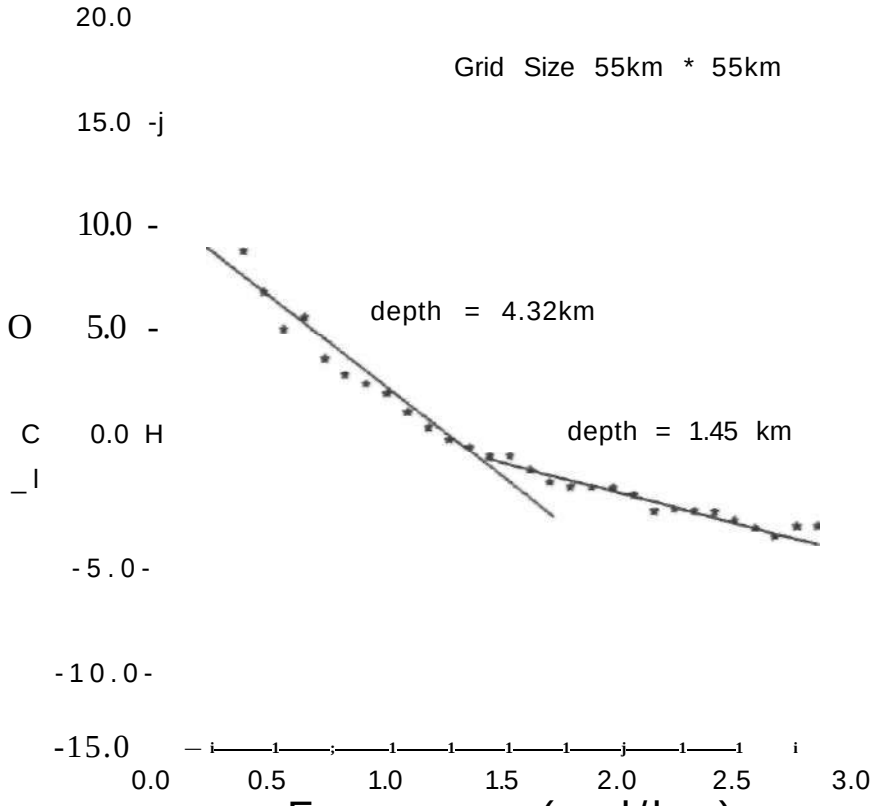
Power Spectrum Analysis for Block 3



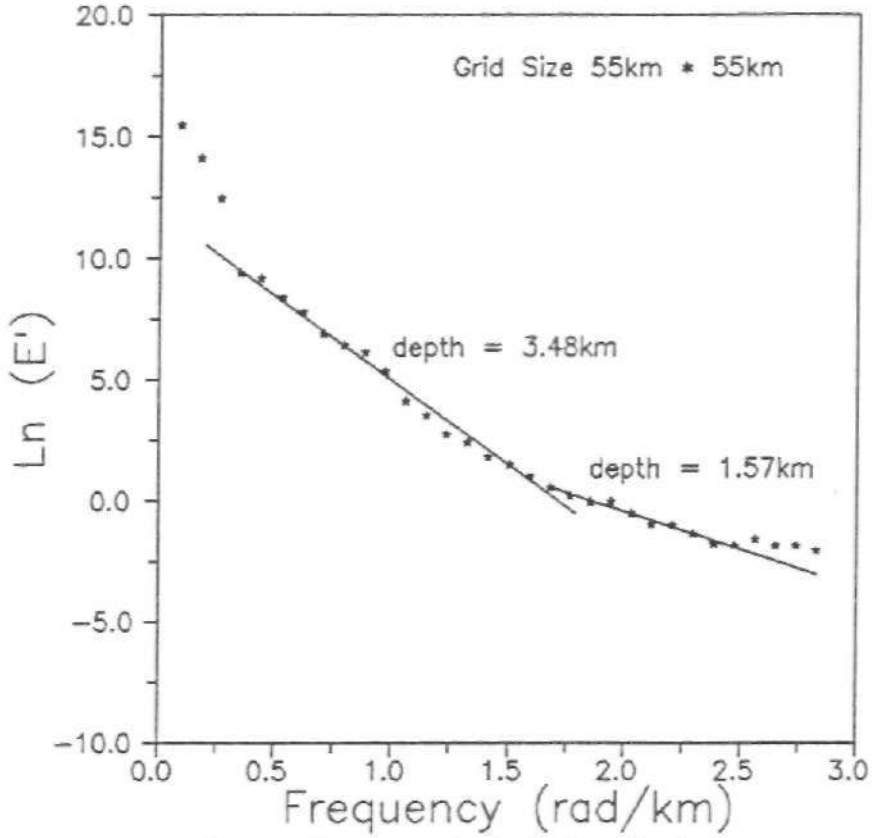
Power Spectrum Analysis for Block 4



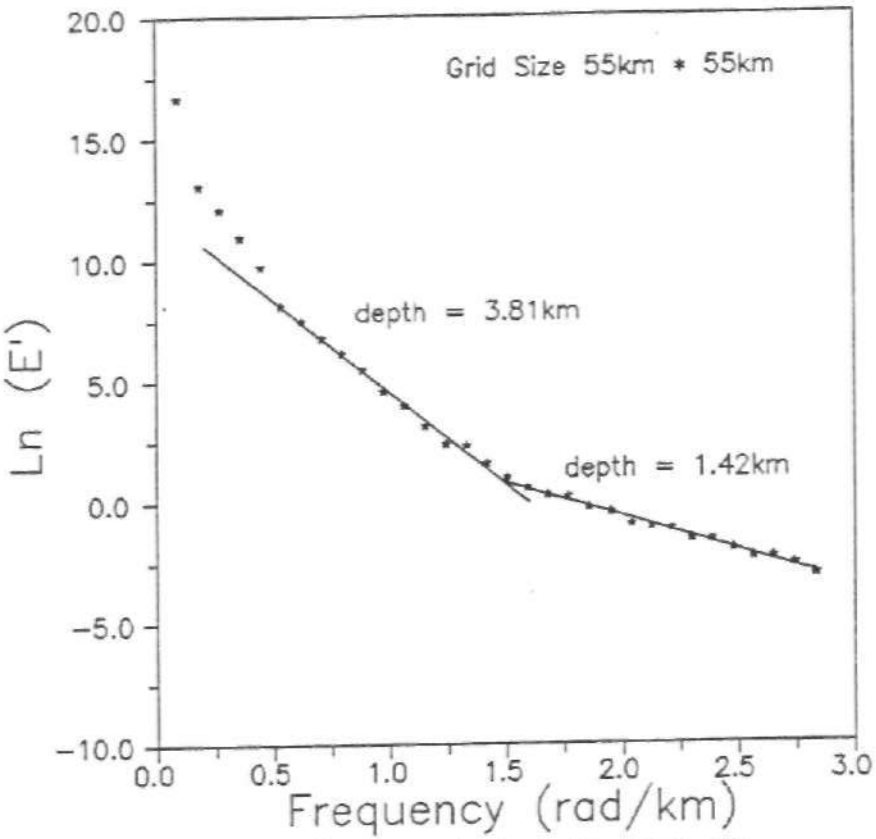
Power Spectrum Analysis for Block 7



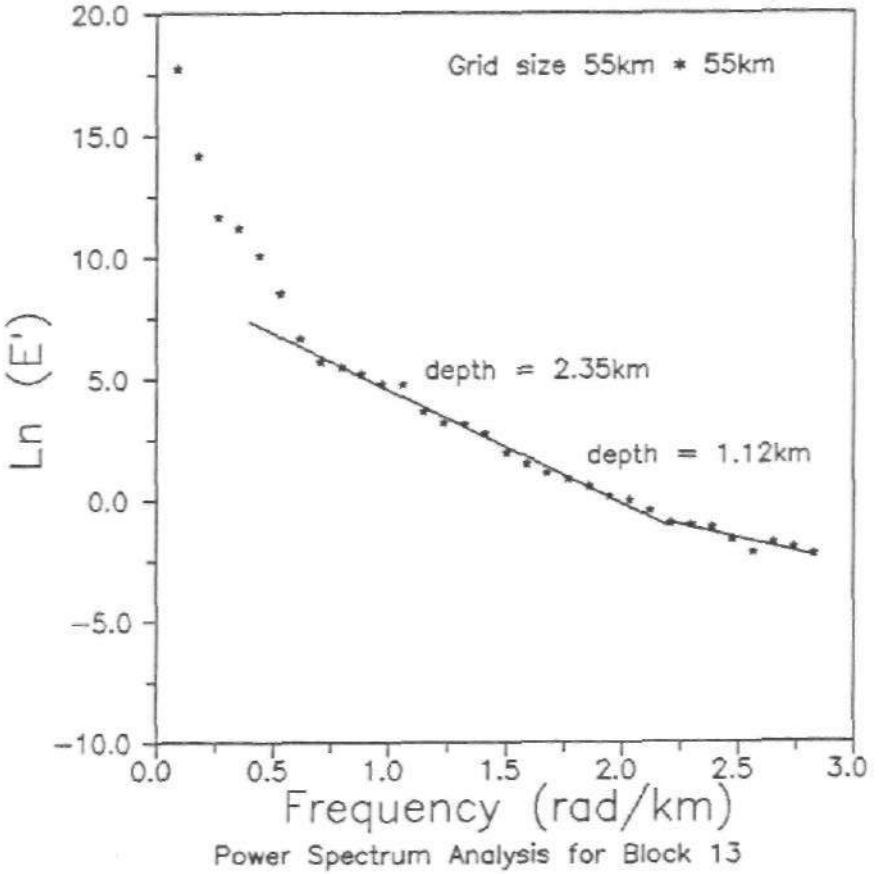
Power Spectrum Analysis for Block 8



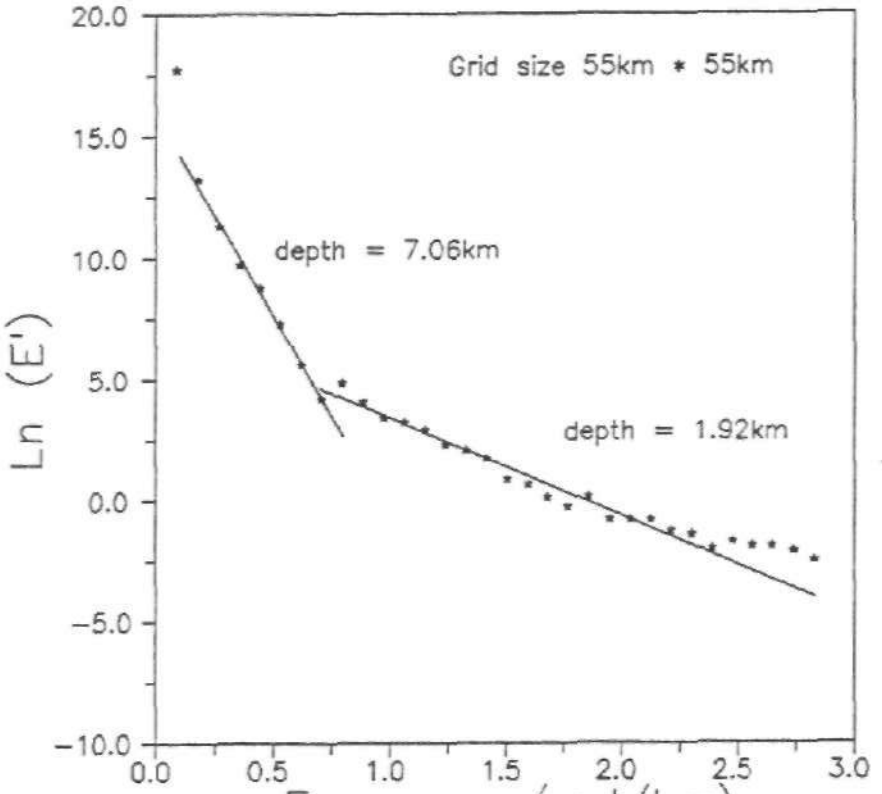
Power Spectrum Analysis for Block 9



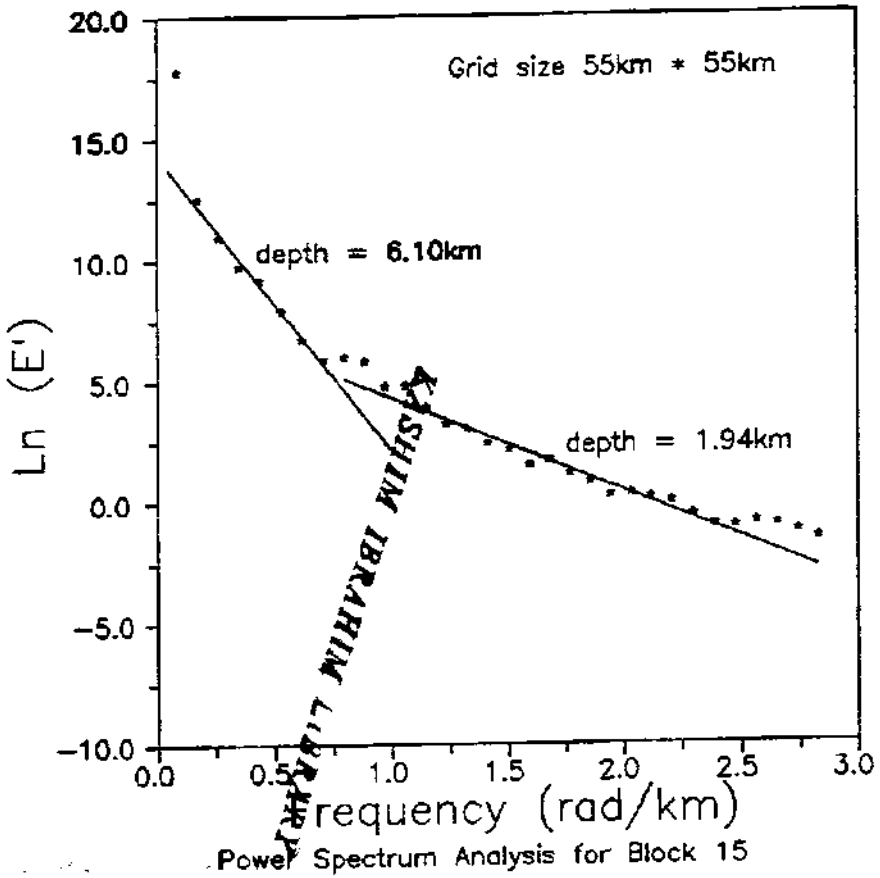
Power Spectrum Analysis for Block 10



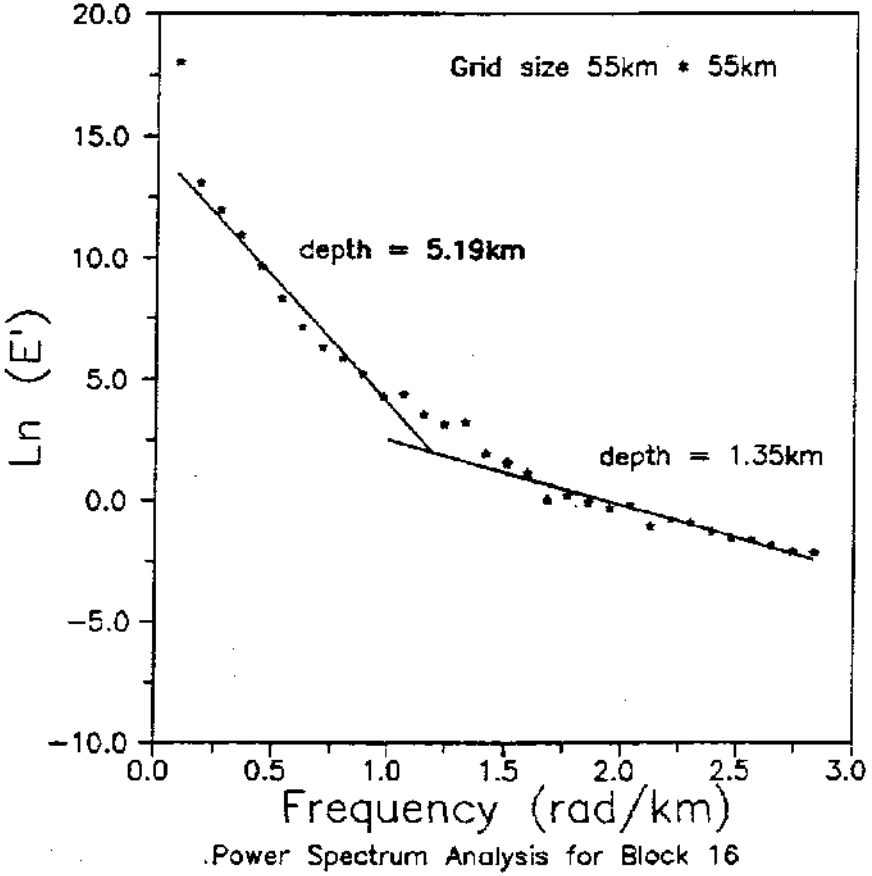
Power Spectrum Analysis for Block 13



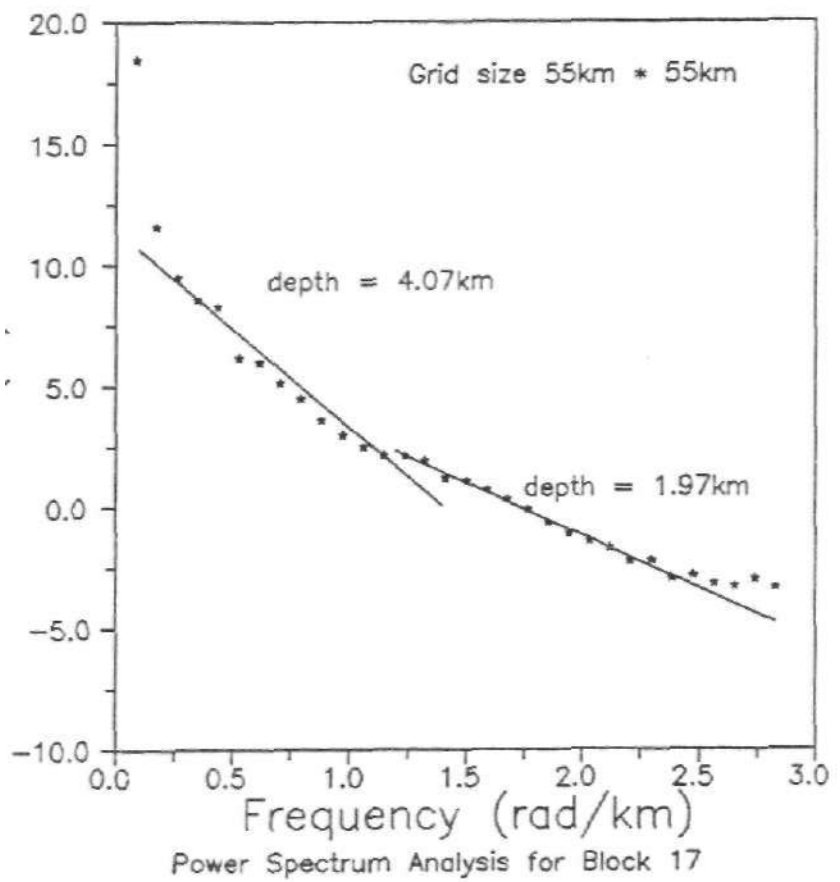
Power Spectrum Analysis for Block 14



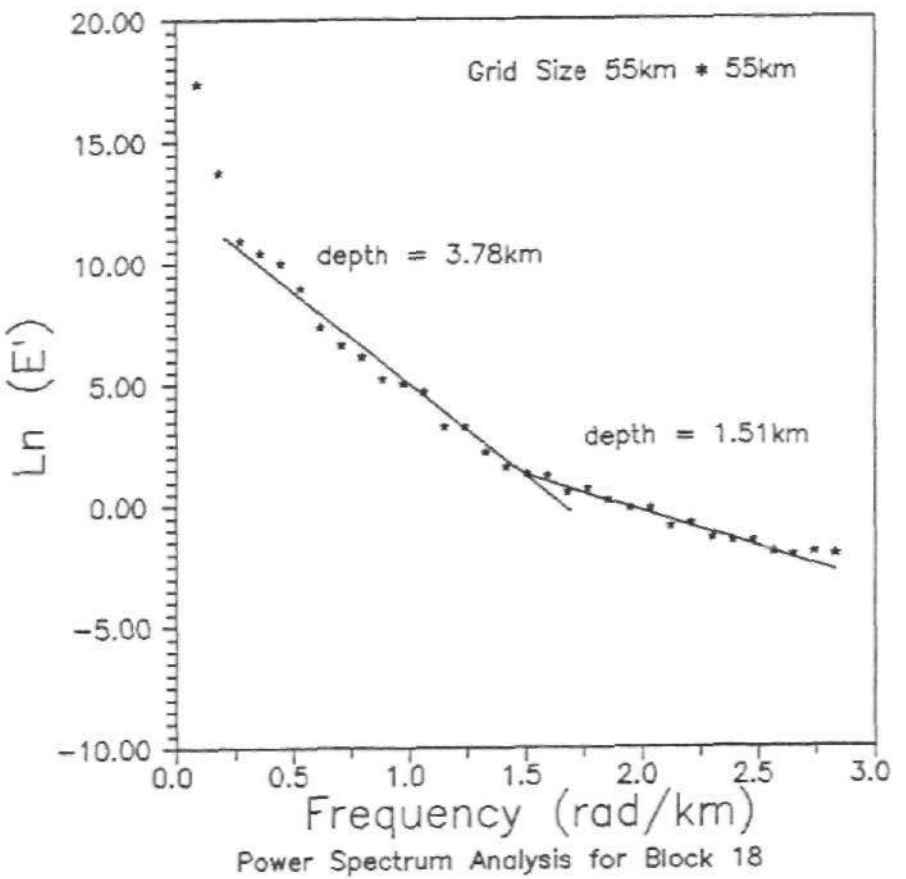
Power Spectrum Analysis for Block 15



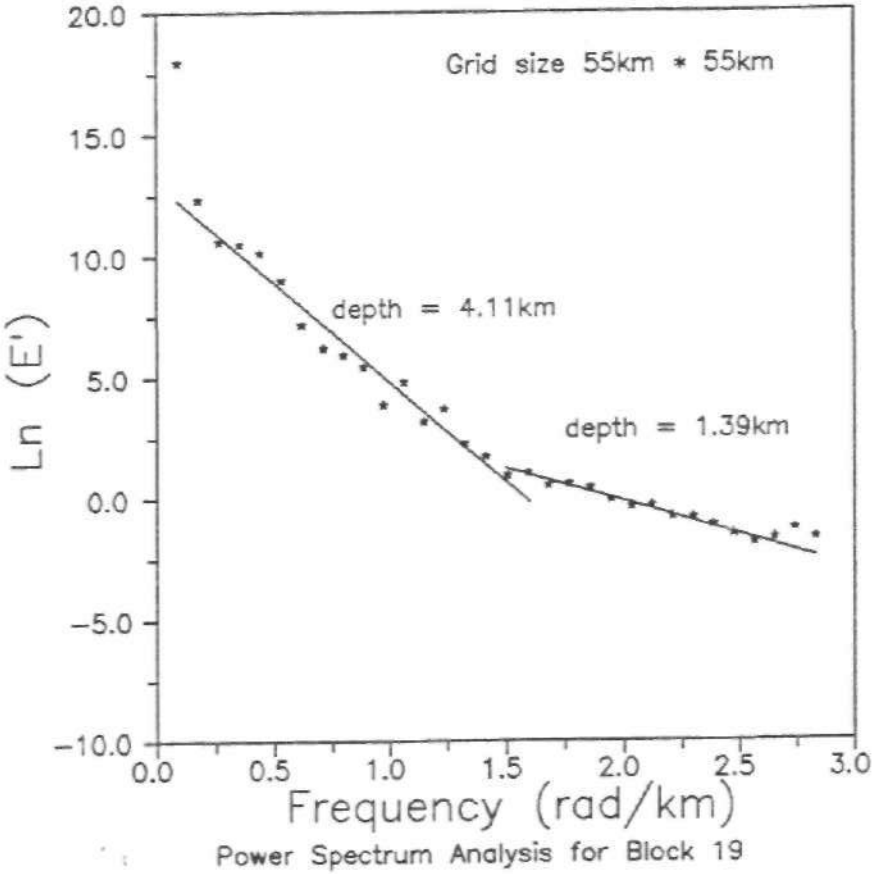
Power Spectrum Analysis for Block 16



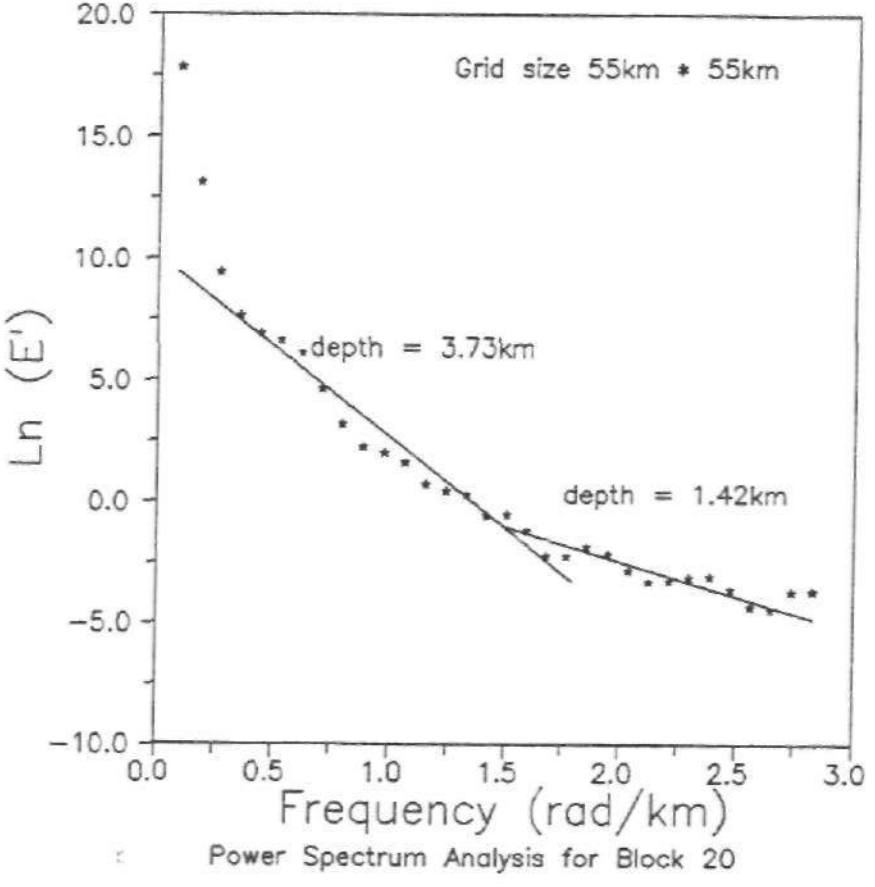
Power Spectrum Analysis for Block 17



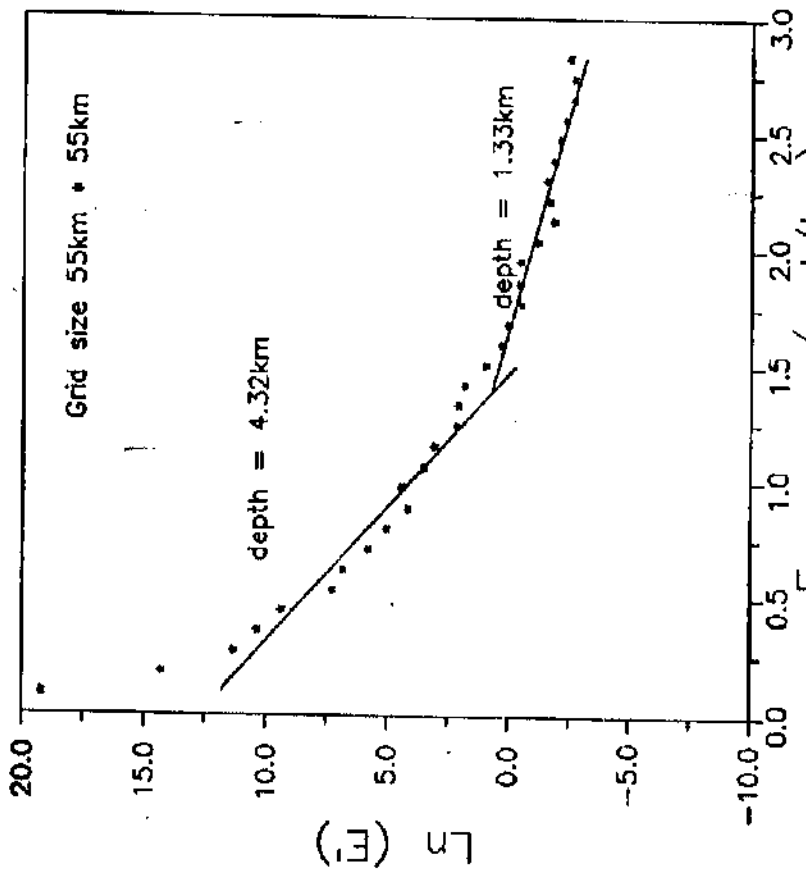
Power Spectrum Analysis for Block 18



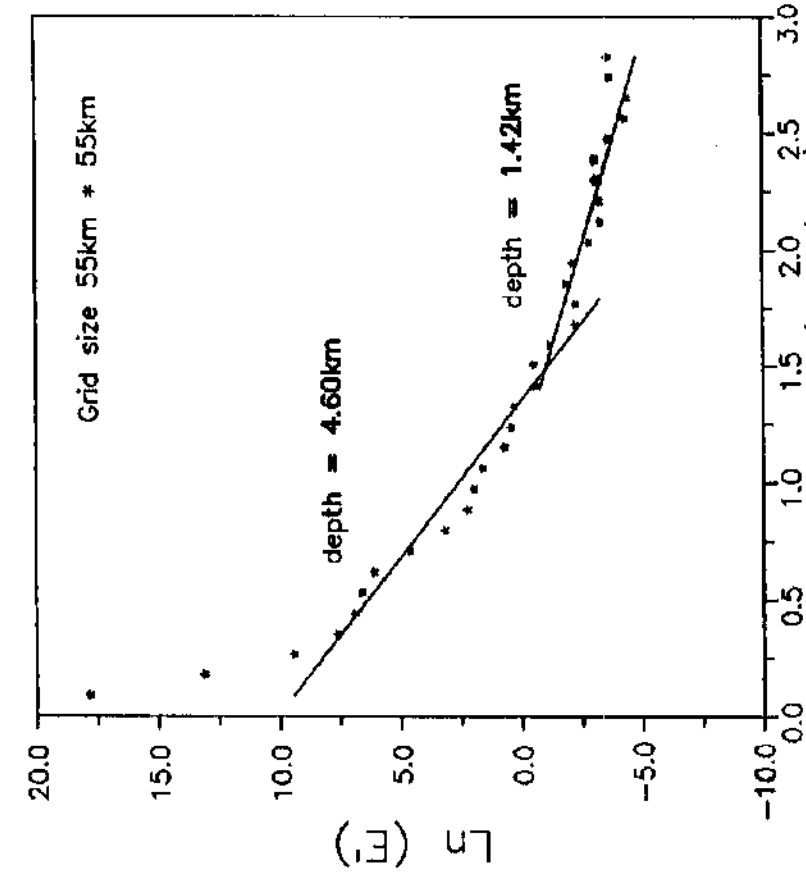
Power Spectrum Analysis for Block 19



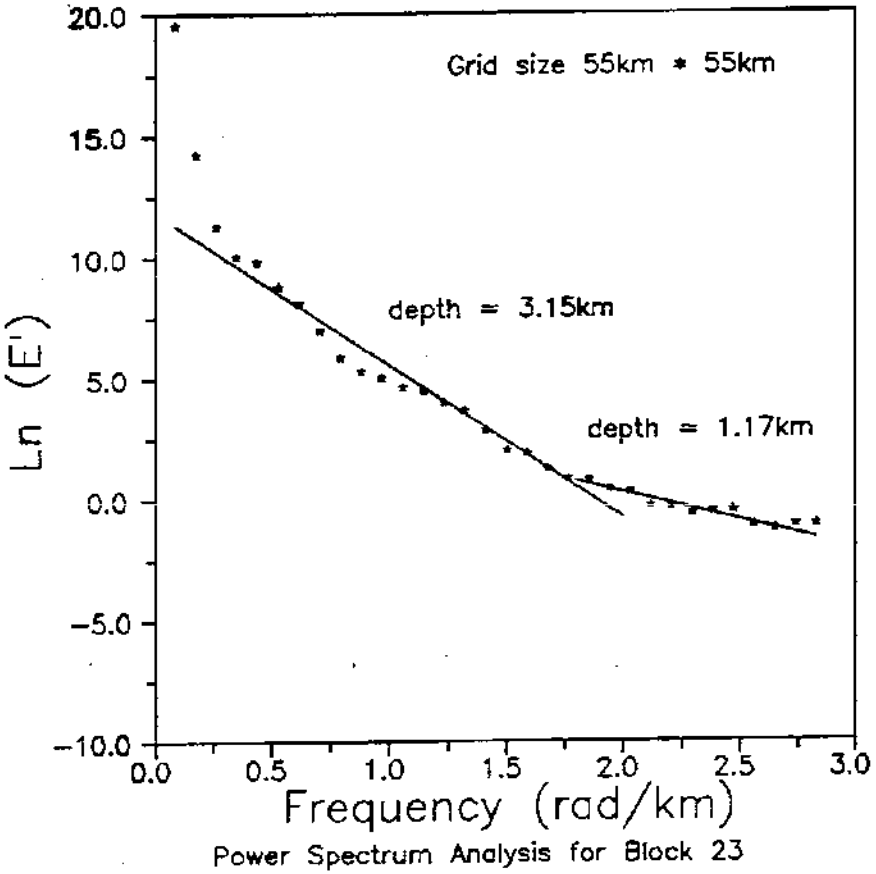
Power Spectrum Analysis for Block 20



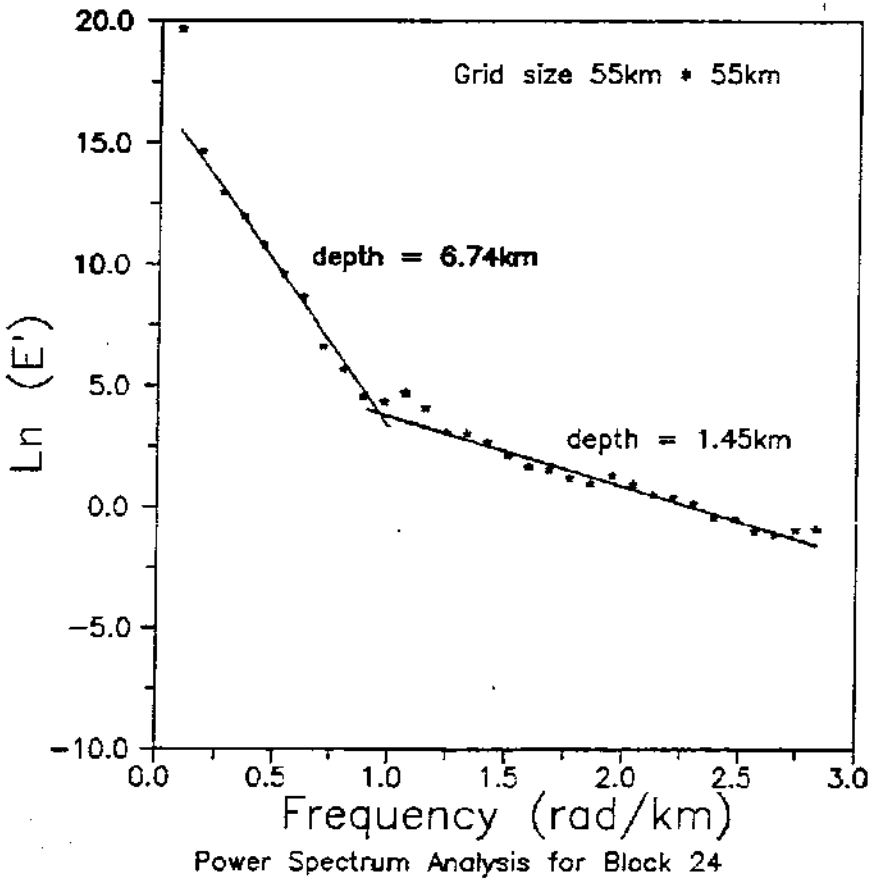
Power Spectrum Analysis for Block 22



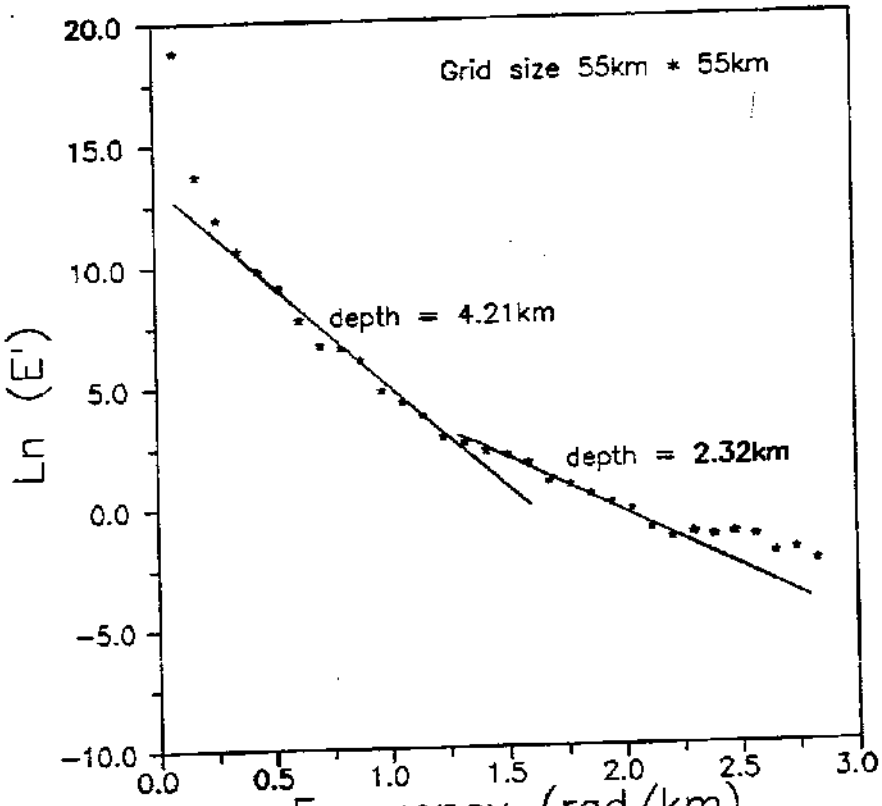
Power Spectrum Analysis for Block 21



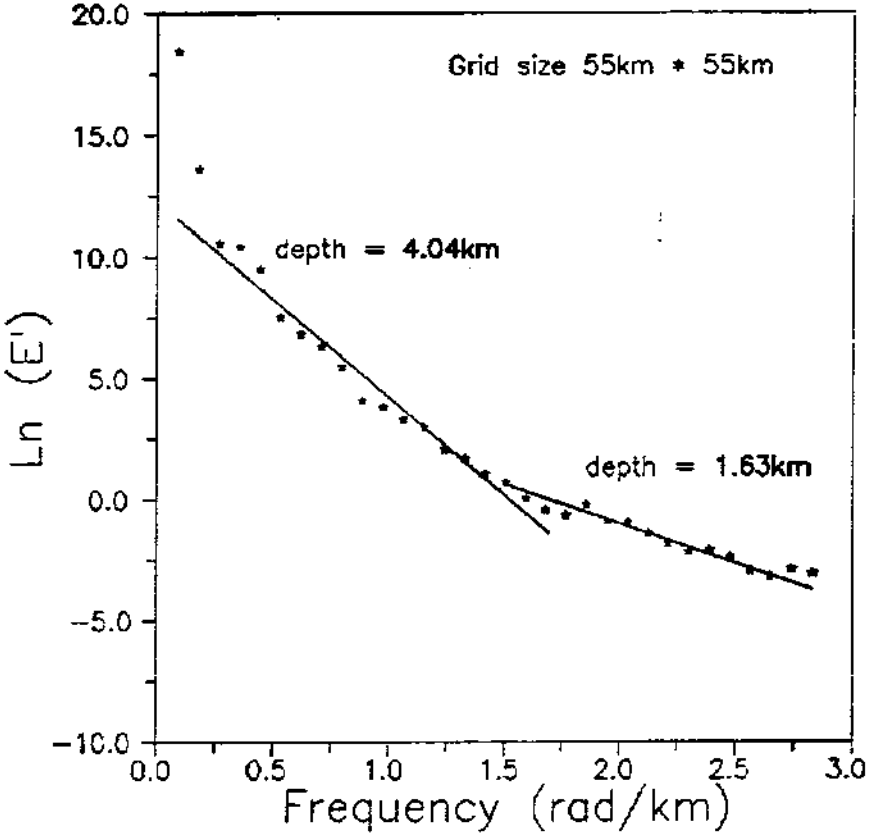
Power Spectrum Analysis for Block 23



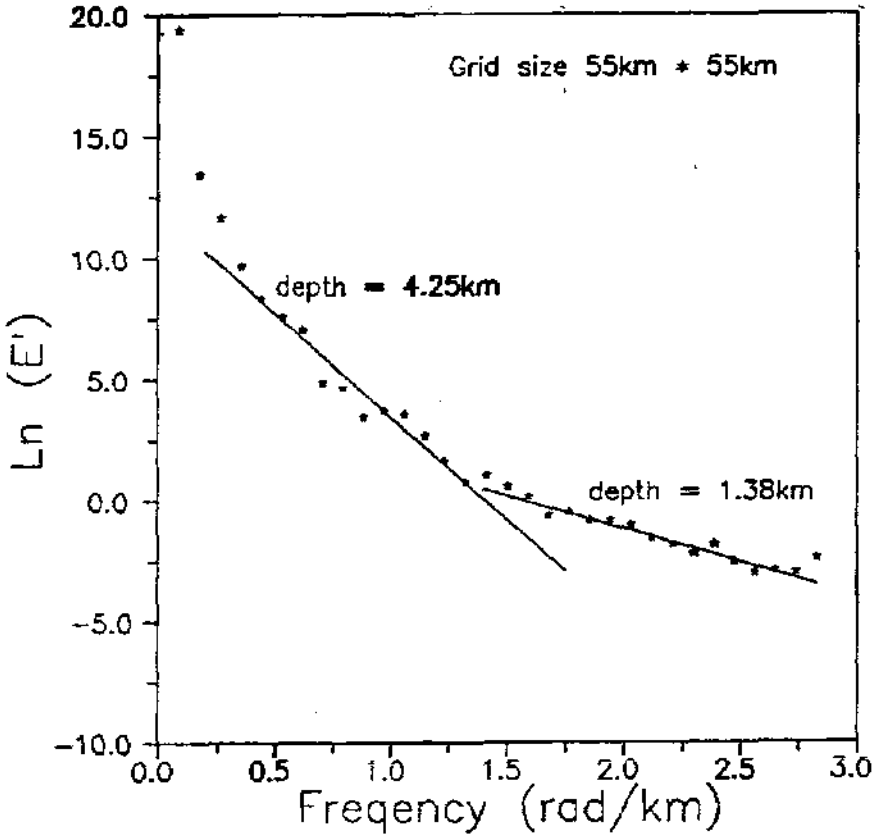
Power Spectrum Analysis for Block 24



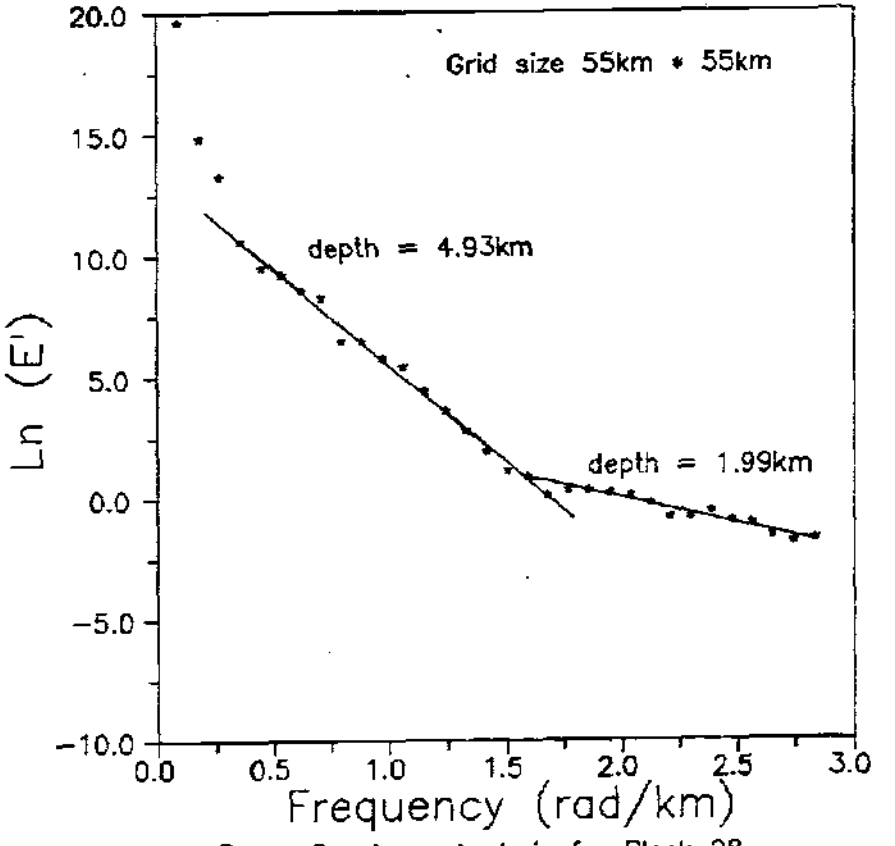
Power Spectrum Analysis for Block 25



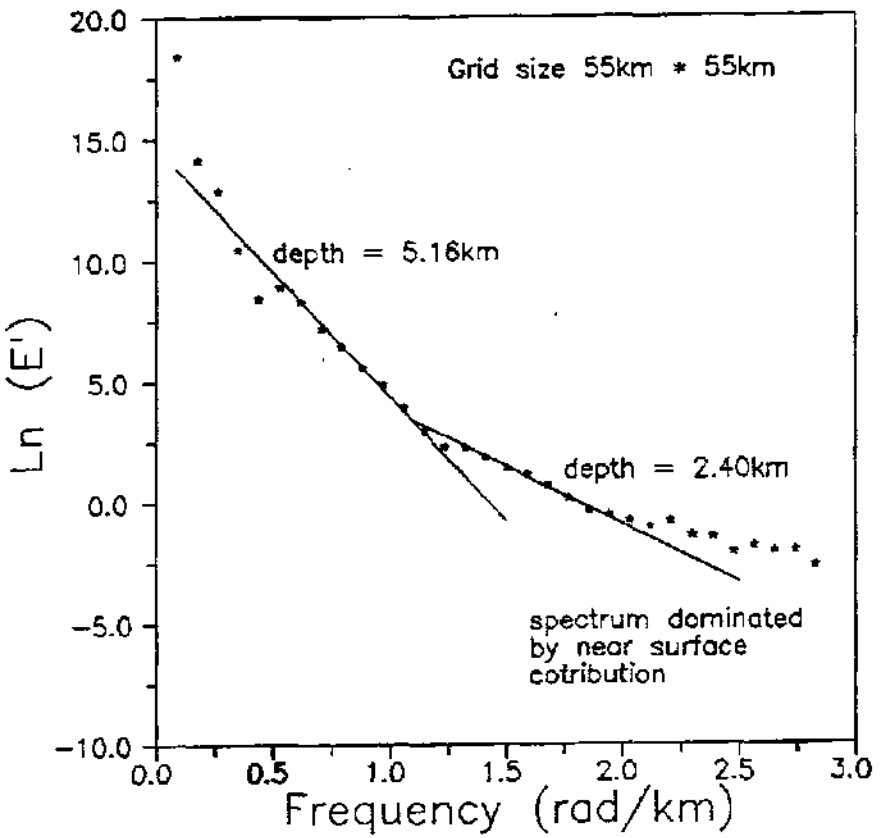
Power Spectrum Analysis for Block 26



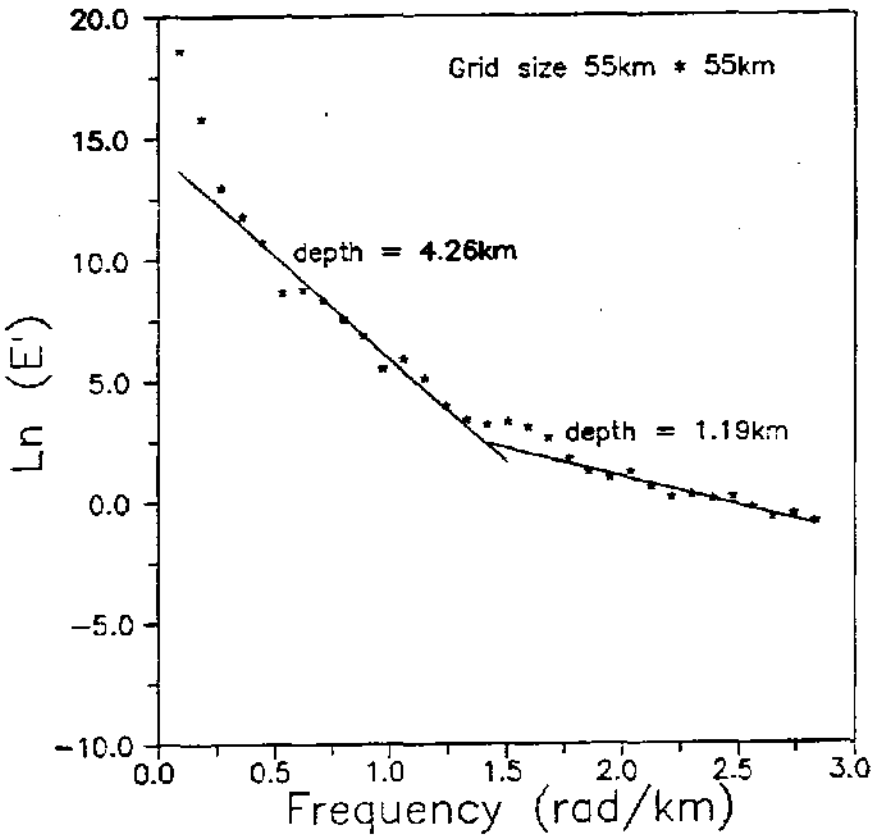
Power Spectrum Analysis for Block 27



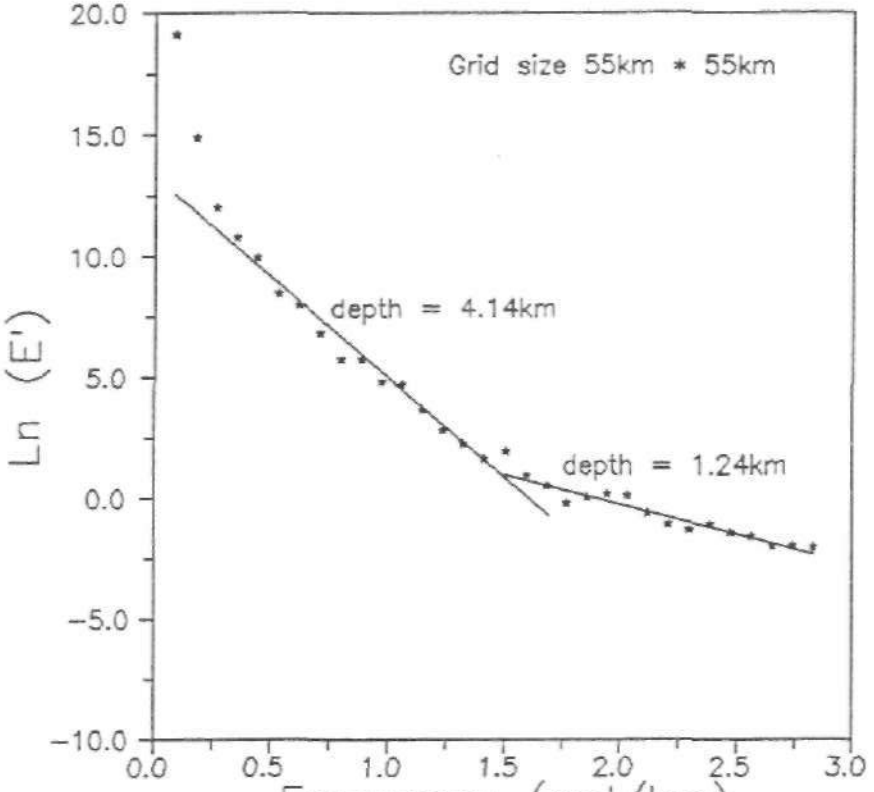
Power Spectrum Analysis for Block 28



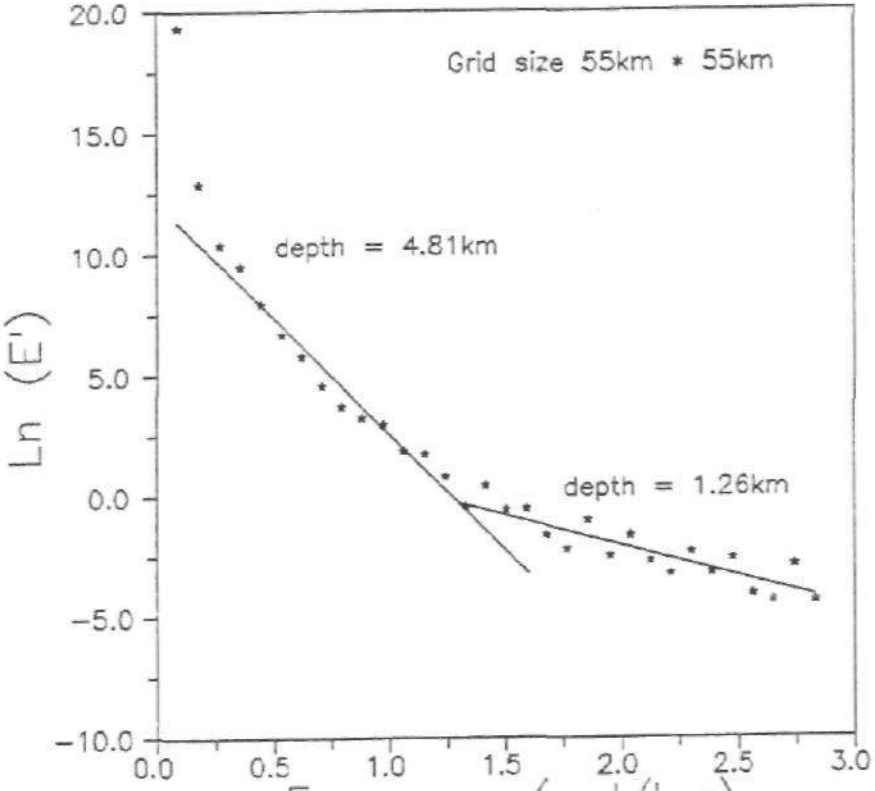
Power Spectrum Analysis for Block 29



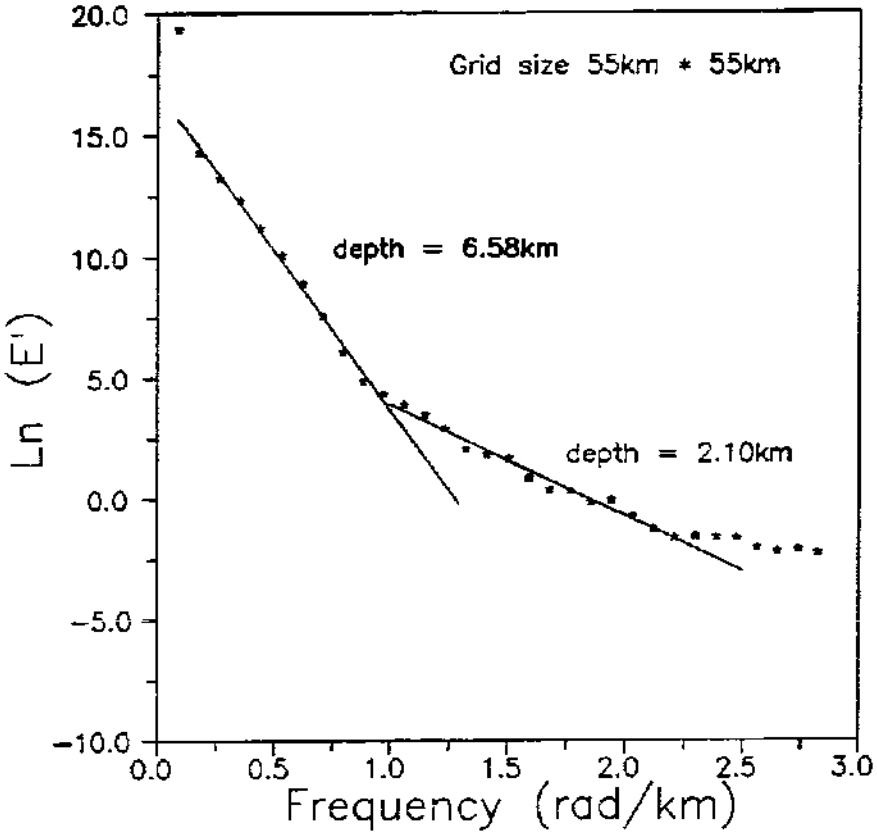
Power Spectrum Analysis for Block 30



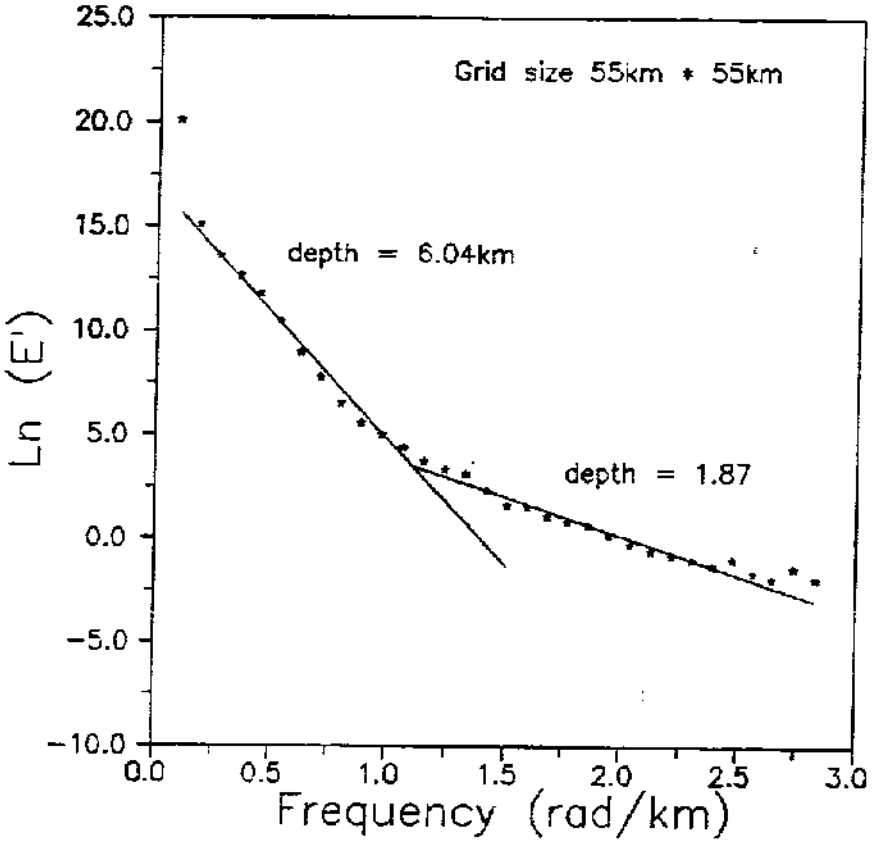
Power Spectrum Analysis for Block 31



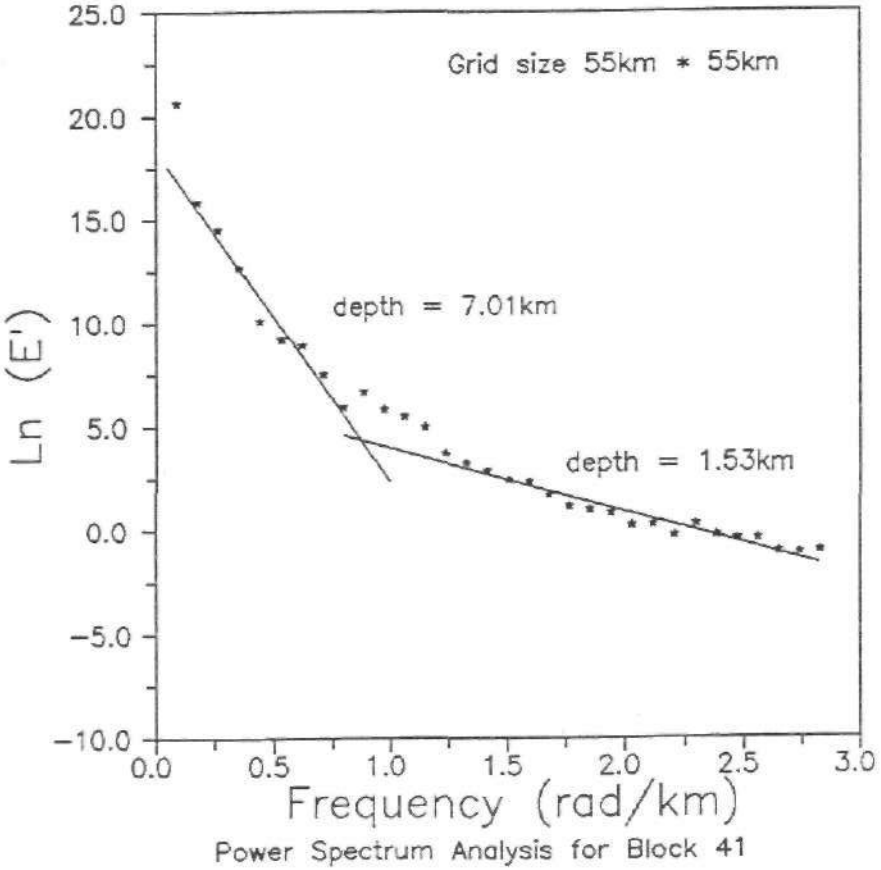
Power Spectrum Analysis for Block 32



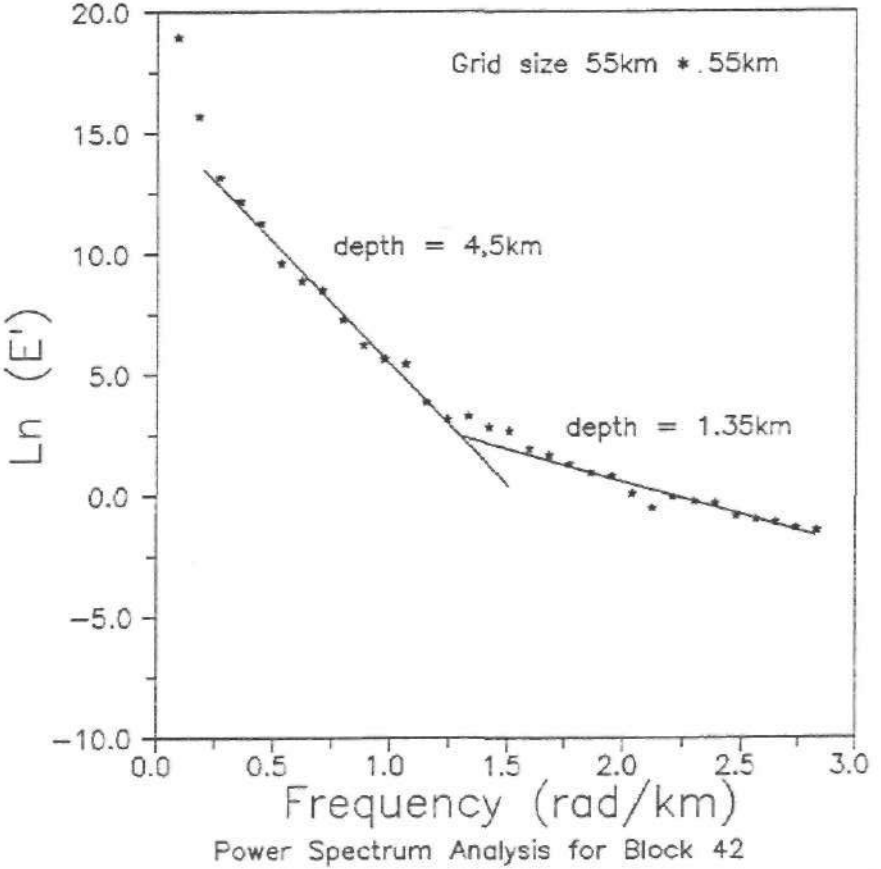
,Power Spectrum Analysis for Block 33



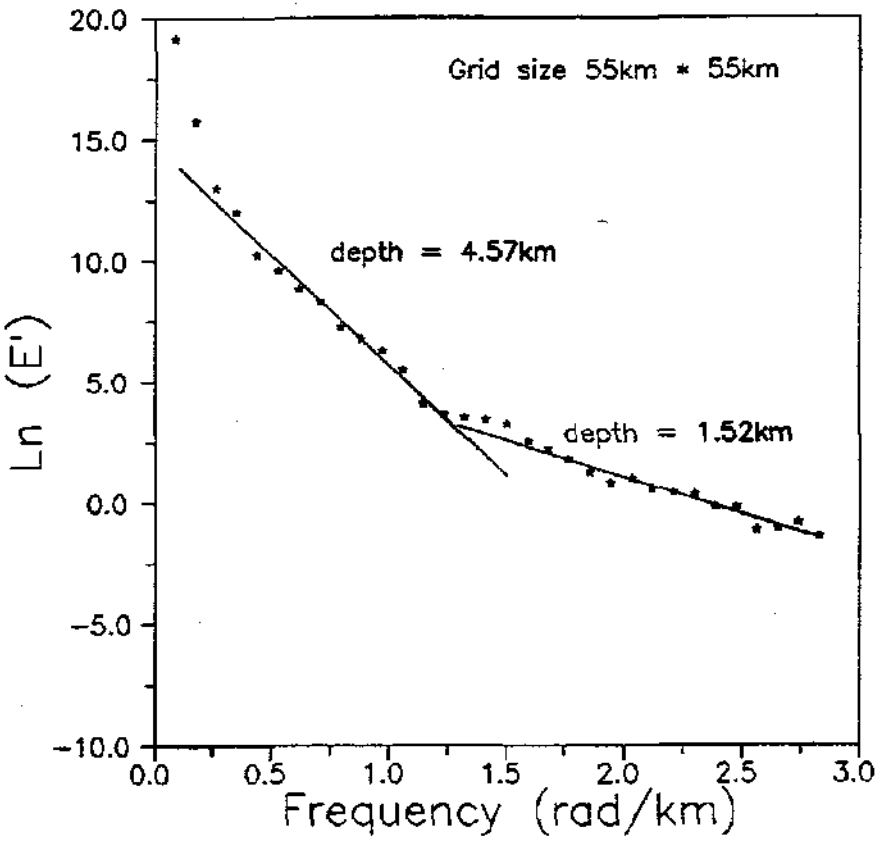
,Power Spectrum Analysis for Block 34



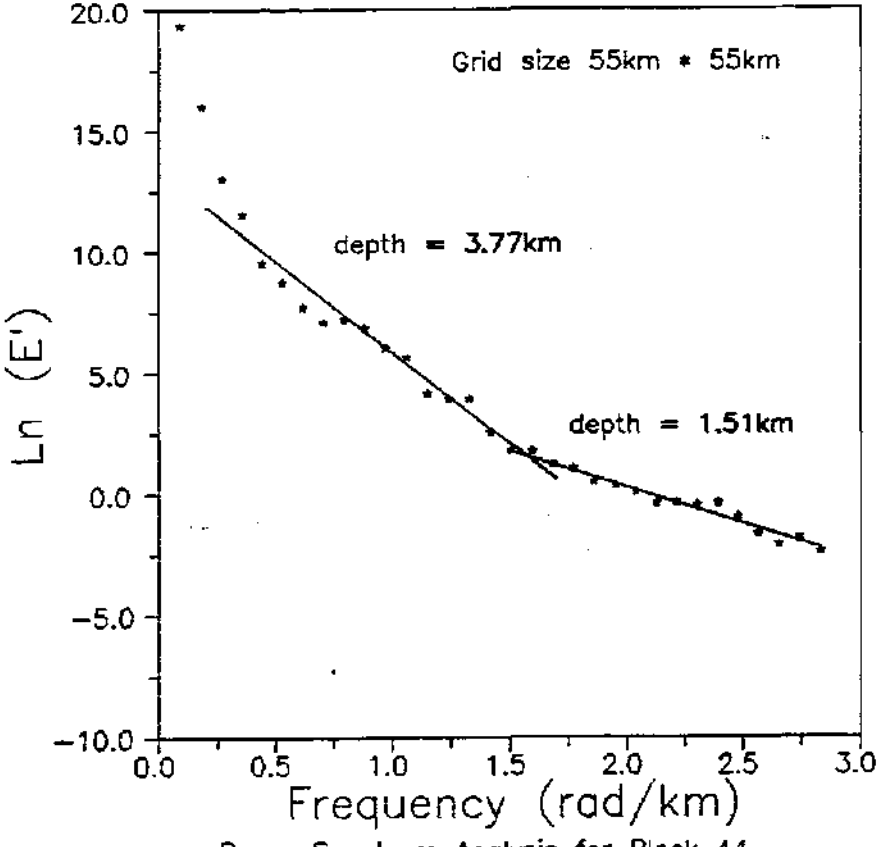
Power Spectrum Analysis for Block 41



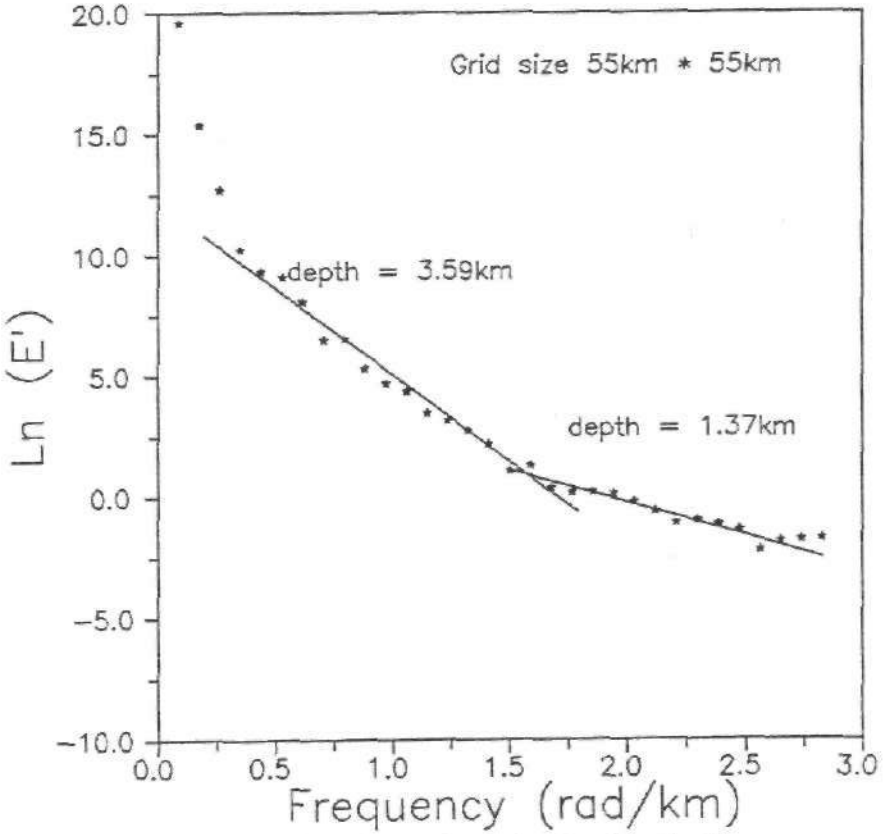
Power Spectrum Analysis for Block 42



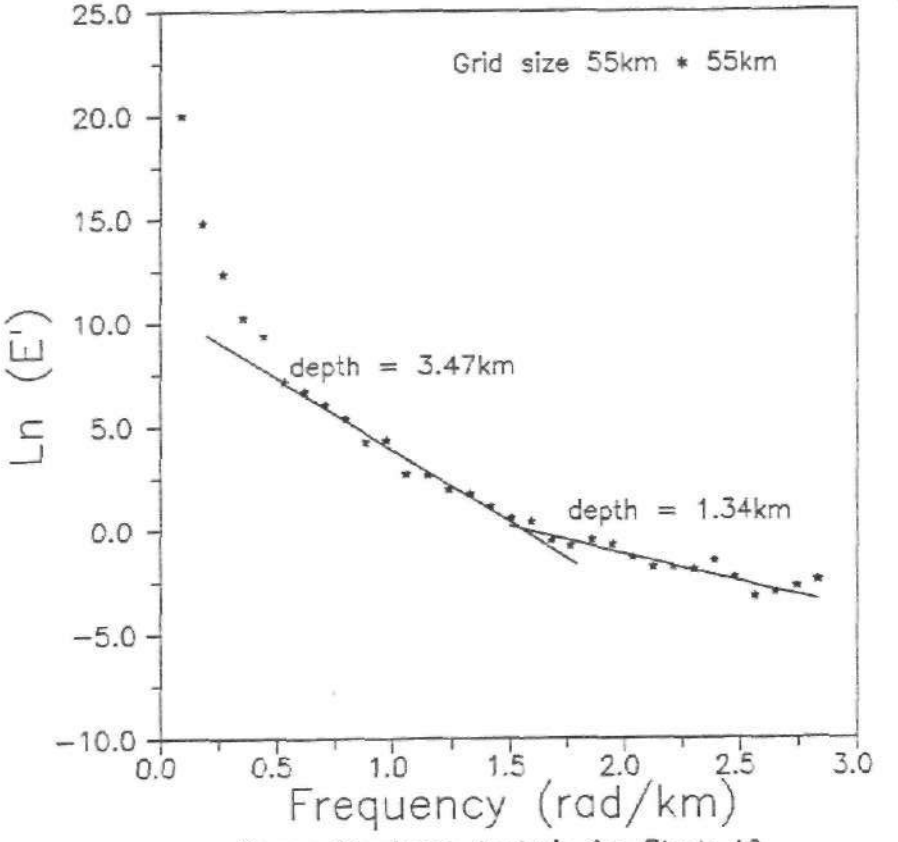
Power Spectrum Analysis for Block 43



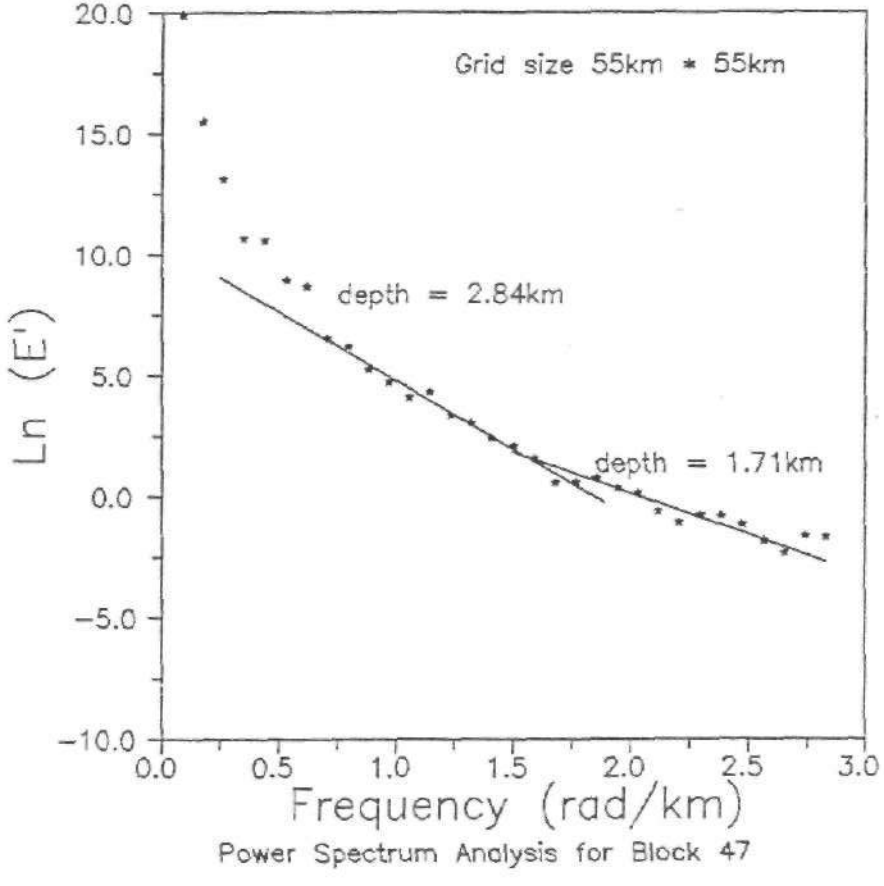
Power Spectrum Analysis for Block 44



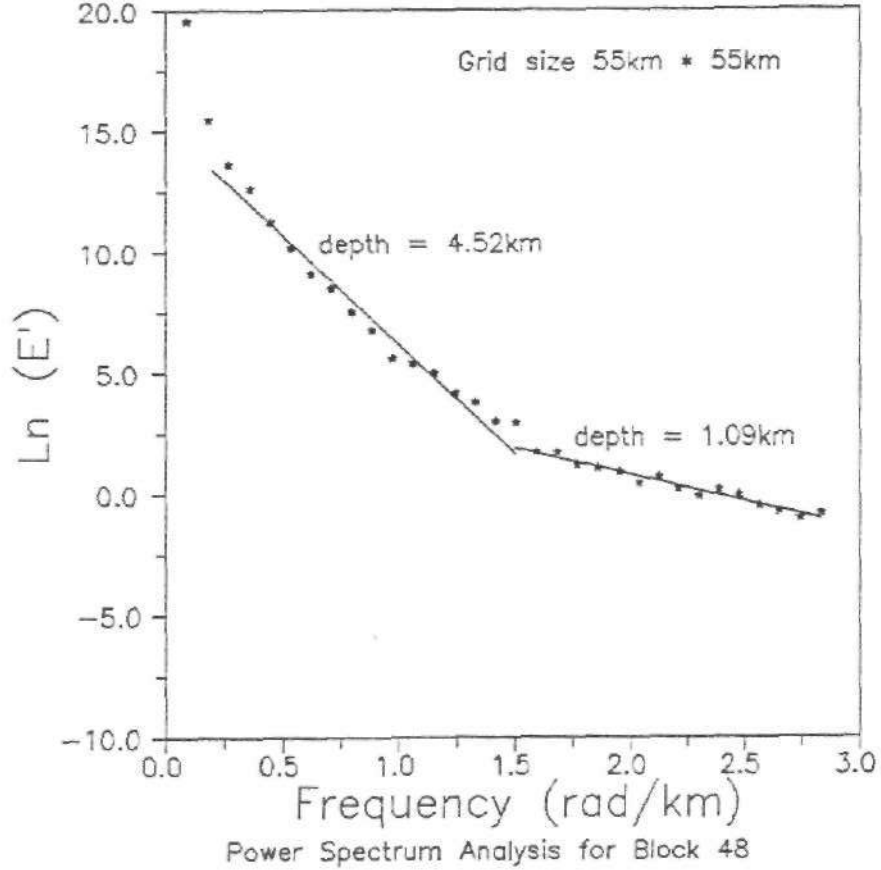
Power Spectrum Analysis for Block 45



Power Spectrum Analysis for Block 46



Power Spectrum Analysis for Block 47



Power Spectrum Analysis for Block 48